Politecnico di Torino

DIMEAS - Dipartimento di Ingegneria Meccanica e Aerospaziale

Politecnico di Torino

Sensitivity of drag coefficient on ground vehicles to different mesh strategies and turbulence models

Advisor:

Renzo Arina

Co-Advisor:

Matteo Gautero

Student:

Edoardo Beatrice

ACADEMIC YEAR 2022-2023

Abstract

The research conducted concerns the field of the computational fluid dynamics and considers various turbulence models of the Reynolds-averaged Navier-Stokes equations. The study has been carried out in collaboration with Politecnico di Torino and Stellantis, which uses this kind of model in order to predict how vehicles react to changes of geometry.

The aim of this project is to analyze how changes in domain meshing processes and turbulence models, can affect the results of the drag coefficient C_x either on different geometry of the same vehicle and on different vehicles. In particular, deltas between different configuration studied will be shown. In order to conduct the study, two different software has been used: $ANSA$ and $StarCCM+$ (in collaboration with Siemens in order to develop a better algorithm of mesh and turbulence model).

The thesis is built in 4 different chapters: the first one is a brief introduction of the topic, which will be developed in following chapters; the second one contains the introduction to the laws which govern aerodynamic flows, the description of the turbulence models used ($\kappa-\epsilon$, $\kappa-\omega$, *Elliptic blending models*) and why they have been introduced in fluid-dynamic computation; the third chapter describes the process followed in order to achieve the results, explaining how many car models were used, which different processes of meshing were followed and which turbulence models were implemented; the fourth chapter is a conclusive one, in which all the results are analyzed and some additional analysis of the study are presented.

Sommario

La tesi che è stata sviluppata si colloca nel campo della fluidodinamica computazionale e si concentra nell'andare a valutare le variazioni di coefficiente di resistenza aerodinamico su differenti geometrie al variare del modo di generare la mesh per il calcolo e del modello di turbolenza. La ricerca è stata sviluppata in collaborazione con il Politecnico di Torino e la Stellantis, la quale usa questi tipi di modelli al fine di prevedere come le modifiche (ad esempio geometriche) influenzino i parametri aerodinamici. Al fine di condurre lo studio sono stati utilizzati due programmi di simulazione aerodinamica: ANSA e Star CCM+.

La prima parte del lavoro di tesi si è concentrata sull'introduzione dell'argomento e degli obiettivi e sull'approfondimento dei modelli di turbolenza che sono stati utilizzati per le analisi. In particolare sono tutti modelli derivati dalle cosiddette RANS, ovvero dalle equazioni di Navier-Stokes mediate alla Reynolds. Le equazioni RANS permettono di studiare i modelli di turbolenza scomponendo la variabile istantanea come sovrapposizione di un valore medio più una fluttuazione (che viene spesso indicata con l'apice " '"). Andando a riscrivere le equazioni di Navier-Stokes imponendo quindi le variabili ϕ come $\phi = \bar{\phi} + \phi'$, ciò che si ottiene è identico alla scrittura di partenza, tranne che per la presenza di un termine addizionale che compare nell'equazione di trasporto del momento e dell'energia. Questo termine, che prende il nome di *tensore degli stress di Reynolds*, dipende dalla densità, dai prodotti mediati delle componenti delle fluttuazioni di velocità e dall'energia cinetica turbolenta. L'obiettivo è dunque quello di avere un modello del tensore degli stress di Reynolds in termini di quantità medie del flusso per poter chiudere il sistema di equazioni di governo. In particolare ci sono due approcci su STAR CCM+ che permettono di fare ciò: gli *eddy viscosity models* ed i *modelli di trasporto dello stress di Reynolds*. Sotto la prima categoria dei modelli ricadono proprio quelli che sono stati utilizzati nel corso del lavoro, ovvero: il modello *Standard* $\kappa - \epsilon$, il modello *SST* $\kappa - \omega$ ed il modello *Lag Elliptic Blending* $\kappa - \epsilon$. Gli *eddy viscoity models* in paricolare, modellizzano il tensore degli stress utilizzando il concetto di viscosità vorticosa turbolenta μ_t che permette di scrivere il tensore stesso in funzione delle quantità medie del fluido. Questi tipi di modelli risolvono equazioni di trasporto aggiuntive per quantità scalari che consentono di derivare la viscosità turbolenta. All'interno del lavoro di tesi sono dunque stati analizzati e presentati i tre modelli di turbolenza appena nominati, descrivendone i vantaggi, gli svantaggi e il modello di utilizzo nell'ambito dell'analisi computazionale svolta.

La seconda parte del lavoro di tesi si è invece concentrata sulla descrizione di ciò che è stato fatto al fine di poter avere i risultati da poter paragonare ed analizzare. Sono stati studiati 4 modelli differenti di veicoli: la Fiat 500X, la Fiat Tipo, lo Stelvio e la Giulia. Il procedimento seguito per tutte le vetture è stato il seguente: per prima cosa utilizzando il software *Ansa* sono stati modificati i nomi di ogni PID al fine di rendere più semplice il lavoro da svolgere su Star CCM+; sono state applicate lo modifiche geometrice al fine di vedere come si sarebbe comportato il coefficiente di resistenza aerodinamico tra le differenti configurazioni; sono stati fatti tutti i controlli geometrici e sulla mesh per evitare di incorrere in errori; sono state esportate le componenti a gruppi di PID per poterli importare successivamente su Star CCM+. La parte successiva che è stata eseguita riguarda tutte le operazioni dopo aver importato i file come *Surface Mesh*: sono stati infati creati i sistemi di riferimento della galleria del vento, delle masse radianti e della macchina; successivamente sono stati costruiti dei volumi di raffinamento in diverse zone al fine di rendere più dettagliata la soluzione in zone come quelle della scia o nelle

zone prossime alla superficie della vettura. Dopo a aver eseguito altre operazioni di preparazione, è stata generata la mesh volumetrica utilizzando degli opportuni *Custom Controls*. Dopo aver generato le celle volumetriche ed aver rimosso quelle che presentavano una qualità inferiore ad una determinata soglia o un volume negativo, ci si è concentrati sui modelli di turbolenza da utilizzare, che sono i medesimi che sono stati presentati nella prima parte del lavoro di tesi. Infine sono stati lanciati i casi e valutati i risultati che vengono riportati all'interno dell'ultimo capitolo della tesi.

La tesi si conclude con il riassunto dei risultati ottenuti ed il loro paragone in particolare concentrandosi sull'influenza del tipo di processo di generazione di mesh utilizzato ed i modelli di turbolenza. I riustati vengono mostrati nelle pagine finali di questo documento.

Contents

Chapter 1

Introduction

Computational fluid dynamics is a branch of physics which deals with the motion of fluid (such as air and water) and their interactions with solid boundaries and It plays a crucial role in a multitude of engineering and scientific applications. From designing more aerodynamically efficient vehicles to optimizing industrial processes involving fluid flows, understanding the intricate interplay between fluid behavior, boundary conditions, and turbulence models is fundamental. One of the most important things that this field has achieved, is the ability to predict non-dimensional coefficient such as lift or drag coefficient. The estimation of the latter one, is a fundamental aspect of fluid dynamics which influences the efficiency and the performance of various systems. Especially in the field of vehicles is crucial, considering for example that improving cars' aerodynamics allows to decrease fuel consumption or can give more stability increasing the down-force. Furthermore, thanks to computational fluid dynamics it is possible also to predict how changes of the geometry can affect either the important non-dimensional coefficients and the aero-acoustic of the model without the need to physically produce the component and test it in the wind tunnel. This master's thesis delves into the realm of computational fluid dynamics (CFD) to explore how alterations in the geometry and turbulence models impact the prediction of the drag coefficient and the lift coefficient.

The drag coefficient is a non-dimensional parameter which quantifies the resistance experienced by an object as it moves through a fluid. Accurate prediction of this coefficient is not only important in automotive engineering, but also in many other different fields such as aerospace, environmental science but also cardiovascular fluid dynamics. Traditionally, the estimation of drag coefficients relied heavily on experimental methods, which can be time-consuming, expensive, and often limited in their ability to capture intricate flow phenomena. With the advancement of computational techniques, CFD has emerged as a powerful tool that enables engineers and researchers to simulate complex fluid flows, providing insights that were once unattainable.

One of the critical factors which influences the accuracy of CFD simulations is the manipulation of the system's geometry. Alterations to the geometry can lead to diverse flow patterns and interactions between the fluid and solid boundaries, thereby directly influencing the drag coefficient estimation. The complexity of these geometrical changes introduces a need to comprehensively explore their effects on drag prediction. This thesis aims to address this aspect by systematically analyzing the impact of geometry variations on drag coefficient estimations through advanced computational fluid dynamics techniques.

Furthermore, turbulence, an inherently chaotic and unsteady flow regime, significantly impacts the accuracy of drag coefficient predictions. Turbulence models are mathematical formulations used within CFD simulations to approximate the complex turbulent behavior of fluids. These models introduce a level of simplification, and their selection can significantly influence the outcomes of simulations. This thesis aims to delve into the comparative analysis of various turbulence models and their effects on the accuracy of drag coefficient estimations under different boundary conditions.

In order to conduct this study, two different aerodynamic simulation software were used: ANSA and Star CCM+. The former was used in order to implement the modifications of the geometry of the model; the latter to build the volumetric mesh, create mesh refinements, set boundary conditions and run the case.

In summation, this master's thesis embarks on an expansive exploration of the intertwined dynamics of boundary conditions, geometry variations, and turbulence models in the realm of drag coefficient estimation using computational fluid dynamics.

Considering that one of the most important topics which has been addressed in this thesis is the way a mesh is produced, it is really important to firstly give an idea of why the its construction is so important.

1.1 Mesh process

Alongside the importance of the turbulence, in this thesis also the construction of the mesh has played a really important role. As a matter of facts, the way a mesh is built in order to solve the equations is of a fundamental importance. In fluid dynamics is essential due to its significant influence on the accuracy, efficiency, and reliability of simulations. But firstly it is useful to give a brief definition of what a mesh is: it is a grid of interconnected points or elements, which discretizes the domain to be analyzed. Following, there are some key points of why the construction of a mesh is essential:

- **Accuracy and Resolution**: in CFD simulations the quality and the density of the mesh directly affect the precision and the reliability of the computation. In areas where gradients are relevant, a fine mesh can capture the phenomena in a more accurate way.

- **Boundary Representation**: meshing plays a crucial role in accurately representing boundaries and surfaces within the domain. Properly resolving solid boundaries and fluid interfaces is essential for capturing boundary layer effects and interactions.

- **Numerical Stability**: a bad constructed mesh can lead to numerical instability and convergence issues during the simulation.

- **Solution Convergence**: A well-structured mesh facilitates convergence to a solution. Iterative solvers in CFD rely on the mesh's quality to converge efficiently and reliably.

- **Resource Efficiency**: it is important to balance the mesh design. Finer mesh results in longer simulation. So, it is imperative to find a trade-off between the need of having a fine mesh (and a better capture of the phenomena as a consequence) and the amount of time spent for the simulation. Usually, in the study of external aerodynamics for vehicles, the domain of the computation is discretized in about 90 million of volumetric cells.

In summary, mesh construction in computational fluid dynamics is a fundamental step which directly influences the quality and reliability of simulation results. A carefully crafted mesh, tailored to the problem's characteristics, ensures accurate predictions of fluid behavior and enhances the overall validity of CFD simulations. As anticipated before, another key point of what will be discussed in thesis is the model of turbulence used in the computation. But before discussing what how turbulence can be modelled, it is useful to give an idea of what a turbulence is.

1.2 The concept of turbulence

The concept of turbulence is widely acknowledged in contemporary times, and in general, its definition is comprehended, particularly by those with technical knowledge. Even though it has been seen that it is a familiar notion, it is not easy to find a satisfactory definition of turbulent flows and it has not been found yet. According to Taylor and Von Karman in 1937 turbulence was defined as "an irregular motion which in general makes it appearance in fluid, gases or liquid, when they flow past solid surfaces or even when neighboring streams of the same fluid flow past or over one another"[12]. One of the important innovations of this definition was the introduction of the condition of irregularity. It is important to have this concept linked to the concept of turbulence because irregularity is the reason why it is impossible to describe the motion in all details as a function of time and space.

The majority part of flows which happens in nature either in nature and in the industrial application can be considered as turbulent. Often, the fluctuations which form are of such a big scale and dimension that is really difficult to solve them in time and space because of the excessive computational costs. So, instead of solving the equations for field which are turbulent, it is less expensive to solve for averaged or filtered quantities and then approximate the impact of these small fluctuating structures [16].

Now it is important to define some properties which characterize turbulence:

- **A random process**: Turbulent flows are time and space dependent and they have a great number of spatial degree of freedom. It is almost impossible to predict its behaviour, but it is indeed possible to reproduce statistical properties. In addition, it can be useful to break down the local speed in two different components: the first one can be and averaged one and the second component can be a fluctuation. It will be seen that this way of breaking down the velocity are used in RANS models.

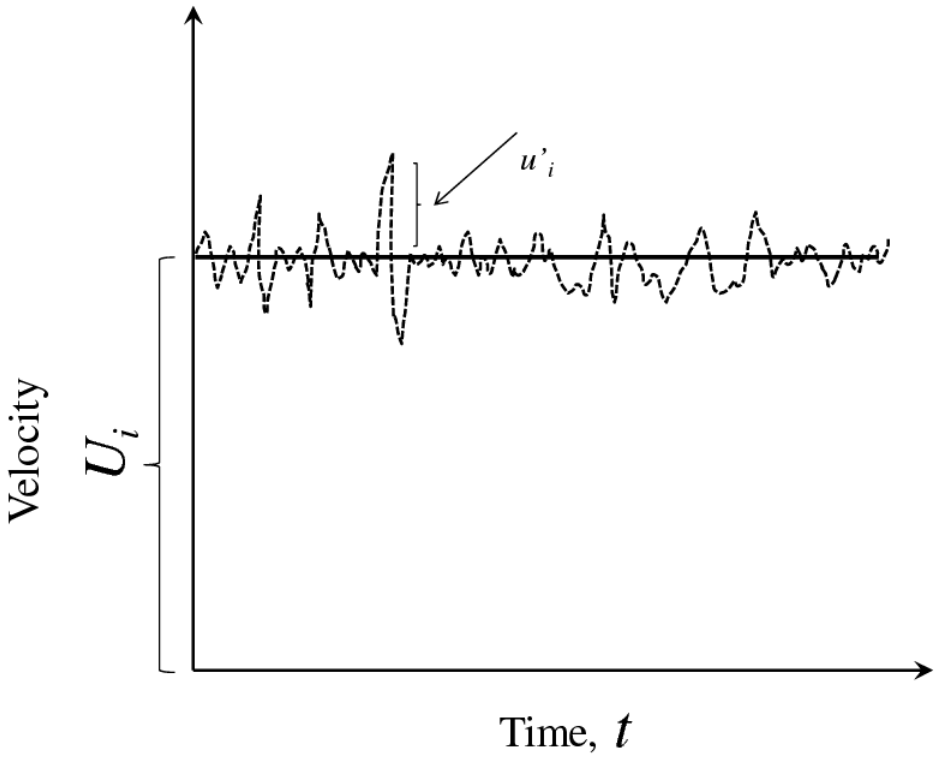

Figure 1.1: Example of how velocity could be broken down in the study of turbulence [8]

- **Wide range of different scales**: the dynamics of turbulence involve a wide range of scales, from the largest one to the smallest one. As a matter of facts, turbulence can be seen as a composition of eddies of different sizes. It is important to remember what an eddy is: it is a motion which happen in a turbulent flow and it is characterized by small rotating structures that form within a complex and chaotic flow. When these large eddies are of a large scale, they are unstable and for this reason they tend to break-up, transferring their energy to some smaller eddies. This process of breaking-up keeps going until the Reynolds number is sufficiently small that the eddy motion is stable and the viscosity is effectively dissipating the turbulent kinetic energy. This condition happens at an eddy scale which is indicated with the Greek letter η and is called *Kolmogorov scale*.

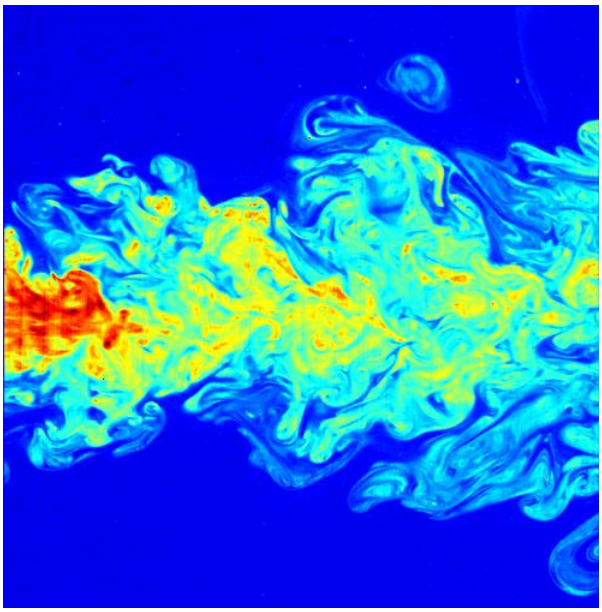

Figure 1.2: Cascade of eddies [11]

- **A rotational field**: as said before, a turbulent flow is characterized by the presence of vorticity. In greater details, the magnitude of the vorticity fluctuation can be much larger than the mean vorticity. By displaying a section of a turbulent flow field, it appears as a collection of streaks, strain regions and swirls which deform and rotate for mutual induction [4].

- **Turbulence arises at high Reynolds numbers**: Transition to turbulence occurs due to the instability of laminar flow at large Reynolds number. As a matter of facts, with rising Reynolds numbers, the convective term in the Navier Stokes equations increases in importance compared to the viscous term and so the tendency of instability, which is damped by the viscosity, increases.

- **Turbulence dissipates energy**: Turbulent kinetic energy is dissipated into heat due to the fluid's viscosity forces. This process of dissipation is essential for the reduction of turbulent energy and its eventual transformation into thermal heat. As a matter of facts, kinetic energy is transferred through a "cascade" from large scales to small scales. Large vortex structures relinquish energy to smaller structures until the energy is dissipated as heat.
  In order to better understand how the dissipation works, it can be useful to recall the vorticity equation [4]:

$$\frac{D\vec{\omega}}{Dt} = \frac{\partial\vec{\omega}}{\partial t} + (\vec{v}\cdot\nabla)\vec{\omega} = \vec{\omega}\cdot\nabla\vec{v} + \nu^2\nabla\vec{\omega} + \nabla\times\vec{f} \tag{1.1}$$

  The term $\vec{\omega}\nabla\vec{v}$ is responsible for the mechanism called *vortex stretching*. It is three-dimensional and it is responsible for transferring the energy from large scale structures to small scale ones, through non-linear interactions, as long as velocity gradients are high enough to allow the dissipation of energy due to viscous actions.

This short paragraph is just a brief introduction to the concept of turbulence which will be dealt in greater detail in the second chapter of this thesis.

Chapter 2

Turbulence models

In order to discuss turbulence model, it is preparatory to have a full knowledge of what are the laws which rule a flow field.

2.1 The Navier Stokes Equations

The Navier-Stokes equations form a system of partial differential equations that describe the behavior of moving fluids, both liquids and gases, in the field of fluid dynamics. Their name pays tribute to the mathematicians Claude-Louis Navier and George Gabriel Stokes, who made significant contributions to the understanding and formulation of these equations during the 19th century.

Navier Stokes equations express three fundamental physical principles:

- Mass is globally conserved.

- The momentum (in the three spatial directions) is conserved. In other words, the second law of Newton in 3D space. As a matter of facts:

$$\vec{F} = \frac{d(m\vec{v})}{dt} = \frac{dm}{dt}\vec{v} + \frac{d\vec{v}}{dt}m$$

  Considering that mass is globally conserved the $\frac{dm}{dt}\vec{v} = 0$ and the result is the second law of Newton indeed:

$$\vec{F} = m\frac{d\vec{v}}{dt}$$

- Energy is conserved. In other words, it is the first law of thermodynamics applied to the fluid.

So, these equations can be defined as equations of balance and conservation, subject to boundary conditions, and are valid as long as the assumption of continuity in the fluid persists.

Now that it has been expressed as a physical model, it is important to translate it into mathematical language. In order to do that, a fluid which respect the continuity hypothesis and which flows through a "virtual" control volume is considered. The adjective "virtual" means that this volume is not physical and so it does not have walls. This control volume is an arbitrary portion of space, defined by a volume, a shape, and a volume's surface. The latter is identified at each point by the unit vector normal to the face. The volume can be used under four different assumption[7]:

- Finite and fixed control volume.

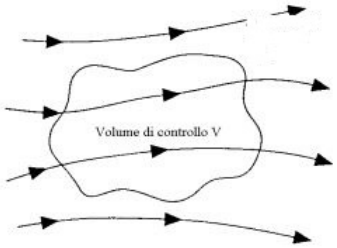

Figure 2.1: Finite and fixed control volume[7]

- Infinitesimal and fixed control volume.

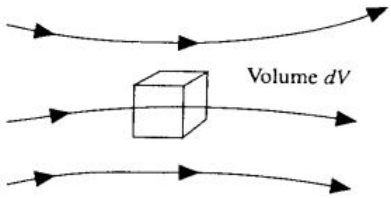

Figure 2.2: Infinitesimal and fixed control volume[7]

- Finite and moving control volume

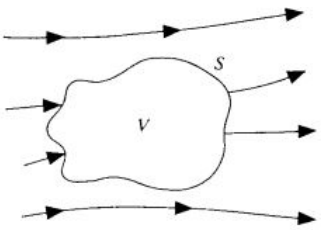

Figure 2.3: Finite and moving control volume[7]

- Infinitesimal and moving control volume.

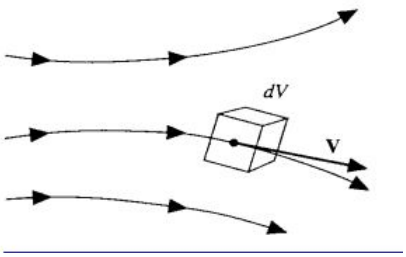

Figure 2.4: Infinitesimal and moving control volume[7]

Fixed volumes in space are defined such that the fluid passing through them is observed whereas volumes in motion are defined in a way that, at the initial instant, the fluid contained within them is "frozen," and then the volume is "tracked" with the moving fluid inside. So, it can be said that the fixed volume represents the *Eulerian point of view* and the moving one is the *Lagrangian point of view*. It is important to underline that, even if the mathematical form in which the laws are derived are different depending on the choice of the control volume, their physical meaning is always the same. In the following chapters it will be seen how to derive the Navier Stokes laws using the different approaches which has just been presented.

2.2 Mass balance equation

In this section the mass balance equation will be derived using the four different ways to define the control volume.

2.2.1 Mass balance equation for a finite and fixed in space control volume

In this paragraph the dissertation will be referred to *Figure 1.3*. In this configuration, the fluid flows through the (stationary) control volume and passes through the so-called control surface (the surface of the control volume). In order to write the mass balance equation, in this case it can be said that net flux of mass coming out from the control volume through surface S is equal to the reduction in time of the mass contained inside the control volume. Now this equation must be written in mathematical language.

The flow of a quantity through an infinitesimal surface dS is equal to that quantity multiplied by the scalar product of the velocity v of the flow and the unit vector normal to the infinitesimal surface at that point, times the same infinitesimal surface dS. So, the net flux through S is given by applying the integral operator to this punctual definition of flow.

$$\int_S \rho\vec{v} \cdot \vec{n} dS$$

Talking about the reduction in time of the mass contained in the control volume, the first thing to do is considering the mass contained in the control volume

$$dm = \rho dV$$

which, if considering all along the domain:

$$m = \int_V \rho dV$$

Considering that the equivalence given before is about the reduction of the mass, it can definitely be define as the temporal derivative of m with a negative sign in front (it is a reduction):

$$-\frac{\partial}{\partial t} \int_V \rho dV$$

So now it is possible to write the mass balance equation for a finite and fixed in space control volume

$$\frac{\partial}{\partial t} \int_V \rho dV + \int_S \rho \vec{v} \cdot \vec{n} dS = 0 \tag{2.1}$$

Since the control volume is finite, it is considered as an *integral* form and, considering that the volume is fixed it is also *conservative*.

2.2.2 Mass balance equation for a finite and moving control volume

As said before, when a moving control volume is considered, it is known that it always contains the same number of particles, so it is like saying that the mass contained inside it remains constant. On the other hand, since this volume is moving, it may happen that it changes its shape or volume. So, it is always true that

$$m = \int_V \rho dV$$

and it must be true that its derived form in time is equal to zero for what has just been said. Now, it must be considered that it is necessary to define the temporary variation of something which is moving so, in addition to the local variation (of a fixed point in a space), also a certain contribution given by the fact that the volume is moving has to be considered. The operator which considers this both effects is called *Lagrangian Derivate*, which can be written as:

$$\frac{D(.)}{Dt} = \frac{\partial(.)}{\partial t} + \vec{v} \cdot \nabla(.)$$

It is important to underline that the scalar product between $\bar{v}$ and ∇ is crucial: remembering that the scalar product introduces the *cos* of the angle between the two quantities just expressed, it means that if the control volume does moves perpendicularly to the gradient, the quantity $\vec{v} \cdot \nabla(.)$ is equal to zero. Summing up, the operator $\frac{D(.)}{Dt}$ says that the quantity (.) may change, either because it changes in time or because the motion happens along a gradient of that quantity. Mathematically, it is expressed by the following equation:

$$\frac{D}{Dt} \int_{V(t)} \rho dV \tag{2.2}$$

which means that the *Lagrangian derivative* of the mass m in the control volume V does not change. This form of the mass balance equation is called *integral* and *non-conservative* (since the volume is moving).

2.2.3 Mass balance equation for an infinitesimal and fixed in space control volume

A Cartesian frame of reference x, y, z is defined, where density and velocity are function of space (x, y, z) and time. An infinitesimal volume element is placed in a point of the space and has the following dimensions: dx, dy, dz [7].

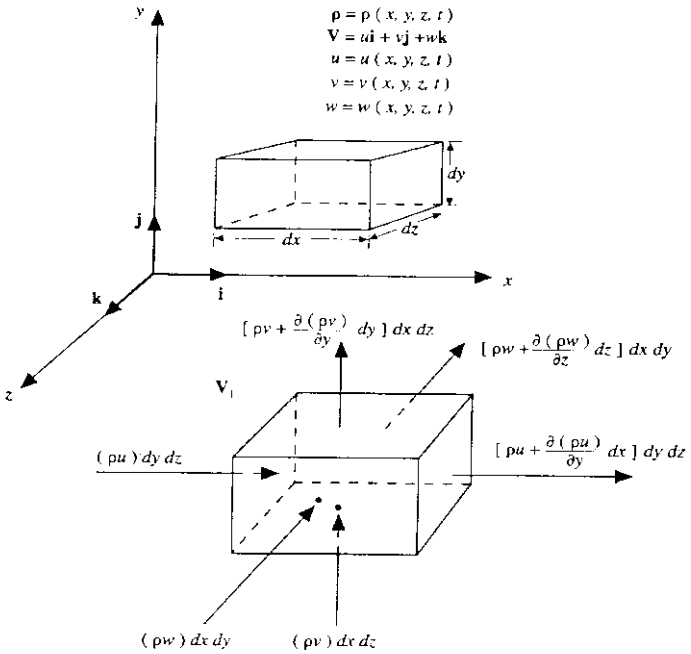

Figure 2.5: Infinitesimal and fixed control volume[7]

Obviously, the vector velocity $\vec{v}$ can be written as the sum of its three Cartesian components:

$$\vec{v} = u\vec{i} + v\vec{j} + w\vec{k}$$

In this way, also the normal vectors of the faces of the cubic control volume considered are represented by (in absolute value) the unit vectors $\vec{i}, \vec{j}, \vec{k}$.

Now let's considered the flux across the six faces of the control volume and let's see what happens to the scalar product $\vec{v} \cdot \vec{n}$. Obviously, the unit vectors are considered positive if they are oriented in the same directions of the axis x, y, z.

The left face of the volume is considered. Its unit vector is oriented outwards the surface, so it points towards the opposite direction of the x axis. So its unit vector is $\vec{n} = -\vec{i}$. If the infinitesimal surface of the face is $dydz$, the flux across it can be written as:

$$\rho\vec{v} \cdot \vec{n} dydz = -\rho y dydz$$

Now the right face is considered. The infinitesimal area is the same of the left one, so $dydz$. The unit vector on the other hand, is the opposite. In fact, the vector which points outwards has the same direction of the x-axis, so the unit vector is $\vec{n} = \vec{i}$. The most important thing which must be said is that now also the flux across the surface has change, because either the density and the velocity are functions of the position. In order to consider what has just been

explained, it is possible to write the flux across the right face (which is far from the left one of a length dx) as a series expansion. In result, the flux can be written as

$$\left[\rho u + \frac{\partial(\rho u)}{\partial x}dx\right] dydz$$

So, the net flux of mass towards x direction is given by the algebraic sum of the two fluxes:

$$-\rho y dydz + \left[\rho u + \frac{\partial(\rho u)}{\partial x}dx\right] dydz = \frac{\partial(\rho u)}{\partial x}dxdydz$$

The same way of proceeding can be done for the top and bottom faces or for the front and back faces. The only two things which changes are the normal vector (it is $|\vec{j}|$ for the former two faces and $|\vec{k}|$ for the latter two) and the infinitesimal area considered ($dxdz$ for the firsts two and $dxdy$ for the other two). The result of the flux along y is

$$\frac{\partial(\rho v)}{\partial y}dxdydz$$

On the other hand, for the flux along z

$$\frac{\partial(\rho w)}{\partial z}dxdydz$$

By adding these three different contributes, the net flux of mass across the infinitesimal control volume results in

$$\left[\frac{\partial u}{\partial x} + \frac{\partial v}{\partial y} + \frac{\partial w}{\partial z}\right] dxdydz = \nabla \cdot (\rho\vec{v})dxdydz$$

Considering what has been previously said, the net flux of mass across the control volume is equal to the reduction of the mass contained inside the same control volume. So, the right term of the equation is now known and it is necessary to find a way to write the left hand side. It is known that the infinitesimal volume dV can be written as

$$dV = dxdydz$$

So, the mass inside it is

$$dm = \rho dV = \rho dxdydz$$

So, the reduction in time of the mass (with the negative sign because the quantity is considered as decreasing), can be written as

$$\frac{dm}{dt} = -\frac{d\rho}{dt}dxdydz$$

By equating the formulation of the net flux and the reduction in time of the mass

$$\nabla \cdot (\rho\vec{v})dxdydz = -\frac{d\rho}{dt}dxdydz \tag{2.3}$$

Bringing the left hand side to the right one, the mass balance equation is obtained:

$$\frac{d\rho}{dt} + \nabla \cdot (\rho\vec{v}) \tag{2.4}$$

It is a conservative and differential form because the volume is infinitesimal and it is fixed in space.

2.2.4 Mass balance equation for an infinitesimal and moving control volume

In this case the mass contained in the infinitesimal control volume is constant and infinitesimal as well and can be written as

$$\partial m$$

The parameter which changes, as in *Section 2.2.2*, is the shape or the volume of the control volume. So, the relation between mass and volume is given by

$$\partial m = \rho \partial V$$

As in *Section 2.2.2*, the *Lagrangian Operator* can be applied and it results in

$$\frac{D}{Dt}(\rho \partial V) = 0$$

Considering that either the density and the infinitesimal volume can change in time, it is possible to expand the *Lagrangian Derivative*:

$$\frac{D}{Dt}(\rho \partial V) = \partial V \frac{D\rho}{Dt} + \rho \frac{D}{Dt}(\partial V) = 0$$

By dividing for ∂V and considering that it is possible to demonstrate that

$$\frac{1}{\partial V}\frac{D}{Dt}(\partial V) = \nabla \cdot \vec{v}$$

it is possible to write that

$$\frac{D\rho}{Dt} + \rho \nabla \cdot v = 0 \tag{2.5}$$

which is the differential and non conservative form of the mass balance equation.

As it has been said, these four different mathematical forms mean the same physical principle. There is only one thing that is important to be said: they cannot always be pick randomly to solve a problem. As a matter of fact, there is a big difference between the integral and the differential form. The integral can be used also if there is a discontinuity in the function (the integral is simply the area under the function itself, so it is not affected by the discontinuity), whereas the differential form needs a continuous function in order to be defined.

At this point, in order to complete the dissertation about the mass balance equation, it will be shown how to pass from a conservative to a non conservative form, either for the differential and for the integral case.

2.2.5 Interchangeability between different equations

In order to explain how to do this passage, two different examples will be taken:

- **From integral and conservative form to differential and non conservative**: in order to do that, it is important to remember *Gauss theorem*, namely that

$$\int_S \vec{f} \cdot \vec{n} dS = \int_V \nabla \cdot f dV$$

So, applying this theorem to *Equation 2.1*,

$$\frac{\partial}{\partial t} \int_V \rho dV + \int_V \nabla \cdot (\rho \vec{v}) dV$$

Considering that the control volume is arbitrary, it can be said that the expression is equal to 0 when the function to be integrate is 0. So, it easy to obtain

$$\frac{\partial \rho}{\partial t} + \nabla \cdot (\rho \vec{v})$$

by expanding $\nabla \cdot (\rho \vec{v})$

$$\frac{\partial \rho}{\partial t} + \rho \nabla \cdot \vec{v} + \vec{v} \cdot \nabla \rho$$

Which using the *Lagrangian derivate* as exposed in *Section 2.2.2*, can be written as

$$\frac{D\rho}{Dt} + \rho \nabla \cdot v = 0 \tag{2.6}$$

which is the differential and non conservative form.

- **From integral and non conservative to integral and conservative**: in this case, the *Theorem of Reynolds Transport* must be used. It can be applied when there is a time derivative of an integral whose domain depends on time:

$$\frac{D}{Dt} \int_{V(t)} f dV = \int_{V(t)} \frac{\partial f}{\partial t} dV + \int_{S(t)} (\vec{v} \cdot \vec{n}) f dS$$

In the studied case, it is traduced in

$$\frac{D}{Dt} \int_{V(t)} \rho dV = \int_{V(t)} \frac{\partial \rho}{\partial t} dV + \int_{S(t)} (\vec{v} \cdot \vec{n}) \rho dS$$

So, the equation becomes

$$\int_{V(t)} \frac{\partial \rho}{\partial t} dV + \int_{S(t)} (\vec{v} \cdot \vec{n}) \rho dS = 0$$

which is the integral and conservative form of the mass balance equation.

2.3 Momentum balance equation

In this section, it will be seen how to derive the momentum balance equation in its differential and non conservative form (so considering an infinitesimal and moving control volume).

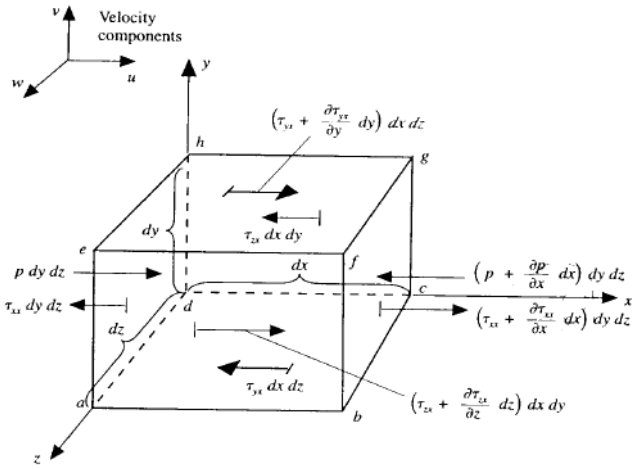

Figure 2.6: Infinitesimal and moving control volume[7]

As said in the previous sections, the momentum balance equation is equivalent to apply the second Newton law, which is a vector equation and so can be broken up in three scalar equations in 3D space. As for the mass balance, considering that the volume is infinitesimal, quantities (force and mass) will be considered infinitesimal (δ). So, the external force, which is applied to the control volume, causes an acceleration which, multiplied by the mass δm, is equal to the infinitesimal force δF. Considering that it is always true that

$$\delta m = \rho dx dy dz$$

and that the acceleration is equal to the derivative (which is the *Lagrangian derivative* because the control volume is moving) in time of the velocity (so every component of the acceleration is the Lagrangian derivative of the same velocity component), it is possible to write

$$\begin{cases} \delta F_x = \rho \frac{Du}{Dt} dx dy dz \\ \delta F_y = \rho \frac{Dv}{Dt} dx dy dz \\ \delta F_z = \rho \frac{Dw}{Dt} dx dy dz \end{cases}$$

The left hand side of these three equations is known since either the velocity and the density are known. It is important to know what are these three components of the force which are applied to the control volume. The forces can be classified in two different categories: volume forces and surface forces.[7]

- **Volume forces**: they are the forces which directly act on the mass contained in the control volume. Some examples of volume forces are the gravitational, the electric and the magnetic forces.

- **Surface forces**: they directly act on the surface of the volume control and can be classified in only two categories:

  - Pressure which the fluid exerts on the surface of the volume control. It is always perpendicular to the surface and it is considered positive if it points towards the inside of the volume.

  - Net pressure force in the x-direction and net friction force along the x-direction. They are linked to the deformation which may happen to the volume control. Net pressure force is considered positive if it points towards the outside of the control volume.

So now, the point is to find a way to write surface forces and volume forces considering the infinitesimal volume $dV = dxdydz$.

- **Volume forces**: A generic volume force per unit of mass can be defined as

$$\vec{f} = f_x\vec{i} + f_y\vec{j} + f_z\vec{k}$$

  This volume force is applied to the infinitesimal mass $\delta m = \rho dxdydz$ and it is obtained by multiplying δm by $\vec{f}$ so the three volume forces along the three directions x, y, z are

$$\begin{cases} \rho\vec{f_x}dxdydz \\ \rho\vec{f_y}dxdydz \\ \rho\vec{f_z}dxdydz \end{cases}$$

  So, these three forces are the are the first three contributions to the resultant force.

- **Surface forces**: every single face of the volume control must be considered. It is important to consider that pressure and normal/shear stress change in space. In order to demonstrate how these quantities can be written, it will be considered x direction and the reasoning can be reproduced along y and z. The demonstration will be referred to *Figure 2.6*.

  - Pressure which acts on the left face (which are is $dydz$) is considered equal to p, so the value of the force along x on the left face can be written as

$$pdydz \tag{2.7}$$

    The pressure which acts on the right face (which obviously has the same area $dxdy$) is dx far from the left one and can be written as a series expansion of p. Considering that it is negative because the pressure goes towards the inside of the volume control (and so it is has the opposite direction of x), the contribution of the pressure to the force along x on the right face is

$$-\left(p + \frac{\partial p}{\partial x}dx\right)dydz$$

By summing the two contributions (of the left and the right face), the results along x axis is found

$$\left[p - \left(p + \frac{\partial p}{\partial x}dx\right)\right] dydz$$

Applying the same procedure also along y axis and z axis, the contribution of the pressure is

$$\left[p - \left(p + \frac{\partial p}{\partial y}dy\right)\right] dxdz$$

$$\left[p - \left(p + \frac{\partial p}{\partial z}dz\right)\right] dxdy$$

- It is known that the net friction force is a tensor which has 9 components. Its components can be classified as $\tau_{i,j}$, where i represents the direction of the normal vector of the face on which the τ acts and j is the direction of the τ itself.

$$\begin{bmatrix} \tau_{xx} & \tau_{xy} & \tau_{xz} \\ \tau_{yx} & \tau_{yy} & \tau_{yz} \\ \tau_{zx} & \tau_{zy} & \tau_{zz} \end{bmatrix}$$

In order to value the contribution along x, every τ has to have $j = x$, whereas i is going to state the direction of the normal vector on which τ is being considered. For example, τ_{xx} acts on the left face (its normal vector is along x) along x. The right face (which is dx far from the left one) is equal to the series expansion of τ_{xx} and so it is

$$\left(\tau_{xx} + \frac{\partial \tau_{xx}}{\partial x}dx\right) dydz$$

Considering that the final value of τ_{xx} along x is given by adding the result of the left face to the result of the right one and that they always point outward the control volume, its final value along x is given:

$$\left[-\tau_{xx} + \left(\tau_{xx} + \frac{\partial \tau_{xx}}{\partial x}dx\right)\right] dydz$$

which results in

$$\frac{\partial \tau_{xx}}{\partial x}dxdydz$$

Along x, there are also of the other four faces. As a matter of facts, τ_{yx} acts on the bottom face (which area is $dxdz$) and by doing the series expansion of τ_{yx} also the contribution of the top face is given:

$$\left(\tau_{yx} + \frac{\partial \tau_{yx}}{\partial y}dy\right) dxdz$$

By adding the two contributions, the total τ_{xy} is given:

$$\frac{\partial \tau_{yx}}{\partial y} dxdydz \tag{2.8}$$

Following the same procedure for the remaining two faces, also τ_{zx} is given:

$$\frac{\partial \tau_{zx}}{\partial z} dxdydz$$

By adding these three contributions, the net friction force along x direction is:

$$\left(\frac{\partial \tau_{xx}}{\partial x} + \frac{\partial \tau_{yx}}{\partial y} + \frac{\partial \tau_{zx}}{\partial z} \right) dxdydz$$

Following the same procedure along y and z, it is easy to find also the other two contributions:

$$\left(\frac{\partial \tau_{xy}}{\partial x} + \frac{\partial \tau_{yy}}{\partial y} + \frac{\partial \tau_{zy}}{\partial z} \right) dxdydz$$

$$\left(\frac{\partial \tau_{xz}}{\partial x} + \frac{\partial \tau_{yz}}{\partial y} + \frac{\partial \tau_{zz}}{\partial z} \right) dxdydz$$

Now it is possible to consider either the resultants of the volume and the surface forces and the result along x, y, z is:

$$\begin{cases} \delta F_x = \left(-\frac{\partial p}{\partial x} + \frac{\partial \tau_{xx}}{\partial x} + \frac{\partial \tau_{yx}}{\partial y} + \frac{\partial \tau_{zx}}{\partial z} + \rho f_x \right) dxdydz \\ \delta F_x = \left(-\frac{\partial p}{\partial y} + \frac{\partial \tau_{xy}}{\partial x} + \frac{\partial \tau_{yy}}{\partial y} + \frac{\partial \tau_{zy}}{\partial z} + \rho f_y \right) dxdydz \\ \delta F_x = \left(-\frac{\partial p}{\partial z} + \frac{\partial \tau_{xz}}{\partial x} + \frac{\partial \tau_{yz}}{\partial y} + \frac{\partial \tau_{zz}}{\partial z} + \rho f_z \right) dxdydz \end{cases}$$

Remembering that δF were also given by

$$\begin{cases} \delta F_x = \rho \frac{Du}{Dt} dxdydz \\ \delta F_y = \rho \frac{Dv}{Dt} dxdydz \\ \delta F_z = \rho \frac{Dw}{Dt} dxdydz \end{cases}$$

equalizing these two different ways of writing, the result is

$$\begin{cases} \rho \frac{Du}{Dt} = -\frac{\partial p}{\partial x} + \frac{\partial \tau_{xx}}{\partial x} + \frac{\partial \tau_{yx}}{\partial y} + \frac{\partial \tau_{zx}}{\partial z} + \rho f_x \\ \rho \frac{Dv}{Dt} = -\frac{\partial p}{\partial y} + \frac{\partial \tau_{xy}}{\partial x} + \frac{\partial \tau_{yy}}{\partial y} + \frac{\partial \tau_{zy}}{\partial z} + \rho f_y \\ \rho \frac{Dw}{Dt} = -\frac{\partial p}{\partial z} + \frac{\partial \tau_{xz}}{\partial x} + \frac{\partial \tau_{yz}}{\partial y} + \frac{\partial \tau_{zz}}{\partial z} + \rho f_z \end{cases}$$

This form is called differential (infinitesimal control volume) and non conservative (moving control volume).

2.3.1 Differential and conservative form

Once that the differential and non conservative form has been found, it is possible (as it was done for the mass balance equation) to pass to the differential and conservative form. In order to do that, it is considered x direction and the procedure will be the same along y and z. The first thing to do is remembering the definition of *Lagrangian derivative*:

$$\rho\frac{Du}{Dt} = \rho\frac{\partial u}{\partial t} + \rho\vec{v}\cdot\nabla u$$

Considering that

$$\frac{\partial(\rho u)}{\partial t} = \rho\frac{\partial u}{\partial t} + u\frac{\partial \rho}{\partial t}$$

it is possible to say that

$$\rho\frac{\partial u}{\partial t} = \frac{\partial(\rho u)}{\partial t} - u\frac{\partial \rho}{\partial t}$$

A similar procedure can also be applied to the second term of the right hand side:

$$\nabla\cdot(\rho u\vec{v}) = u\nabla\cdot(\rho\vec{v}) + \rho\vec{v}\cdot\nabla u \tag{2.9}$$

$$\rho\vec{v}\cdot\nabla u = \nabla\cdot(\rho u\vec{v}) - u\nabla\cdot(\rho\vec{v})$$

By replacing these two formulations inside the definition of the *Lagrangian derivative*:

$$\rho\frac{\partial u}{\partial t} + \rho\vec{v}\cdot\nabla u = \frac{\partial(\rho u)}{\partial t} - u\frac{\partial \rho}{\partial t} + \nabla\cdot(\rho u\vec{v}) - u\nabla\cdot(\rho\vec{v})$$

Collecting terms which have u:

$$\rho\frac{Du}{Dt} = \frac{\partial(\rho u)}{\partial t} + \nabla\cdot(\rho u\vec{v}) - u\left[\frac{\partial \rho}{\partial t} + \nabla\cdot(\rho\vec{v})\right]$$

the term $\frac{\partial \rho}{\partial t} + \nabla\cdot(\rho\vec{v})$ is equal to 0 following the mass balance equation and the left hand side is given by the momentum balance equation in the differential and non conservative form and it is equal to

$$\rho\frac{Du}{Dt} = -\frac{\partial p}{\partial x} + \frac{\partial \tau_{xx}}{\partial x} + \frac{\partial \tau_{yx}}{\partial y} + \frac{\partial \tau_{zx}}{\partial z} + \rho f_x$$

So, it is now possible to write

$$\frac{\partial(\rho u)}{\partial t} + \nabla\cdot(\rho u\vec{v}) = -\frac{\partial p}{\partial x} + \frac{\partial \tau_{xx}}{\partial x} + \frac{\partial \tau_{yx}}{\partial y} + \frac{\partial \tau_{zx}}{\partial z} + \rho f_x \tag{2.10}$$

Along y and z the result is analogous

$$\frac{\partial(\rho v)}{\partial t} + \nabla\cdot(\rho v\vec{v}) = -\frac{\partial p}{\partial y} + \frac{\partial \tau_{xy}}{\partial x} + \frac{\partial \tau_{yy}}{\partial y} + \frac{\partial \tau_{zy}}{\partial z} + \rho f_y \tag{2.11}$$

$$\frac{\partial(\rho w)}{\partial t} + \nabla\cdot(\rho w\vec{v}) = -\frac{\partial p}{\partial z} + \frac{\partial \tau_{xz}}{\partial x} + \frac{\partial \tau_{yz}}{\partial y} + \frac{\partial \tau_{zz}}{\partial z} + \rho f_z \tag{2.12}$$

These three equations represents the formulation of the momentum balance equation in a differential and conservative form.

Considering that τ_x ,τ_y and τ_z can be written as

$$\begin{cases} \tau_x = \tau_{xx}\vec{i} + \tau_{xy}\vec{j} + \tau_{xz}\vec{k} \\ \tau_y = \tau_{yx}\vec{i} + \tau_{yy}\vec{j} + \tau_{yz}\vec{k} \\ \tau_z = \tau_{zx}\vec{i} + \tau_{zy}\vec{j} + \tau_{zz}\vec{k} \end{cases}$$

it is also possible to write the momentum balance equation as

$$\begin{cases} \frac{\partial(\rho u)}{\partial t} + \nabla \cdot (\rho u \vec{v}) + \frac{\partial p}{\partial x} = \nabla \cdot \tau_x + \rho f_x \\ \frac{\partial(\rho v)}{\partial t} + \nabla \cdot (\rho v \vec{v}) + \frac{\partial p}{\partial y} = \nabla \cdot \tau_y + \rho f_y \\ \frac{\partial(\rho w)}{\partial t} + \nabla \cdot (\rho w \vec{v}) + \frac{\partial p}{\partial z} = \nabla \cdot \tau_z + \rho f_z \end{cases}$$

2.3.2 Integral and conservative form

It is possible to pass from the differential and conservative form to the integral and conservative. By applying the integral computed on the volume V to the conservative and differential form and by using *Gauss theorem*, it is possible to write:

$$\begin{aligned} \frac{\partial}{\partial t}\int_V \rho u dV + \int_S \rho u \vec{v} \cdot \vec{n} dS + \int_S p n_x dS &= \int_S \tau_x \cdot \vec{n} dS + \int_V \rho f_x dV \\ \frac{\partial}{\partial t}\int_V \rho v dV + \int_S \rho v \vec{v} \cdot \vec{n} dS + \int_S p n_y dS &= \int_S \tau_y \cdot \vec{n} dS + \int_V \rho f_y dV \\ \frac{\partial}{\partial t}\int_V \rho w dV + \int_S \rho w \vec{v} \cdot \vec{n} dS + \int_S p n_z dS &= \int_S \tau_z \cdot \vec{n} dS + \int_V \rho f_z dV \end{aligned} \tag{2.13}$$

It is important to underline that the pressure becomes the product of the pressure itself and the normal vector $\vec{n} = (n_x, n_y, n_z)$ because it is possible to see for example $\frac{\partial p}{\partial x}$ as

$$\frac{\partial p}{\partial x} = \nabla \cdot p\vec{i}$$

As a matter of fact, by applying the integral and the *Gauss theorem* is verified that

$$\int_V \nabla \cdot p\vec{i} dV = \int_S p\vec{i} \cdot \vec{n} dS = \int_S p n_x dS$$

Obviously, the integral and conservative form means exactly the same as the other forms, which is that the imbalance in time of momentum inside the finite control volume is balance by the momentum flux through the surface and by the forces which act on the volume and surface themselves.

2.3.3 Compact forms for momentum balance equations

It has been seen that the momentum balance equations are three (direction x,y,z), but it is possible to summarize them in one vector equation.

- Where there are the three different components of the velocity.
- Where there is the derivative of the pressure along one of the three Cartesian axis, it can be put ∇p, which is the gradient of the pressure.
- Where there is the vector of the net friction force, a matrix $\bar{\tau}$ can be put.
- Where there is the component of the volume force along x, y, z, a vector $\vec{f} = (f_x, f_y, f_z)$ can be put.

In this way it is possible to write the momentum balance equation in a conservative e differential form like:

$$\frac{\partial(\rho\vec{v})}{\partial t} + \nabla \cdot (\rho\vec{v}\vec{v}) + \nabla p - \nabla \cdot \bar{\tau} = \rho f \tag{2.14}$$

By integrating and using again the *Gauss theorem* it is possible to write the integral form which is

$$\frac{\partial}{\partial t}\int_v \rho\vec{v}dV + \int_S \rho\vec{v}\vec{v}\cdot\vec{n}dS + \int_S p\bar{\bar{I}}\cdot\vec{n}dS - \int_S \bar{\tau}\cdot\vec{n}dS = \int_V \rho\vec{f}dV \tag{2.15}$$

2.3.4 Frictional forces in a Newtonian fluid

It has been seen how in the momentum balance equation appears the frictional forces matrix $\bar{\tau}$. Considering that air is a Newtonian fluid, it is important to know what a Newtonian fluid is and how frictional forces can be written for a fluid like this.

First of all, a Newtonian fluid is a fluid where frictional forces are proportional to the gradients of the velocity of the fluid. As just said, considering that in aerodynamics air has this characteristic, the mathematical relation is given by

$$\tau_{i,j} = \delta_{i,j}\lambda\nabla\cdot\vec{v} + \mu\left(\frac{\partial u_i}{\partial x_j} + \frac{\partial u_j}{\partial x_i}\right) \tag{2.16}$$

where $\delta_{i,j}$ is known as *Kronecker delta* and it is equal to 1 if $i = j$, otherwise it is 0. This fact implies that only normal forces (for which $i = j$) has a sort of influence on the term which contains $\nabla \cdot \vec{v}$, whereas the tangential components only have the contribution to the viscosity. The coefficient λ is called *bulk viscosity* and plays a role when the volume expands, so it is linked to the divergence. In aerodynamics, it can be calculated from *Stokes' relation*

$$\lambda = -\frac{2}{3}\mu$$

where μ is the *dynamic viscosity*, which is a function of temperatures, but it can be considered constant if those are low.

2.4 Energy balance equation

In this section it will be shown how the energy balance equation can be derived. The energy balance equation is the last "law" which is necessary in order to model an aerodynamic problem. The physical principle that *energy is conserved*, is translated in math using the *first law of thermodynamics*, which states that in a closed system, total energy is conserved. This means that if it changes in time, there must be a net heat flux across the volume control and/or a certain work carried out by volume or surface forces. So, all these three contribution will be seen and then they will be put together in a scalar equation which is the energy balance equation. As it was done for the momentum balance equation, the reasoning will be developed considering the infinitesimal and moving control volume which is shown in the following picture.

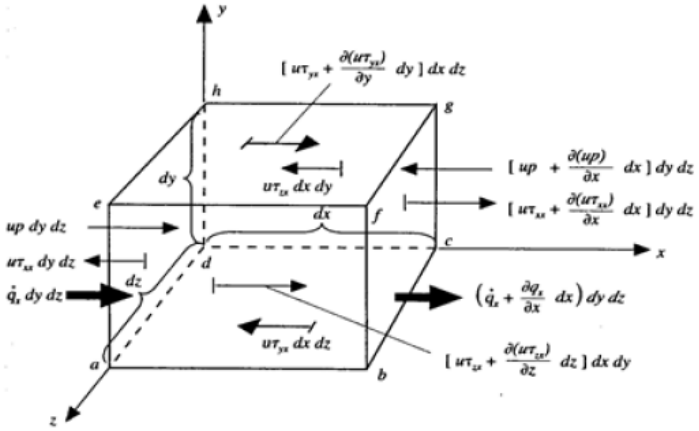

Figure 2.7: Infinitesimal and moving control volume[7]

Following, it will be shown how to write the contribution of work and net heat flux to the energy balance equation.

- Work done per unit time on the control volume by forces considering separately the contribution of the volumetric ones and the surface ones.

  - The work done by the volumetric forces can be calculated by considering that force is equal to the multiplication between mass and the force per unit of mass $\vec{f}$. This means that work per unit of time is equal to force times velocity. Considering all the contributions along the three different directions, it is possible to write:

$$\rho \vec{f} \cdot \vec{v} dx dy dz$$

  - The work done by the pressure can be similarly evaluated, by multiplying the force (which can be considered as pressure times surface) and the velocity. it is possible to initially focus on those forces which are directed along the x-axis. On the left and the right sides of the control volume, the work done by pressure forces is:

$$\left[up + \left(up + \frac{\partial (up)}{\partial x} dx \right) \right] dydz = -\frac{\partial (up)}{\partial x} dxdydz$$

Along y-axis and z-axis it can be similarly written that:

$$\left[vp + \left(vp + \frac{\partial(vp)}{\partial y}dy\right)\right] dxdz = -\frac{\partial(vp)}{\partial y}dxdydz$$

$$\left[wp + \left(wp + \frac{\partial(wp)}{\partial z}dz\right)\right] dxdy = -\frac{\partial(wp)}{\partial z}dxdydz$$

By adding these three results, it is possible to evaluate the contribution to the work by the pressure:

$$\left[-\frac{\partial(up)}{\partial x}dxdydz - \frac{\partial(vp)}{\partial y}dxdydz - \frac{\partial(wp)}{\partial z}dxdydz\right]$$

- The same reasoning can be made with the friction forces. Differently from pressure forces (whose normal vector is directed towards the inside of the control volume), friction forces contribution is positive when the direction points outwards the volume, so their net contribution is considered positive. Along x-axis, it is possible to write:

$$\left[\left(u\tau_{xx} + \frac{\partial(u\tau_{xx})}{\partial x}dx\right) - u\tau_{xx}\right] dydz = \frac{\partial(u\tau_{xx})}{\partial x}dxdydz$$

By keeping into account the other faces also, the total work done by surface forces on the surface of the control volume in the x-direction is

$$\left[\frac{\partial(u\tau_{xx})}{\partial x} + \frac{\partial(u\tau_{yx})}{\partial y} + \frac{\partial(u\tau_{zx})}{\partial z}\right] dxdydz$$

By making the same reasoning also along y-direction and z-direction, it is possible to write:

$$\left[\frac{\partial(v\tau_{xy})}{\partial x} + \frac{\partial(v\tau_{yy})}{\partial y} + \frac{\partial(v\tau_{zy})}{\partial z}\right] dxdydz$$

$$\left[\frac{\partial(w\tau_{xz})}{\partial x} + \frac{\partial(w\tau_{yz})}{\partial y} + \frac{\partial(w\tau_{zz})}{\partial z}\right] dxdydz$$

It is now possible to put all together by summing the contributions of the pressure, the friction forces and the volumetric forces along all three directions. The result is the work per unit of time done by forces and can be written as

$$\left[-\frac{\partial(up)}{\partial x} - \frac{\partial(vp)}{\partial y} - \frac{\partial(wp)}{\partial z}\right] dxdydz+$$

$$+\left[\frac{\partial(u\tau_{xx})}{\partial x} + \frac{\partial(u\tau_{yx})}{\partial y} + \frac{\partial(u\tau_{zx})}{\partial z} + \frac{\partial(v\tau_{xy})}{\partial x} + \frac{\partial(v\tau_{yy})}{\partial y} + \frac{\partial(v\tau_{zy})}{\partial z}\right] dxdydz+$$

$$+\left[\frac{\partial(w\tau_{xz})}{\partial x} + \frac{\partial(w\tau_{yz})}{\partial y} + \frac{\partial(w\tau_{zz})}{\partial z}\right] dxdydz + \rho\vec{f}\cdot\vec{v}dxdydz$$

This equation can also be written as:

$$\left[-\nabla \cdot (\rho \vec{v}) + \nabla \cdot (\bar{\tau} \cdot \vec{v}) + \rho \vec{f} \cdot \vec{v}\right] dxdydz$$

- The other contribution to the energy balance equation is given by the net heat flux. It can be split into two different parts:

  - **Volumetric heating**: one example is represented by radiation absorption or emission. It can be expressed as the product between the infinitesimal mass and a certain quantity of heat absorbed per unit time and unit mass. Its contribution can be written as

    $$\rho \dot{\xi} dxdydz$$

    Usually, in aerodynamics, this contribution is not really important in terms of value.

  - **Thermal conduction**: if there is a thermal conduction, it means that there is a certain net flux which crosses every face of the infinitesimal control volume. This flux is due to the diffusion of the kinetic energy of every particle, caused by the presence of a temperature gradient.
    Considering the net heat flux in the x-direction:

    $$\left[\dot{q}_x - \left(\dot{q}_x + \frac{\partial \dot{q}_x}{\partial x} dx\right)\right] dydz = -\frac{\partial \dot{q}_x}{\partial x} dxdydz$$

    Using the same approach along y-direction and z-direction:

    $$\left[\dot{q}_y - \left(\dot{q}_y + \frac{\partial \dot{q}_y}{\partial y} dy\right)\right] dxdz = -\frac{\partial \dot{q}_y}{\partial y} dxdydz$$

    $$\left[\dot{q}_z - \left(\dot{q}_z + \frac{\partial \dot{q}_z}{\partial z} dz\right)\right] dxdy = -\frac{\partial \dot{q}_z}{\partial z} dxdydz$$

    By summing these three contributions, it is possible to evaluate the net heat flux towards the control volume due to heat conduction as:

    $$-\left(\frac{\partial \dot{q}_x}{\partial x} + \frac{\partial \dot{q}_y}{\partial y} + \frac{\partial \dot{q}_z}{\partial z}\right) = -\nabla \cdot \dot{\vec{q}} dxdydz$$

    Now it is possible to express the net heat flux along the three directions using the *Fourier Law*, which links the flux itself to the temperature gradient:

    $$\dot{\vec{q}} = -k \nabla T$$

    Which can also be written separately for the three directions:

    $$\dot{q}_x = -k \frac{\partial T}{\partial x}$$

    $$\dot{q}_y = -k \frac{\partial T}{\partial y}$$

$$\dot{q}_z = -k\frac{\partial T}{\partial z}$$

Where k is a coefficient which depends on the temperature and the type of gas. It takes into account the energy transport (analogously to the dynamic viscosity which considers the transport of momentum). It can be seen that there is a minus sign in the expression: as a matter of fact, the gradient is positive when temperature increases and it is known that the flux moves from areas with higher temperatures to the ones with lower ones.

It is now possible to write the net heat flux towards the control volume as

$$(\rho\dot{\xi} - \nabla\dot{q})dxdydz = \left[\rho\dot{\xi} + \frac{\partial}{\partial x}\left(k\frac{\partial T}{\partial x}\right) + \frac{\partial}{\partial y}\left(k\frac{\partial T}{\partial y}\right) + \frac{\partial}{\partial z}\left(k\frac{\partial T}{\partial z}\right)\right]$$

- Lastly, it must be considered also the rate of change of total energy in the control volume. First of all, it is important to define what the total energy is: it represents the sum of every type of energy of the fluid. In this case the two types of energy which belong to the flux are the internal energy and the kinetic energy (gravitational potential energy is not considered as it has been taken into account in the work done by volumetric forces).

  - **Internal energy**: it considers the chaotic motion of the molecules (so it is present even if the velocity is equal to zero on average, which is steady state), due to translation, rotation, vibration.

  - **Kinetic energy**: it takes into account the statistic average speed of the particles, which is the motion of the whole fluid.

  Considering this breakdown, the total energy can be written as

$$e + \frac{1}{2}|\vec{v}|^2$$

  Where e represents the internal energy, whereas the second term is the kinetic energy. Considering that it is being studied a moving control volume, it is possible to write the Lagrangian variation in time of the total energy:

$$\rho\frac{D}{Dt}\left(e + \frac{1}{2}|\vec{v}|^2\right)dxdydz$$

  where it is possible to note that ρ is outside the operator of derivative because it is considered constant.

Now that every contribution has been explicitly written, it is possible to equal the rate of change of total energy in control volume with the sum of volumetric heating, conduction heat flux and work done per unit time on the control volume by volumetric and surface forces:

$$\rho\frac{D}{Dt}\left(e+\frac{1}{2}\rho|\vec{v}|^2\right)=\rho\dot{\xi}+\nabla\cdot(k\nabla T)-\nabla\cdot(p\vec{v})+\nabla\cdot(\bar{\tau}\cdot\vec{v})+\rho\vec{f}\cdot\vec{v} \tag{2.17}$$

The equation which has just been written represents the energy balance equation in differential and non-conservative form.

As it has been done for the other balance equations, it is possible to pass to the conservative form as it follows. First of all, it is possible to manipulate the Lagrangian derivative:

$$\rho\frac{D\left(e+\frac{1}{2}|\vec{v}|^2\right)}{Dt}=\rho\frac{\partial\left(e+\frac{1}{2}|\vec{v}|^2\right)}{\partial t}+\rho\vec{v}\cdot\nabla\left(e+\frac{1}{2}|\vec{v}|^2\right)$$

Considering that the mass balance equation is equal to zero, it is possible to multiply it by total energy per unit of mass:

$$\rho\frac{D\left(e+\frac{1}{2}|\vec{v}|^2\right)}{Dt}=\rho\frac{\partial\left(e+\frac{1}{2}|\vec{v}|^2\right)}{\partial t}+\rho\vec{v}\cdot\nabla\left(e+\frac{1}{2}|\vec{v}|^2\right)+\left(e+\frac{1}{2}|\vec{v}|^2\right)\left[\frac{\partial\rho}{\partial t}+\nabla\cdot(\rho\vec{v})\right]=$$

$$=\rho\frac{\partial\left(e+\frac{1}{2}|\vec{v}|^2\right)}{\partial t}+\left(e+\frac{1}{2}|\vec{v}|^2\right)\frac{\partial\rho}{\partial t}+\rho\vec{v}\cdot\nabla\left(e+\frac{1}{2}|\vec{v}|^2\right)+\left(e+\frac{1}{2}|\vec{v}|^2\right)\nabla\cdot(\rho\vec{v})=$$

$$\frac{\partial\left[\rho\left(e+\frac{1}{2}|\vec{v}|^2\right)\right]}{\partial t}+\nabla\cdot\left[\rho\left(e+\frac{1}{2}|\vec{v}|^2\right)\vec{v}\right]$$

It is possible to indicate with E the total energy per unit volume:

$$E=\rho\left(e+\frac{1}{2}|\vec{v}|^2\right)$$

and consequently:

$$\rho\frac{D\left(e+\frac{1}{2}|\vec{v}|^2\right)}{Dt}=\frac{\partial E}{\partial t}+\nabla\cdot(E\vec{v})$$

By substituting it into the *Equation 2.17*, the differential and conservative form is obtained:

$$\frac{\partial E}{\partial t}+\nabla\cdot(E\vec{v})=\rho\dot{\xi}-\nabla\cdot\dot{\vec{q}}-\nabla\cdot(p\vec{v})+\nabla\cdot(\bar{\tau}\cdot\vec{v})+\rho\vec{f}\cdot\vec{v} \tag{2.18}$$

or

$$\frac{\partial E}{\partial t}+\nabla\cdot[(E+p)\vec{v}]=\rho\dot{\xi}-\nabla\cdot\dot{\vec{q}}+\nabla\cdot(\bar{\tau}\cdot\vec{v})+\rho\vec{f}\cdot\vec{v} \tag{2.19}$$

By integrating the e differential conservative equation over a finite volume and by using the Gauss' Theorem, it is possible to obtain the integral conservative form:

$$\int_V\frac{\partial E}{\partial t}dV+\int_V\nabla\cdot[(E+p)\vec{v}]\,dV-\int_V\nabla\cdot(\bar{\tau}\cdot\vec{v})dV+\int_V\nabla\cdot\dot{\vec{q}}dV=\int_V\rho\dot{\xi}dV+\int_V\rho\vec{f}\cdot\vec{v}dV \tag{2.20}$$

Which can also be written as

$$\int_V\frac{\partial E}{\partial t}dV+\int_S(E+p)\vec{v}\cdot\vec{n}dS-\int_S(\bar{\tau}\cdot\vec{v})\cdot\vec{n}dS+\int_S\dot{\vec{q}}\cdot\vec{n}dS=\int_V\rho\dot{\xi}dV+\int_V\rho\vec{f}\cdot\vec{v}dV \tag{2.21}$$

2.5 Notes on governing equations of fluid dynamics

It is important to note that the knowledge of the balance equations gives a total of five equations of fluid dynamics: one for the conservation of the mass, three for the momentum balance and one for the conservation of energy. By counting the unknowns which are present in the equation, it is possible to notice that there are seven of them (ρ, u, v, w, p, e, t). In order to close the system, two additional equations are needed.
In typical aerodynamics application, the two following equations are used:

- **Perfect gas law**: the assumption is that the gas behaves as a perfect gas:

$$p = \rho \frac{R}{M} T = \rho R^* T \tag{2.22}$$

- The last equation is given by a mathematical relation which links the thermodynamics variables, such as

$$e = e(T, P)$$

  For a perfect gas the specific heats are constant, so that the seventh equation is:

$$e = c_v T \tag{2.23}$$

  where c_v is the specific heat at constant volume.

So now there are 7 equations and 7 unknowns; this system is non-linear of partial differential equations. They are not easy to solve and, at this time, a general solution in closed form does not exist. For this reason, it is important to find a way to numerically solve them.

2.6 Statistical description of turbulence

The complexity of describing a turbulent flow lays on the way to develop a theory which can represent the complex motion of the fluid (as a matter of facts, it is three-dimensional, unsteady, many different scales.
Eddies, which as said in *Chapter 1* are irregular regions of the fluid, behave in a stochastic way, either in space and in time. For this reason, it is necessary to introduce a statistical description of the phenomena. The theory which describes the properties of the turbulent motion variables is known as *statistical theory of turbulence*.
If $u(x,t)$ is a stochastic variable, it is possible to define N values of the variable u. It is possible to define the ensemble average, written as the arithmetic average of the N data[4]:

$$\bar{u}(x,t) \equiv \frac{1}{N} \sum_{n=1}^{N} u(x,t;n)$$

If $N \to \infty$, the ensemble average is the expected value. This mean operation has the effect to remove the random fluctuations.
As long as the stochastic variable u can be considered independent in time, that is $\bar{u}(x)$, the

ensemble average can be obtained by using data of the variable u collected in different moments. By using the definition of ensemble average:

$$\bar{u}(x) = \frac{1}{N}\sum_{n=1}^{N} u(x,t;n) = \frac{1}{N}\sum_{n=1}^{N}\int_{t_0+(n-1)\Delta t}^{t_0+n\Delta t} u(x,t)\frac{dt}{\Delta t}$$

where the integral represents a single realization. If $t = N\Delta T$, the time average is obtained:

$$\bar{u}(x) = \frac{1}{T}\int_{t_0}^{t+T} u(x,t)dt \tag{2.24}$$

where T is the sampling interval and it must be $T \to \infty$, so that it is sufficiently bigger than the characteristic time of the oscillation.

The average operator indicated in the *Equation 2.24* is linear and the following properties (where u and v are two stochastic variables statistically stationary) can be obtained [4]:

$$\begin{cases} \overline{u \pm v} = \bar{u} + \bar{v}, \\ \overline{ku} = k\bar{u}\ (k = constant), \\ \bar{\bar{u}} = \bar{u}, \\ \overline{u - \bar{u}} = \bar{u} - \bar{\bar{u}} = 0 \end{cases}$$

but

$$\overline{u\bar{v}} \neq \bar{u}\bar{v}$$

2.7 Reynolds decomposition

Reynolds decomposition was introduced for the first time in 1985 [10]. It is a mathematical technique used indicate the instant value of a quantity as a sum of a mean quantity and a fluctuation. If the Cartesian components (2D) are considered, it can be written that

$$u_i(\vec{x},t) = U_i(\vec{x}) + u_i'(\vec{x},t) \tag{2.25}$$

Where $U_i(\vec{x})$ is the mean quantity and $u_i'(\vec{x},t)$ is the fluctuation.

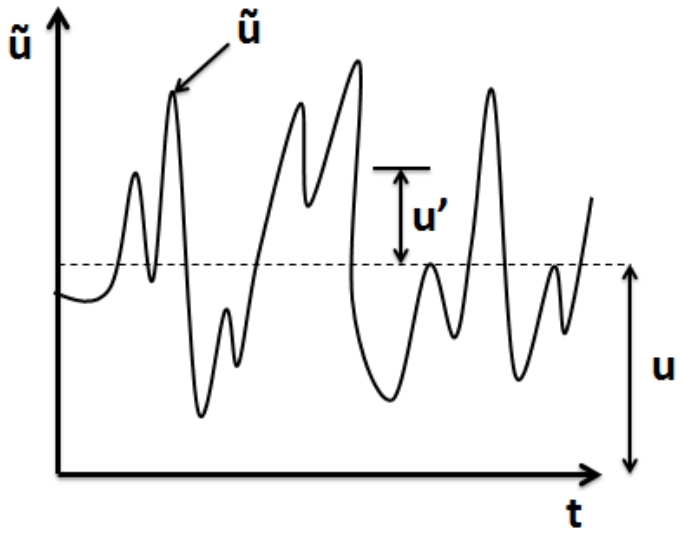

Figure 2.8: Diagram of the Reynolds Decomposition [14]

$U_i(\bar{x})$ is considered equal to

$$U_i(\vec{x}) \equiv \bar{u_i}(x) = \frac{1}{T}\int_{t_0}^{t_0+T} u_i(\vec{x},t)dt$$

and it is the average stationary field , whereas the fluctuation $u_i'(\vec{x},t)$ are defined as

$$u_i'(\vec{x},t) \equiv u_i(\vec{x},t) - U_i(\vec{x})$$

By using the definition of mean value and by using the properties of the average operator indicated in the *Section 2.6*, it is possible to say

$$\bar{U_i}(\vec{x}) = U_i(\vec{x})$$

$$\bar{u_i'} = \frac{1}{T}\int_{t_0}^{t_0+T} \left[u_i(\vec{x},t) - U_i(\vec{x})\right] dt = U_i(\vec{x}) - \bar{U_i}(\vec{x}) = 0$$

The same approach can be done also with the other variables which appears in the Navier-Stokes equations, so it is possible to write:

$$p(\vec{x},t) = P(\vec{x}) + p'(\vec{x},t)$$

$$T(\vec{x},t) = \Theta(\vec{x}) + T'(\vec{x},t)$$

2.8 Reynolds-Averaged Navier-Stokes (RANS)

Firstly, it is important to remember how continuity and momentum equations can be written in Cartesian coordinates:

$$\begin{cases} \frac{\partial u_i}{\partial x_i} = 0 \\ \rho\frac{\partial u_i}{\partial t} + \rho\frac{\partial u_i u_j}{\partial x_j} = -\frac{\partial p}{\partial x_i} + \mu\frac{\partial^2 u_i}{\partial x_j^2} \end{cases}$$

It is possible to average the continuity equation and below it is shown what it is obtained:

$$\frac{\partial \bar{u}_i}{\partial x_i} = \frac{\partial \bar{u}_i}{\partial x_i} = \frac{\partial}{\partial x_i}\left(U_i + \bar{u_i'}\right) = 0$$

Considering that U_i is a constant, the continuity equation can be resumed in these two equations:

$$\frac{\partial U_i}{\partial x_i} = 0 \tag{2.26}$$

$$\frac{\partial \bar{u_i'}}{\partial x_i} = 0 \tag{2.27}$$

It is possible to follow the same procedure also for the momentum equation. The three components which are derived by x can be analyzed as it follows:

$$\frac{\partial}{\partial x_j}(\overline{u_i u_j}) = \frac{\partial}{\partial x_j}\overline{\left[(U_i + u_i')(U_j + u_j')\right]} = \frac{\partial}{\partial x_j}\left(U_i U_j + \overline{u_i' u_j'}\right)$$

$$\frac{\partial \bar{p}}{\partial x_i} = \frac{\partial P}{\partial x_i}$$

$$\frac{\partial^2 \bar{u}_i}{\partial x_j} = \frac{\partial^2 U_i}{\partial x_j^2}$$

So, it is possible to write the momentum equation for the mean motion as:

$$\rho\frac{\partial}{\partial x_j}(U_i U_j) = -\frac{\partial P}{\partial x_i} + \mu\frac{\partial^2 U_i}{\partial x_j^2} - \rho\frac{\partial}{\partial x_j}\left(\overline{u_i' u_j'}\right)$$

which can also be written as

$$\rho U_j\frac{\partial U_i}{\partial x_j} = -\frac{\partial P}{\partial x_i} + \frac{\partial}{\partial x_j}\left(\tau_{ij} - \rho\overline{u_i' u_j'}\right) \tag{2.28}$$

where τ_{ij} represents the viscous stress connected to the mean motion of the fluid. It can be written as:

$$\tau_{ij} = \mu\left(\frac{\partial U_i}{\partial x_j} + \frac{\partial U_i}{\partial x_j}\right) \tag{2.29}$$

The *Equation 2.26* and the *Equation 2.28* are called *Reynolds-Averaged Navier-Stokes equations*, which rule the mean motion of the fluid. They are formally equal to Navier-Stokes equation, except for the term $R_{ij}(\vec{x}, t) = -\rho\overline{u_i' u_j'}$. This term is called *Reynolds stress tensor* and it takes into account the effects of fluctuations over the mean motion and every term R_{ij} represents the mean turbulent stress. It is possible to explicitly write the tensor:

$$\rho\overline{u_i' u_j'} = \rho\begin{bmatrix} \overline{u_i' u_i'} & \overline{u_i' u_j'} & \overline{u_i' u_k'} \\ \overline{u_j' u_i'} & \overline{u_j' u_j'} & \overline{u_j' u_k'} \\ \overline{u_k' u_i'} & \overline{u_k' u_j'} & \overline{u_k' u_k'} \end{bmatrix}$$

Considering the correlation

$$\overline{u_i' u_j'} = \overline{u_j' u_i'}$$

among these nine components of the tensor, only six of them are independent of each other. Another important thing is that the tensor is symmetric. Components on the diagonal ($i = j$) are the normal stress which contributes to increase the mean pressure, whereas the others ($i \neq j$) represent the shear stresses.

By proceeding in the same way using the energy equation (by using the Reynolds decomposition) and neglecting the term Φ, it can be obtained the following expression:

$$\rho e \left\{ \frac{\partial}{\partial t}(\Theta + T') + \frac{\partial}{\partial x_i}[(U + u_i') + (\Theta + T')] \right\} = \kappa \frac{\partial^2}{\partial x_i}(\Theta + T')$$

By averaging the previous equation:

$$\rho c U_i \frac{\partial \Theta}{\partial x_i} = \frac{\partial}{\partial x_i} \left(\kappa \frac{\partial \Theta}{\partial x_i} - \rho c \overline{u_i' T'} \right) \tag{2.30}$$

Where $\rho c \overline{u_i' T'}$ represent the contribution of the turbulent fluctuations to the heat flux.

As said few lines above, the appearance of the *Reynolds Stress Tensor* introduces three additional terms which are not known. For this reason, in order to close the system, six additional equations are needed. In order to provide the closure of the system, Boussinesq hypothesis is introduced.

2.9 Boussinesq hypothesis

As said in the previous section, by introducing fluctuations using *Reynolds decomposition*, there is the problem of closing the system. In order to do that, *Boussinesq hypothesis* is introduced. It assumes that momentum transport in turbulent flows is mainly due to the biggest and most energetic eddies. Boussinesq stated that the Reynolds stress tensor is proportional to the mean strain rate tensor, multiplied by a constant, which is called *turbulent eddy viscosity* μ_t. The Boussinesq hypothesis simplifies the process of turbulence modeling by shifting the focus from calculating the six turbulent stresses in the RANS model to identifying a suitable value for the turbulent eddy viscosity. This hypothesis (or assumption) straightforwardly asserts that, akin to fluid viscosity in laminar flows, a flow-dependent turbulent viscosity can be incorporated alongside molecular agitation to depict turbulent mixing or diffusion ($\tau_{total} = (\mu + \mu_t)\nabla \bar{u}$). It is a rough and imperfect approximation of the actual physics, but it has been shown to be accurate when adhering to good standard practices.

By applying Boussinesq hypothesis to an incompressible flow modelled with RANS, it is possible to write Reynolds stress tensor as

$$R_{ij}(\vec{x}, t) = -\rho \overline{u_i' u_j'} = 2\mu_t \overline{S_{ij}} - \frac{2}{3}\rho k \delta_{ij} \tag{2.31}$$

Where $\overline{S_{ij}}$ is the *Reynolds-averaged shear stress tensor* which can be considered equal to

$$\overline{S_{ij}} = \frac{1}{2} \left(\frac{\partial \bar{u}_i}{\partial x_j} + \frac{\partial \bar{u}_j}{\partial x_i} \right)$$

The variable k represents the turbulent kinetic energy:

$$K = \frac{1}{2}\overline{u_i' u_j'}$$

δ_{ij} is the Kronecker delta and is define as follows:

$$\delta_{ij} = \begin{cases} 1 \;\; if \;\; i = j \\ 0 \;\; otherwise \end{cases}$$

In expand form, the Boussinesq hypothesis can be written as:

$$R_{ij}(\vec{x}, t) = -\rho\overline{u_i' u_j'} = \begin{bmatrix} 2\mu_t S_{11} - \frac{2}{3}k & 2\mu_t S_{12} & 2\mu_t S_{13} \\ 2\mu_t S_{21} & 2\mu_t S_{22} - \frac{2}{3}k & 2\mu_t S_{23} \\ 2\mu_t S_{31} & 2\mu_t S_{32} & 2\mu_t S_{33} - \frac{2}{3}k \end{bmatrix}$$

By using the *Reynolds decomposition*, it is possible to express the *dynamic viscosity coefficient* as a sum of a laminar and a turbulent component:

$$\mu = \mu_L + \mu_t \tag{2.32}$$

The use of Reynolds-averaged equations and the inclusion of turbulent dynamic viscosity term, form the basis of turbulence models with first-order closure commonly employed for turbulent flow simulations. However, this approach proves to be limited for certain flow types, excluding cases such as flows with significant streamlines curvature, flows characterized by stratification and rotation, secondary flows in ducts, flows with boundary layer separation and reattachment and flows featuring abrupt changes in mean strain rate.
In order to address this issue, various corrections are introduced within different turbulence models. Additionally, to achieve the same goal, it is possible to switch to a non-linear treatment of eddy viscosity by introducing higher-order terms for the strain and rotation tensors.

2.10 Non-dimesional quantities and wall treatment for turbulence

Before digging deeper into the models used to approximate the *Reynolds stress tensor*, it is important to have a look to the non-dimensional quantities used and how the problem is analyzed near the wall.

The Reynolds number is the predominant non-dimensional quantity employed in turbulence modeling, representing the balance between inertial and viscous forces. Within the realm of turbulence modeling, the following parameters are some of the most important:

- Wall-distance Reynolds Number:

$$Re_d = \frac{\sqrt{k}d}{\nu}$$

  where k is the turbulent kinetic energy, d is the distance from the wall and ν is the kinematic viscosity.

- Turbulent Reynolds Number:

$$Re_t = \frac{k^2}{\nu\epsilon}$$

or

$$Re_t = \frac{k}{\nu\omega}$$

where ϵ is the turbulent dissipation rate and ω is the specific dissipation rate.

Talking about the wall treatment, it is important to say that walls introduce vorticity in the majority of practical flow scenarios. Hence, providing a precise forecast of the boundary layer flow near the wall is imperative. In the field of fluid mechanics, the wall boundary layer pertains to the slender region close to a surface where viscosity has a notable influence. Within this layer, flow velocity transitions from zero at the surface to the free stream velocity further away. The standard thickness of the boundary layer is determined as the distance perpendicular to the wall, at which the velocity reaches 99% of the free stream velocity. Beyond this juncture, the impact of viscous stresses becomes negligible.
The flow within the boundary layer can exhibit two states: laminar or turbulent, contingent upon the Reynolds number of the flow. At low Reynolds numbers, the boundary layer remains laminar, featuring a gradual, uniform alteration of streamwise velocity away from the surface. Conversely, at high Reynolds numbers, the boundary layer becomes turbulent, displaying fluctuating swirling currents within its confines.
It is possible to define some characteristic variables of the turbulent boundary layer:

$$u_\tau = \frac{\tau_w}{\rho}$$

where τ_w represents the viscous stresses on the wall and ρ is the density.

$$l_\tau = \frac{\nu}{u_\tau}$$

where ν is the kinematic viscosity.

By using these two parameters it is possible to evaluate some wall functions which are essential to characterize the turbulent boundary layer:

$$y^+ = \frac{y\rho u_\tau}{\mu} \tag{2.33}$$

which is the non-dimensional distance from the wall and the parameters which appear in the relation are the usual known.

$$u^+ = \frac{u}{u_\tau} \tag{2.34}$$

which is the non-dimensional wall-tangential component u of the velocity vector.

The following diagram shows the velocity profile of a turbulent boundary layer:

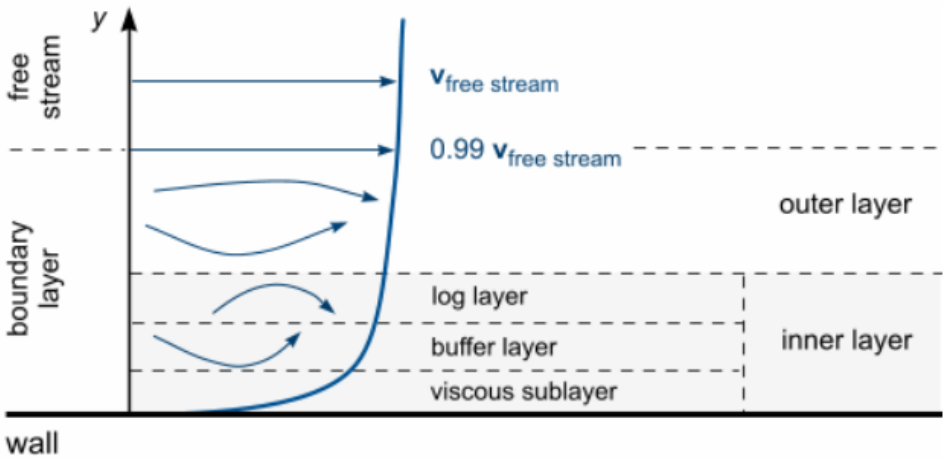

Figure 2.9: Velocity profile of a turbulent boundary layer [16]

As it is shown from the previous picture, turbulent boundary layer has a multilayer structure which may be divided as it follows:

- **Viscous sublayer**: Near the wall, there is the viscous sublayer, where viscous forces dominate, and the velocity profile $u(y)$ is approximately linear. In this part of the boundary layer, it is true that [1]:

$$y^+ = u^+ \quad 5 \leq y^+$$

- **Buffer layer**: Following the viscous sublayer is a transitional region called the buffer layer, which extends to the logarithmic region where the velocity profile, in terms of wall variables, follows a logarithmic law.
  In the viscous sublayer, there is a heightened level of turbulent activity, which contributes to the generation of turbulent kinetic energy.

- **Log layer**: In this region, the average velocity profile is characterized by a logarithmic law of the type [1]:

$$u^+ = \frac{1}{k} ln(y^+) + C \quad 30 \leq y^+ \leq 500 - 1000$$

  where $k = 0.41$ is Von Karman's constant and $C = 5.1$ is Cole's constant.

After having introduced some important wall function, it is possible to discuss the wall treatment, since the use of turbulence models requires the imposition of boundary conditions at the walls and the imposition of specific turbulence values on the centroids of the near-wall cells.

For the turbulence models in Simcenter STAR-CCM+, the following approaches of accounting for turbulent wall boundary layers are available [16]:

- *High-y^+*: The high-y^+ wall treatment mirrors the conventional wall-function methodology. This method employs algebraic relationships derived from the presumed distribution of velocity, temperature, and turbulence properties within the boundary layer. These relations furnish boundary conditions when the centroid of a cell near the wall is situated within the logarithmic layer of the boundary layer. The effectiveness of the wall-function approach hinges on how closely the assumptions and estimations encapsulated in the functions align with the actual conditions of the application. While many standard wall functions are designed for equilibrium conditions, Simcenter STAR-CCM+ broadens their scope to encompass non-equilibrium effects.

- *Low-y^+*: Typically, the low-y^+ wall treatment aligns with the conventional low Reynolds number approach. This involves using a finely layered mesh to resolve the boundary layer, with no additional modeling required beyond assuming laminar flow in the near-wall cells.

- *All-y^+*: The all-y^+ wall treatment employs the use of blended wall functions and offers accurate boundary conditions for flow, energy, and turbulence properties across a broad spectrum of near-wall mesh densities.

- *Two-layer all y^+*: The two-layer all y^+ wall treatment, accessible for the two-layer turbulence models, follows the same methodology as the all-y^+ wall treatment. Nevertheless, it introduces specific values for turbulence dissipation rates at the centroids of near-wall cells to ensure consistency with the two-layer formulation of the underlying turbulence model.

2.11 Turbulence models

There are different turbulence models which can provide a closure of the system and everyone is more suitable than the others for particular conditions. So, it is really important to understand when a model is *better* than the others in order to have a solution which is as precise as possible.
As said in the previous section, turbulence models are essentially used to approximate *Reynolds stress tensor* in the RANS equations. In particular, turbulence models with first-order closure are used to compute *eddy viscosity* μ_t, because they use Boussinesq hypothesis.

2.11.1 Spalart-Allmaras model

Spalart-Allmaras model is a one-equation model which solves transport equation for the variable $\tilde{\nu}$, which is linked to eddy viscosity through the density and it is called *modified diffusivity*. This approach differs from many early one-equation models, which solved an equation for turbulent kinetic energy transport and relied on an algebraic specification of a length scale [17].
The model is based on empirical data and dimensional analysis, allowing for accurate results in describing the flow field, even in the presence of adverse pressure gradients or during a gradual

transition from laminar to turbulent flow. However, it is essential to specify in advance the point at which this transition will occur. The Spalart-Allmaras model, like the other models that will be discussed later, can be applied to both structured and unstructured grids, with the advantage of not requiring a particularly refined grid near the walls. Furthermore, the model is a local model, meaning that the solution at one point is not influenced by that at other points in the computational domain.
As for the initial conditions, the initial value of $\tilde{\nu}$ must be set and it usually is considered equal to $\tilde{\nu} = 0.1$ [17]. As for the boundary conditions, it is required to set the value of $\tilde{\nu}$ on the inlet wall, whereas on the outlet wall, it is computed. It is possible to set $\tilde{\nu} = 0$ on the solid walls [17], which corresponds with $\mu_t = 0$.

The Spalart-Allmaras model, in its standard form, operates as a low-Reynolds number model, indicating its application without the use of wall functions. As per the model's formulation, it allows for the precise resolution of the complete turbulent boundary layer, encompassing the viscous sublayer. This renders the model suitable for application on finely discretized grids (small values of $y+$) [16]. Using this approach, it is possible to represent the turbulent eddy viscosity μ_t as:

$$\mu_t = \rho f_{v1} \tilde{\nu}$$

where ρ is the density and f_{v1} is a damping function.

The equation of the transport for the modified diffusivity $\tilde{\nu}$ can be written as:

$$\frac{\partial}{\partial t}(\rho\tilde{\nu}) + \nabla \cdot (\rho\vec{\bar{v}}\tilde{\nu}) = \frac{1}{\sigma_{\tilde{\nu}}}\nabla \cdot [(\mu + \rho\tilde{\nu})\nabla\tilde{\nu}] + P_{\tilde{\nu}} + S_{\tilde{\nu}} \tag{2.35}$$

where

- $\vec{\bar{v}}$ is the mean velocity;
- $\sigma_{\tilde{\nu}}$ is a Model Coefficient which can be considered equal to $\frac{2}{3}$ [16];
- μ is the dynamic viscosity;
- $P_{\tilde{\nu}}$ is the Production Term which can be written as shown below:

$$P_{\tilde{\nu}} = D_{\tilde{\nu}} + G_{\tilde{\nu}} + G_{nl} - \Upsilon_{\tilde{\nu}}$$

where the contributions to the productive term are:

- $D_{\tilde{\nu}}$ is called *Non-conservative diffusion*:

$$D_{\tilde{\nu}} = \frac{C_{b2}}{\sigma_{\tilde{\nu}}}\rho(\nabla\tilde{\nu} \cdot \nabla\tilde{\nu})$$

where C_{b2} is a model coefficient and it is equal to 0.622.

- $G_{\tilde{\nu}}$ takes into account the turbulent production and can be expressed as:

$$G_{\tilde{\nu}} = \rho(1 - f_{t2})C_{b1}f_{r1}\tilde{S}\tilde{\nu}$$

where f_{t2} is a damping function (which is a function which mimics the decrease of the turbulent mixing near the walls) and can be written as:

$$f_{t2} = 1.1e^{-2\chi^2}$$

with $\chi = \frac{\tilde{\nu}}{\nu}$
C_{b2} is a model coefficient and it is equal to 0.1355; f_{r1} is a rotation function; $\tilde{S}$ is the deformation parameter which is calculated as:

$$\tilde{S} = \widehat{S} + \frac{\tilde{\nu}}{\kappa^2 d^2} f_{v2}$$

where f_{v2} is a damping function which depends on χ, κ is a model coefficient, d is the distance from the wall and $\widehat{S}$ of the magnitude of the vorticity;

- G_{nl} is a non-linear production;

- $\Upsilon_{\tilde{\nu}}$ which is a turbulent dissipation and can be written as:

$$\rho\left(C_{w1}f_w - \frac{C_{b1}}{\kappa^2}f_{t2}\right)\left(\frac{\tilde{nu}}{d}\right)^2$$

where C_{w1}, f_w, C_{b1} f_{t2} are typical constant of the model.

2.11.2 $\kappa - \epsilon$ model

The K-Epsilon turbulence model is a two-equation formulation that addresses the transport of turbulent kinetic energy κ and turbulent dissipation rate ϵ, which are essential in calculating turbulent eddy viscosity.

Over several decades, different versions of the K-Epsilon model have been employed, establishing it as the predominant choice for industrial applications. Throughout its evolution, numerous endeavors have been made to enhance its performance. Notably, Simcenter STAR-CCM+ has integrated the most substantial advancements in this model.

There are six variants of the $\kappa - \epsilon$ model which are implemented on STAR-CCM+, which are resumed in the following table:

Model Variant	Abbreviation
Standard K-Epsilon	SKE
Standard K-Epsilon Two-Layer	SKE 2L
Standard K-Epsilon Low-Re	SKE LRe
Realizable K-Epsilon	RKE
Realizable K-Epsilon Two-Layer	RKE 2L

Table 2.1: $\kappa - \epsilon$ model variants

- *Standard* $\kappa - \epsilon$: The Standard K-Epsilon model represents a widely accepted variant of the two-equation model, incorporating transport equations for both turbulent kinetic energy κ and its dissipation rate ϵ. In Simcenter STAR-CCM+, supplementary terms have been introduced to address factors like buoyancy and compressibility. Additionally, an alternative non-linear constitutive relation is made available as an option.

- *Standard* $\kappa-\epsilon$ *Two-Layer*: The Standard K-Epsilon Two-Layer model integrates the Standard K-Epsilon model with a two-layer approach. While the coefficients remain consistent across both models, this integration provides the additional advantage of employing an all-wall treatment for added versatility.

- *Standard* $\kappa - \epsilon$ *Low-Re*: The Standard K-Epsilon Low-Reynolds Number model merges the Standard K-Epsilon model with the low-Reynolds number methodology.

- *Realizable* $\kappa - \epsilon$: The Realizable K-Epsilon model introduces a new transport equation specifically for the turbulent dissipation rate ϵ. Moreover, it employs a variable damping function f_μ, dependent on mean flow and turbulence properties, which is applied to the pivotal coefficient of the model C_μ. This enables the model to adhere to certain mathematical constraints regarding normal stresses, in accordance with turbulence physics (realizability). This notion of a damped C_μ is also in alignment with experimental observations in boundary layers.

  For many applications, this model demonstrates significant improvements over the Standard K-Epsilon model and generally provides results of equal or greater accuracy. Simcenter STAR-CCM+ offers both the standard and realizable models, along with the option of utilizing a two-layer approach, enabling their use with finely detailed meshes that accurately represent the viscous sublayer.

- *Realizable* $\kappa - \epsilon$ *Two-Layer*: The Realizable Two-Layer K-Epsilon model integrates the Realizable K-Epsilon model with a two-layer approach. While the coefficients remain consistent across both models, this integration provides the additional advantage of employing an all-y^+ wall treatment for added flexibility.

In $\kappa - \epsilon$ models, the turbulent eddy viscosity μ_t which is used to evaluate *Reynolds stress tensor* is calculated as:

$$\mu_t = \rho C_\mu f_\mu k T \tag{2.36}$$

where

- ρ is the density;
- C_μ is a model constant which is equal to 0.09 for every variation of $\kappa - \epsilon$ model;
- f_μ is a damping function which is equal to 1 for SKE and SKE 2L whereas it is a function of the wall-distance Reynolds number, of some model coefficients, of C_μ, of the mean strain tensor S and of the modulus of the mean vorticity tensor W;
- T represents the turbulent time scale which for SKE, SKE 2L, SKE LRe is equal to

$$T = max\left(T_e, C_t\sqrt{\frac{\nu}{\epsilon}}\right)$$

  where $T_e = \frac{\kappa}{\epsilon}$, C_t is a model coefficient and ν is the kinematic viscosity. For RKE and RKE 2L, the turbulent time scale can be simply assumed equal to T_e.

The two transport equations, which the $\kappa - \epsilon$ model adds to the already known equations in order to close the system, are transport equations for the kinetic energy κ and the turbulent dissipation rate ϵ:

$$\frac{\partial}{\partial t}(\rho\kappa) + \nabla\cdot(\rho\kappa\overline{\vec{v}}) = \nabla\cdot\left[\left(\mu + \frac{\mu_t}{\sigma_\kappa}\right)\nabla\kappa\right] + P_k - \rho(\epsilon - \epsilon_0) + S_k \tag{2.37}$$

$$\frac{\partial}{\partial t}(\rho\epsilon) + \nabla\cdot(\rho\epsilon\overline{\vec{v}}) = \nabla\cdot\left[\left(\mu + \frac{\mu_t}{\sigma_\epsilon}\right)\nabla\epsilon\right] + \frac{1}{T_e}C_{\epsilon1}P_\epsilon - C_{\epsilon2}f_2\rho\left(\frac{\epsilon}{T_e} - \frac{\epsilon_0}{T_0}\right) \tag{2.38}$$

where

- $\overline{\vec{v}}$ represents the mean velocity;
- μ is the dynamic viscosity;
- σ_κ, σ_ϵ, $C_{\epsilon1}$, $C_{\epsilon2}$ are model coefficients;
- P_κ and P_ϵ are productive terms;
- f_2 is a damping function;

- S_κ and S_ϵ are the user-specified source terms.

ϵ_0 represents the ambient turbulence value within the source terms, working in opposition to the decay of turbulence. The option to apply an ambient source term also gives rise to the establishment of a distinct time-scale T_0, which is characterized as:

$$T_0 = max\left(\frac{\kappa_0}{\epsilon_0}, C_t\sqrt{\frac{\nu}{\epsilon_0}}\right)$$

The formulation of the productive terms depends on the variant of the model. Their expression is resumed in the table below:

Model Variant	$\boldsymbol{P_k}$	$\boldsymbol{P_\epsilon}$
SKE	$G_k + G_{nl} + G_b - \Upsilon_M$	$G_k + G_{nl} + C_{\epsilon 3}G_b$
SKE 2L	$G_k + G_{nl} + G_b - \Upsilon_M$	$G_k + G_{nl} + C_{\epsilon 3}G_b + \frac{\rho}{C_{\epsilon 1}}\Upsilon_y$
SKE LRe	$G_k + G_{nl} + G_b - \Upsilon_M$	$G_k + G_{nl} + G' + C_{\epsilon 3}G_b + \frac{\rho}{C_{\epsilon 1}}\Upsilon_y$
RKE	$f_c G_k + G_b - \Upsilon_M$	$f_c Sk + C_{\epsilon 3}G_b$
RKE 2L	$f_c G_k + G_b - \Upsilon_M$	$f_c Sk + C_{\epsilon 3}G_b$

Table 2.2: Productive terms in $\kappa - \epsilon$ model variants

Where

- $C_{\epsilon 3}$ is a model coefficient;

- f_c is the curvature correction factor. The turbulent kinetic energy transport equation, as designed, does not inherently account for stabilizing or destabilizing influences commonly linked with significant (streamline) curvature and frame rotation. To accommodate these effects, a curvature correction factor can be introduced, modifying the production term of turbulent kinetic energy based on the local rates of rotation and vorticity.

- G_k represents a turbulent production and can be assumed equal to

$$G_k = \mu_t S^2 - \frac{2}{3}\rho k \nabla \cdot \overline{\vec{v}} - \frac{2}{3}\mu_t \left(\nabla \cdot \overline{\vec{v}}\right)^2$$

  where the parameters which appears are those already explained in the previous sections.

- G_b is the buoyancy production, whose formulation is:

$$G_b = \beta \frac{\mu_t}{Pr_t}(\nabla \overline{T} \cdot \vec{g})$$

  where

  - β is the coefficient of thermal expansion and for constant density flows which use Boussinesq approximation, it must be specified by the user;

- Pr_t is the turbulent Prandtl number;
- $\overline{T}$ is the mean temperature;
- $\vec{g}$ is the gravitational vector.

- G_{nl} represents a "non-linear production";
- G' is an additional production which can be assumed equal to

$$G' = Df_2 \left(G_k + 2\mu \frac{\kappa}{d^2} \right) e^{-ERe_d^2}$$

where

- D and E are model coefficients;
- f_2 is a damping function;
- d is the distance from the wall;
- Re_d is the wall-distance Reynolds nuber which was given in the *Section 2.10*.

- Υ_M represents a compressibility modification which can be assumed equal to

$$\frac{\rho C_M \kappa \epsilon}{c^2}$$

where C_M is a model coefficient and c is the speed of sound.

- Υ_y is a yap correction which is a correction which takes into accounts the effects of the curvatures of the flow lines. Its formulation is

$$\Upsilon_y = C_W \frac{\epsilon^2}{\kappa} max \left[\left(\frac{l}{l_\epsilon - 1} \right) \left(\frac{l}{l_\epsilon} \right)^2, 0 \right]$$

where

- C_w is a model coefficient;
- l and l_ϵ are length scales defined as $l = \frac{\kappa^{\frac{3}{2}}}{\epsilon}$ and $l_\epsilon = C_l d$ where C_l is a model coefficient.

2.11.3 $\kappa - \omega$ model

The K-Omega turbulence model is a two-equation model that addresses transport equations for both turbulent kinetic energy κ and specific dissipation rate ω, representing the dissipation rate per unit turbulent kinetic energy ($\omega \propto \frac{\epsilon}{\kappa}$), with the aim of calculating the turbulent eddy viscosity.

A noted benefit of the K-Omega model, compared to the K-Epsilon model, lies in its enhanced effectiveness in handling boundary layers subject to unfavorable pressure gradients. Nevertheless, its most noteworthy advantage lies in its applicability across the entire boundary layer, including the region dominated by viscosity, without the need for additional adjustments. Additionally, the standard K-Omega model can be employed in this manner without necessitating the calculation of wall distance.

The primary drawback of the original form of the K-Omega model is its susceptibility to changes in the free-stream values of k and ω, particularly manifesting as heightened sensitivity to inlet boundary conditions in internal flows—a concern not encountered with K-Epsilon models. Variants of the K-Omega model integrated into Simcenter STAR-CCM+ have undergone adjustments in an effort to mitigate this limitation.

There are two different $\kappa - \omega$ models which are implemented on Star CCM+ and they are shown in the following table:

Model Variant	**Abbreviation**
Standard K-Omega	SKO
SST K-Omega	SSTKO

Table 2.3: $\kappa - \omega$ model variants

- **Standard K-Omega**: In 2006, D.C. Wilcox published a revised model of his previous one, correcting some deficiencies in the original version (1998) [19]. This formulation included:

  - A revised set of model coefficient.

  - The incorporation of a cross-diffusion term bears resemblance to its utilization in the SST K-Omega model.

  - An adjustment aimed at enhancing the spreading rates in free shear flows of the model.

  - A compressibility correction.

  - Modifications tailored for low Reynolds numbers that enhance the applicability of the K-Omega model in predicting flows characterized by low Reynolds numbers and transitional behavior.

Nonetheless, it's important to note that the validation results presented in Wilcox's book primarily pertain to two-dimensional, predominantly parabolic flows. Until comprehensive validations for intricate flows become more widely available, it is advisable to exercise caution when applying these corrections. Hence, each correction has been incorporated as an optional feature in Simcenter STAR-CCM+.

- **SST K-Omega**: Menter [15] tackled the sensitivity to free-stream/inlet conditions by realizing that the transport equation of the Standard K-Epsilon model could be converted into an ω transport equation through variable substitution.

  The modified equation closely resembles that of the Standard K-Omega model, but introduces an extra non-conservative cross-diffusion term incorporating the dot product $\nabla k \cdot \nabla \omega$. By incorporating this term in the ω transport equation, the K-Omega model may yield results akin to those of the K-Epsilon model. Menter proposed the use of a blending function (which encompasses functions dependent on wall distance) that incorporates the cross-diffusion term far away from walls, but not in close proximity to them. This method effectively combines a K-Epsilon model in the distant field with a K-Omega model near the wall. Some concerns may be raised about the arbitrary nature of the blending function's crossover location, as it could potentially obscure certain crucial aspects of the turbulence. Nonetheless, it remains a fact that this approach resolves the primary limitation in applying the K-Omega model to practical flow simulations.

  Menter further innovated by introducing a modification to the linear constitutive equation, dubbing the model that incorporates this adjustment the SST (Shear-Stress Transport) K-Omega model. Nonetheless, the linear correlation between Reynolds stresses and mean strain rate often leads to a significant underestimation of turbulence anisotropy. In the majority of intricate flows, such as those featuring intense swirl, streamline curvature, shear layers, or boundary layers, turbulence exhibits anisotropic behavior. This anisotropy in Reynolds stresses not only impacts the flow pattern but also influences the turbulent transport of scalars like temperature, concentration, and passive scalar.

  To address turbulence anisotropy, Simcenter STAR-CCM+ provides the following nonlinear constitutive relations:

  - Quadratic;

  - Cubic.

  The cubic constitutive relation is obtained from a Reynolds stress transport model, making it an Explicit Algebraic Reynolds Stress Model (EARSM). While Reynolds stress transport models excel in handling anisotropic turbulence, they can become unstable in complex flow scenarios. Hence, the cubic model serves as a balanced compromise between these two approaches.

The SST model has found extensive application in the aerospace industry, particularly in scenarios involving resolved viscous flows, where turbulence models are implemented across the boundary layer.

In $\kappa - \omega$ models, the turbulent eddy viscosity μ_t which is used to evaluate *Reynolds stress tensor* is calculated as:

$$\mu_t = \rho k T \tag{2.39}$$

where

- ρ is the density;
- T is the turbulent time scale which for SKO is equal to

$$\frac{\alpha^*}{\omega}$$

and for SSTKO is

$$min\left(\frac{\alpha^*}{\omega}, \frac{a_1}{SF_2}\right)$$

where a^* and a_1 are model coefficients, S is the mean strain rate tensor, F_2 is a blending function which depends on a model coefficient β^*, the distance from the wall d, the kinematic viscosity ν, the turbulent kinetic energy κ and the specific dissipation rate ω.

The two transport equations, which the $\kappa - \omega$ model adds to the already known equations in order to close the system, are transport equations for the kinetic energy κ and the specific dissipation rate ω:

$$\frac{\partial}{\partial t}(\rho\kappa) + \nabla \cdot (\rho\kappa\overline{\vec{v}}) = \nabla \cdot [(\mu + \sigma_\kappa \mu_t)\nabla\kappa] + P_\kappa - \rho\beta^* f_{\beta^*}(\omega\kappa - \omega_0\kappa_0) + S_\kappa \tag{2.40}$$

$$\frac{\partial}{\partial t}(\rho\omega) + \nabla \cdot (\rho\omega\overline{\vec{v}}) = \nabla \cdot [(\mu + \sigma_\omega \mu_t)\nabla\omega] + P_\omega - \rho\beta f_\beta(\omega^2\omega_0^2) + S_\omega \tag{2.41}$$

where:

- $\overline{\vec{v}}$ is the mean velocity;
- μ is the dynamic viscosity;
- σ_κ and σ_ω are model coefficients;
- P_κ and P_ω are production terms;

- f_{β^*} is the free-shear modification factor; Considering that for flows in which free-shear layer are predominant or for those in which free-stream turbulence is high, K-Omega models tend to under-predict the production of ω, so free-shear modifications are needed;

- f_β is the vortex-stretching modification factor. In practice, nearly all two-equation models have a tendency to overestimate the spreading rate in round jets compared to plane jets, contrary to what is observed in experiments. This is why this modification is needed;

- S_κ and S_ω are the user-specified source terms;

- κ_0 and ω_0 re the ambient turbulence values that counteract turbulence decay.

The formulation of the productive terms depends on the variant of the model. Their expression is resumed in the table below:

Model Variant	$\boldsymbol{P_k}$	$\boldsymbol{P_\epsilon}$
SKO	$G_k + G_b$	G_ω
SSTKO	$G_k + G_{nl} + G_b$	$G_\omega + G_\omega$

Table 2.4: Productive terms in $\kappa - \omega$ model variants

Where

- G_k represents a turbulent production and may be assumed equal to

$$\mu_t f_c S^2 - \frac{2}{3}\rho\kappa\nabla\cdot\overline{\vec{v}} - \frac{2}{3}\mu_t(\nabla\cdot\overline{\vec{v}})^2$$

  where all the parameters which appears are those already explained in the previous sections.

- G_b is the bouyancy production, whose formulation is:

$$G_b = \beta\frac{\mu_t}{Pr_t}(\nabla\overline{T}\cdot\vec{g})$$

  where the parameters are the same which have been explained in the section regarding production terms in $\kappa - \epsilon$ models.

- G_{nl} represents a "Non-linear production".

- G_ω is the specific dissipation production which have two different formulations for SKO and SSTKO: for SKO it is considered equal to:

$$G_\omega = \rho\alpha \left[\left(\alpha^* S^2 - \frac{2}{3}(\nabla \cdot \vec{\overline{v}})^2 \right) - \frac{2}{3}\omega \nabla \cdot \vec{\overline{v}} \right]$$

  For SSTKO, it is equal to

$$G_\omega = \rho\gamma \left[\left(S^2 - \frac{2}{3}(\nabla \cdot \vec{\overline{v}})^2 \right) - \frac{2}{3}\omega \nabla \cdot \vec{\overline{v}} \right] \tag{2.42}$$

  where α, α^* and γ are model coefficients.

- D_ω represents the cross-diffusion term which is given by the following formulation:

$$D_\omega = 2\rho(1 - F_1)\sigma_{\omega_2} \frac{1}{\omega} \nabla\kappa \cdot \nabla\omega$$

  where σ_{ω_2} is a model coefficient and F_1 is a blending function which combines the near-wall contribution of a coefficient with its value far away from the wall. It depends on the distance to the wall d, the kinematic viscosity ν and the cross-diffusion coefficient $CD_{\kappa\omega} = max\left(\frac{1}{\omega}\nabla\kappa \cdot \nabla\omega, 10^{-20}\right)$.

2.11.4 Elliptic blending model

The Elliptic Blending turbulence model resolves transport equations for turbulent kinetic energy κ, turbulent dissipation rate ϵ, normalized (reduced) wall-normal stress component $\phi = \frac{\overline{\theta^2}}{\kappa}$, and the elliptic blending factor α to ascertain the turbulent eddy viscosity.

Durbin [9] introduced the concept of elliptic relaxation for Reynolds-stress models. The original model necessitated solving six extra transport equations, but this was subsequently streamlined to just one additional equation.

There are two different variants of the Elliptic Blending model implemented on Star CCM+ and they are shown in the following table:

Model Variant	**Abbreviation**
Standard Ellipting Blending	EBS
Lag Elliptic Blending	EBL

Table 2.5: Elliptic Blending model variants

- **Standard Elliptic Blending**: The introduction of the elliptic relaxation model paved the way for the development of several two-equation eddy viscosity models, commencing with the $\overline{\theta^2} - f$ model. As stated by its creators, the model $BL - \frac{\overline{\theta^2}}{\kappa}$developed by Billard and Laurence is regarded as one of the most robust [16]. Significant alterations to this model render it highly reliable for intricate flow geometries.
  Two major benefits can be seen using this model:

- An enhancement over the current realizable $\kappa - \epsilon$ model in terms of accuracy, particularly in the vicinity of the wall;

- An enhancement in terms of stability compared to the SST $\kappa - \omega$ model.

- **Lag Elliptic Blending**: The Lag Elliptic Blending model integrates the Standard Elliptic Blending model with the stress-strain lag concept. The lag concept consists on the delay of the stress response $\sigma(t)$ to a strain input $\epsilon(t)$.

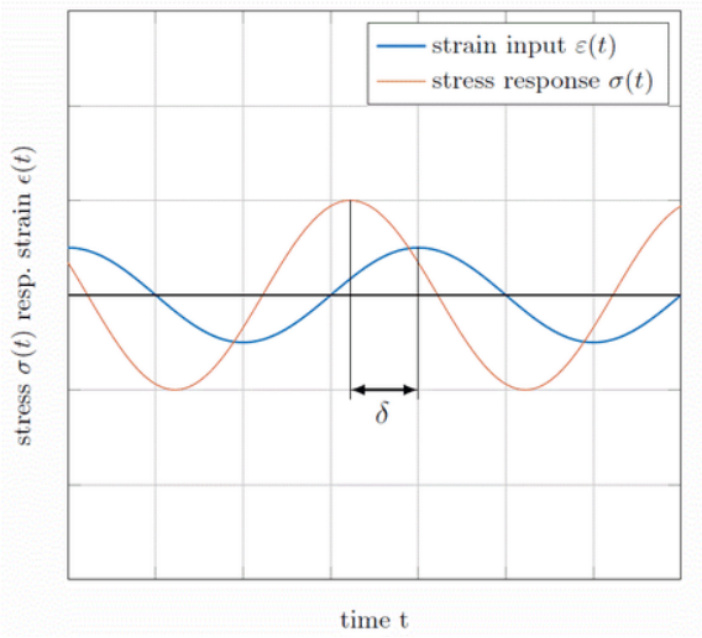

Figure 2.10: Phase lag between strain input and stress response [13]

In areas of flow characterized by non-equilibrium effects causing a deviation between the principal components of stress and strain-rate tensors, linear eddy viscosity models often exhibit an overestimation of the production of κ. To address this, the Lag Elliptic Blending model considers the angle between these components. Moreover, it introduces supplementary terms to account for anisotropic effects, similar to non-linear constitutive relations, as well as for curvatures and rotational effects, akin to curvature correction. These adjustments are directly incorporated into the transport equation governing the reduced stress function ϕ [16].

The Lag Elliptic Blending model demonstrates effective predictive capabilities in scenarios involving separated or unsteady flow (such as vortex shedding) and in flows influenced by rotation or significant streamline curvature.

In elliptic models, the turbulent eddy viscosity μ_t which is used to evaluate Reynolds stress tensor is calculated as:

$$\mu_t = \rho C_\mu \phi \kappa \, min\left(T, \frac{C_T}{\sqrt{3} C_\mu \phi S}\right) \tag{2.43}$$

where

- ρ is the density;
- C_μ and C_T are model coefficients;
- T is the turbulent time scale which is evaluated as:

$$T = \sqrt{T_e^2 + C_t^2 \frac{\nu}{\epsilon}} \tag{2.44}$$

  where $T_e = \frac{\kappa}{\epsilon}$ is the large-eddy time scale, C_t is a model coefficient and ν is the kinematic viscosity.

- S is the mean strain rate tensor.

Elliptic blending models use four additional transport equations to add to those already known in order to close the system. The variables which are involved are: the turbulent kinetic energy κ, the turbulent dissipation rate ϵ, the wall-normal stress component ϕ and the elliptic blending factor α.

$$\frac{\partial}{\partial t}(\rho\kappa) + \nabla \cdot (\rho\kappa\overline{\vec{v}}) = \nabla \left[\left(\frac{\mu}{2} + \frac{\mu_t}{\sigma_\kappa} \nabla\kappa \right) \right] + P_\kappa - \rho(\epsilon - \epsilon_0) + S_\kappa \tag{2.45}$$

$$\frac{\partial}{\partial t}(\rho\epsilon) + \nabla \cdot (\rho\epsilon\overline{\vec{v}}) = \nabla \left[\left(\frac{\mu}{2} + \frac{\mu_t}{\sigma_\epsilon} \nabla\epsilon \right) \right] + \frac{1}{T_e} C_{\epsilon 1} P_\epsilon - C^*_{\epsilon 2} \rho \left(\frac{\epsilon}{T_e} - \frac{\epsilon_0}{T_0} \right) + S_\epsilon \tag{2.46}$$

$$\frac{\partial}{\partial t}(\rho\phi) + \nabla \cdot (\rho\phi\overline{\vec{v}}) = \nabla \left[\left(\frac{\mu}{2} + \frac{\mu_t}{\sigma_\phi} \nabla\phi \right) \right] + \rho \frac{\epsilon_0 \phi_0}{\kappa_0} + P_\phi + S_\phi \tag{2.47}$$

$$\nabla \cdot \left(L^2 \nabla\alpha \right) = \alpha - 1 \tag{2.48}$$

where

- $\overline{\vec{v}}$ is the mean velocity;
- μ is the dynamic viscosity;
- P_κ, P_ϵ and P_ϕ are production terms;
- $C_{\epsilon 1}$, $C^*_{\epsilon 2}$, σ_κ, σ_ϵ and σ_ϕ are model coefficients;
- S_κ, S_ϵ and S_ϕ are the user-specified source terms;

- L is the turbulent length scale calculated as:

$$L = C_L \sqrt{\frac{\kappa^2}{\epsilon^2} + C_\eta^2 \sqrt{\frac{\nu^3}{\epsilon}}}$$

  where C_L and C_η are model coefficients;

- ϵ_0, κ_0 and ϕ_0 represent the ambient turbulence values within the source terms, working in opposition to the decay of turbulence. The option to apply an ambient source term also gives rise to the establishment of a distinct time-scale T_0, which is characterized as:

$$T_0 = max\left(\frac{\kappa_0}{\epsilon_0}, C_t\sqrt{\frac{\nu}{\epsilon_0}}\right)$$

  where C_t is a coefficient model.

The formulation of the productive terms depends on the variant of the model. Their expression is resumed in the table below:

Model Variant	$\boldsymbol{P_\kappa}$	$\boldsymbol{P_\epsilon}$
EBS	$G_k + G_b - \Upsilon_M$	$G_\kappa + C_{\epsilon 3} G_b + \frac{1}{C_{\epsilon 1}} E$
EBL	$G_k + G_b - \Upsilon_M$	$G_\kappa + C_{\epsilon 3} G_b + \frac{1}{C_{\epsilon 1}} E$

Table 2.6: Productive terms in elliptic blending model variants

Model Variant	$\boldsymbol{P_\phi}$
EBS	$-\frac{\phi}{\kappa}(G_\kappa + G_b) + \rho(1-\alpha^3) f_w + \rho\alpha^3 f_h$
EBL	$-(2 - C_{\epsilon 1})\frac{\phi}{\kappa}(G_\kappa + G_b) + \rho(1-\alpha^3) f_w + \rho\alpha^3 f_h$

Table 2.7: Productive terms in elliptic blending model variants

Where

- G_κ, G_b and Υ_M are parameters which has already been formulated in *Section 2.11.2*;

- E (which accounts for viscous wall-effects) is an additional production which can be assumed equal to

$$E = C_\kappa (1-\alpha)^3 \nu \mu_t \frac{\kappa}{\epsilon} \left[\nabla \cdot (|2\vec{S}\vec{n}|\vec{n})\right]^2$$

  where C_κ is a model coefficient, and $\vec{n}$ is the wall normal direction. Other parameters are those already known;

- f_w and f_h are functions expressed how it follows for EBS:

$$f_w = -\frac{1}{2}\frac{\phi}{T_e}$$

$$f_h = -\frac{1}{T}\left(C_1 - 1 + C_2\frac{G_\kappa + G_b}{\rho\epsilon}\right)\left(\phi - \frac{2}{3}\right)$$

  Considering EBL model, these functions are more complicated and they depend on some model coefficients which are shown in the following point, Reynolds-stress anisotropy tensor and the modified absolute vorticity tensor;

- C_1, C_1^*, C_2, C_3^*, C_4, C_5, $C_{\epsilon 2}$, , $C_{\epsilon 3}$, C_μ and C_{P3} are model coefficients;

Chapter 3

Comparative analysis between two strategies of computational simulations

This chapter is dedicated to elucidating the processes undertaken to achieve significant results in the field of automotive engineering. It focuses on the transformative methodologies employed, encompassing both geometric modifications facilitated by Ansa and the computational procedures carried out using Star CCM+. The chapter is divided into different sections.

Firstly, it is presented how alterations in geometry have been executed through the versatile tool, ANSA BETA CAE. This software played a crucial role in shaping the vehicle profiles, paving the way for subsequent computational analysis.

Secondly, the two procedures, which have been used on Star CCM+ in order to obtain the results, are presented. Special attention will be given to the process of mesh generation and the definition of turbulence models which have already been presented in the previous chapter.

Lastly, the last section presents the four different models which have been analyzed, giving a deeper focus on the modifications which have been implemented in order to compute deltas between different configurations.

3.1 ANSA BETA CAE procedure: Model preparation

ANSA, developed by BETA CAE Systems, is a powerful and versatile engineering tool which is often used in computational simulations and virtual prototyping. Being used for the process of model preparation, it allows the user to execute efficient meshing and pre-processing tasks.

The procedure, which is going to be presented, has been used for all four different models of vehicles which have been analyzed.

Firstly, after having open the project, all the components of the vehicles have been renamed, using a special tools called "AutoNames". This tool allows to rename all the PIDs (Produc Identification) under a Standard Naming Convention, which is useful especially in the definitions of the parts to use in the meshing process on Star CCM+. For each group it is possible to define a primary system, such as the engine (ENG), the external parts (EXT) or the back suspensions (SOVP). In order to complete the rename process, it is fundamental to assign to the PID also

a secondary system, a sub-system and the name of the component. Lastly, it is important to define the boundary type which can be of three different types:

- **Wall**: which refers to those components which are surfaces or walls with a non-infinitesimal thickness in the geometric model.

- **Baffle**: similar to the walls, but baffles are surfaces with an infinitesimal thickness.

- **Internal**: surfaces that allow the passage of airflow applied in specific areas of the vehicle (such as air intake inlets, etc.) through which it is possible to take account of the airflow rate.

The following table shows few examples of a PID with the Standard Name Convention:

Component	**Standard Name Convention**	**Boundary Type**
Side doors	Wall	EXT_EXT_side-doors_main
Front-left rim	Wall	WHL_WHL_FRT-LFT_rim
Rear shock absorber	Wall	SOVP_SOVP_shock-abosrber_main
Compressor cap	Baffle	BFL-ENG_CLI_compressor_cap
Lower grille	Internal	I-EXT_EXT_grille_lower-intake

Table 3.1: Example of Standard Name used in the definition of PIDs name

After having renamed all the PIDs, in order to check that no duplicated names where present, the boundaries check called *Duplicate PIDs name* has been run. In case it gave an error, the procedure consisted in finding the two PIDs with the same name and changing one of them, by choosing a different definition or by adding a variant to the Standard Name.

After having completed this process, the modification of the geometry was carried out. Firstly, through the option *merge*, the component to be inserted to the vehicle was added to the project. In order to correctly merge this component with the vehicle, it was necessary to manipulate the geometry and the surfaces. As a matter of facts, some faces were overlapping, resulting into geometry errors. In order to solve this problem, different options which are present on ANSA BETA CAE were used such as:

- **Delete**: it allows to delete surfaces which are overlapping or which may produce errors.

- **New**: after having deleted the faces, it may be necessary to close some holes or rebuild some faces in order to have the best surface possible. In order to do that, there are four different surface types which can be used [5]:

  - **Existing surface**: allow to build a surface on an already existing surface which is present on the model.

  - **Planar**: it allows to create a surface based on a user-specified plane. This option is useful when a planar or flat surface is requested.

- **Coons**: it is ideal for defining surfaces whose surrounding boundaries are already defined.

- **Fitted**: it is used for the definition of a non-planar Face. The created Face fits to the selected boundaries.

The next step consisted in evaluating whether there were any geometric errors. In order to give a deeper look into this part of the process, some examples of geometry errors are reported below:

- **Intersections**: ANSA can detect situations where surfaces or volumes intersect, which could cause issues in calculating properties like volume or surface area.

- **Duplicates**: Finding and flagging entities (such as nodes, edges, or surfaces) that are duplicated in the model, which can lead to ambiguity or errors during analysis.

- **Unclosed surfaces**: Identifying surfaces that do not form a closed boundary or volume, which could cause issues during analysis.

- **Needle shaped faces**: they are faces with a shape of a needle which may result in a worsening of the mesh quality.

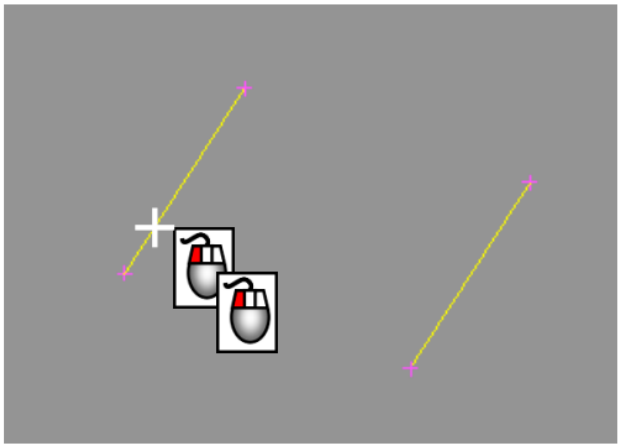

Figure 3.1: Example of needle shape faces [5]

After having solved all the problems related to the geometry, the attention switched to the generation of the mesh. Considering that the whole vehicle already had the surface mesh, it has only been necessary to rebuild it on those new faces which were created in order to merge the car with the new components. In order to do that, the option *Batch mesh* has been used. This option allows the user to generate a surface mesh by giving as input an already predefined scenario.

Once that the surface mesh has been generated, as for the geometry, some checks were implemented:

- **Unmeshed Check**: this check is fundamental because it allows to find all the surfaces which have not been meshed. In order to fix this problem, it is possible to find the faces not meshed and fix them by using some mesh generation tools.

- **Penetration Check**: element penetration can arise when there are misaligned geometry components in the CAD file, causing parts to intersect. This can also be a result of a relatively coarse mesh resolution or even an incompatible mesh. ANSA has the capability to detect and pinpoint these Intersection errors in both the Geometry and FE-Model mesh.
  Another scenario to consider is that, even in the absence of intersecting geometries, element penetration can occur. This may be attributed to the thickness of shell elements in areas where parts are closely situated.
  One example of penetration check which have been implemented is *Intersection*. This feature identifies and addresses intersections among lines, shell elements, and external facets of solid elements. If there are no penetrations in the model, the "Penetration: Intersections" category will be indicated by a green check-mark in its status field within the Checks Manager window, otherwise the check-mark will be red and will indicate the problems.

- **Non-manifold nodes**: this tool identifies shells with non-manifold nodes.

Once all geometric and mesh checks were completed, the focus shifted towards configuring the model in order to initiate the simulation. In order to do that, a tool called "AutoSetup" was used. This tool allows the user to decide the set up of the vehicle and define some parameters which will be used either to build an ANSA file which contains the vehicle and the wind tunnel specified, and to define solver settings (Star CCM+). Below, some steps required to do what has just been said:

- **Tunnel Setup**: in particular, the type of tunnel (open air) and ground (moving ground) has been specified.

- **Ride Height**: it is required to decide the front right and the rear height of the vehicle. In addition, it is also important to define which entities are assigned to rigid translation (wheels) and which to morphing (suspension).

- **Heat Exchangers**: in order to start the simulation, it is essential to give the inertial coefficient and the viscous coefficient of radiators.

- **Solver**: The version of Star CCM+ to use must be specified.

- **Run**: in this section the free-stream parameters such as the velocity has to be decided and also the maximum number of iterations executed by the solver must be set.

It is important to underline that all the process described in this section, has been followed for all the vehicles.

After having completed all these steps and having saved the file, by using the software MobaXterm, the computation was launched. As anticipated before, one of the important things that the process does, is the merging between the vehicle and the wind tunnel specified in AeroSetup. After setting up the machine as instructed and performed new mesh and geometry checks, the components are imported into Star CCM+. The software then proceeds with the operations in order to initiate the simulation. The actions performed in Star pertain to the initial strategy used to obtain the results, which will be further elaborated in the following section.

3.2 First strategy of computational simulation

In this section, the operations implemented by Star CCM+ following the first strategy to initiate the simulation will be described.

As anticipated before, the components prepared on the software ANSA BETA CAE were imported on Star CCM+ as surface mesh format. A surface mesh is a digitalized portrayal of specific regions essential for volume mesh creation. It is composed of faces (typically triangles) and vertices. The optimal surface mesh exhibits the following characteristics:

- **Closed**: it does not include any unconnected edges or discrepancies.
- **Manifold**: edges are shared by a maximum of two triangles.
- **Non-intersecting**: the surface does not intersect itself.

These three properties have already been checked before importing the mesh, immediately after having set up the vehicle in the wind tunnel. The next step consisted in executing the following operation:

- **Subtract Operation**: This operation in Boolean logic involves the subtraction of a defined shape from the volume of a designated target part. In order to do that a group called "RAW-AIR-geometry" which contains all the parts of the vehicle (except for MRF walls) and the wind tunnel are subtracted from an auxiliary volume.
- **Contact Creator Operation**: The contact creator enables the establishment of contacts between surfaces of different parts. There are four types of contact which may be implemented: Weak Contact, Baffles, Periodic Translation and Periodic Rotation. The one implemented in this process is the Weak Contact. This option allows to create contacts between part surfaces.
- **Automated Mesh Operation**: It is an operation to resurface and/or generate a volume mesh. Some of the actions which this operation executes are resumed below:

- It automatically creates a mesh on the surfaces of the model's geometries based on the surface of the imported parts.

- It extends the mesh from the surface to the internal volume of the model, creating a three-dimensional mesh representing the flow domain.

- It automatically applies quality control criteria to ensure the mesh meets certain accuracy and precision standards.

It is also possible to select various custom controls, such as the number of prism layers. As a matter of facts, it can be useful to examine the flux near the wall, by using a different number of prism layer (for example on the external surface of the car rather than on wind tunnel walls).
It is also possible to thicken the mesh by increasing the number of cells where necessary (for example on the grills or on those areas where velocity gradients are high). Another important thing which can be implemented in this operation as a custom control is the implementation of a volumetric control, which can be useful to refine the volumetric mesh in important areas such as the wake which develops downstream the vehicle or near wheels.

- **Directed Mesh Operation**: It is a specialized technique designed for creating superior swept meshes on geometries. This process involves systematically sweeping a mesh from the surfaces of a geometry, extending through its volume, and terminating on a corresponding target surface. It is important to use this kind of mesh especially for radiators because, considering that there is a law governing pressure drop within the radiators in terms of x-direction, a directed mesh is able to provide a smooth variation in x for each cell to the solver, without any approximations.

Special attention must be given to those parts called MRFs. MRFs are the acronym of *Moving Reference Frame* and they are used to take into account the effect of rotating parts such as the wheels. With the MRF approach, the mesh does not physically move during the simulation. Instead, a rotating coordinate system (the moving reference frame) is used in which the flow is considered to be stationary. This means that the mesh and the airflow are fixed relative to the coordinate system "attached" to the rotating part (such as a wheel or a fan). Considering that MRFs are not a real wall, it is important to act on the custom controls especially by deciding how to build the prism layer.

After having built the volumetric mesh and having check that there are no negative volume cells, the attention switched to the definition of the physics of the problem.

Considering that this part is common also to the second strategy of computational simulation, this topic will be dealt later.

3.3 Second strategy of computational simulation

In this section, the operations implemented by Star CCM+ following the first strategy to initiate the simulation will be described.

This second approach is a test of a template provided by Siemens. In order to proceed with the simulation, it has been requested to export parts from ANSA BETA CAE as the format ".nas", following their instructions. For example the three PIDs which belongs to the HT radiator (inlet, outlet and wall) were exported a unique file .nas" called HEX_HEX_RadHT; another example is the one related to the wind tunnel: all the PIDs containing as a primary system *WT* were grouped in a *.nas* file called *Tunnel*.
The next step consisted in importing all the ".nas" files in Star CCM+ by using the option *Import surface mesh*. Once that all the components of the simulations have been imported and grouped under different categories (rims or MRFs), the tool "Surface Repair" was used.
This tool allows to check the surface mesh examines the geometry to identify surface and feature errors, categorizing them into color-coded groups:

- **Pierced Faces**: A pierced face refers to a face intersected by one or more edges of another face. The color associated to this kind of error is "red".

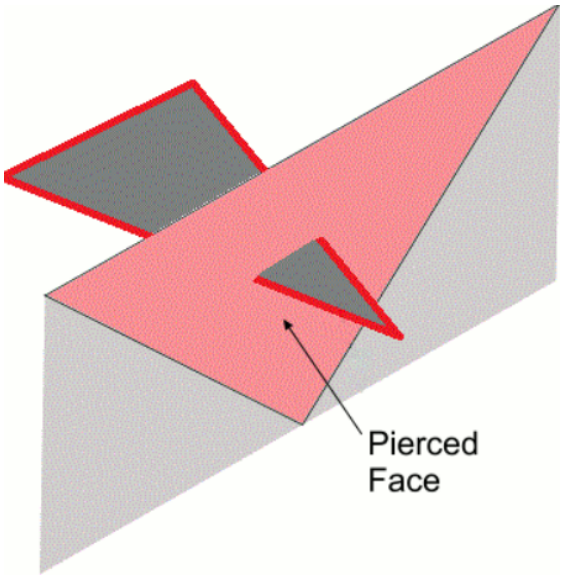

Figure 3.2: Example of pierced face [16]

- **Face quality**: It assesses how closely a face resembles the ideal shape, which is an equilateral triangle. The color which to this kind of error is "yellow".

- **Face Proximity**: It evaluates the distance between two faces. Faces with a face proximity of less than 0.05 (default value) are categorized as being in close proximity. The color which to this kind of error is "orange".

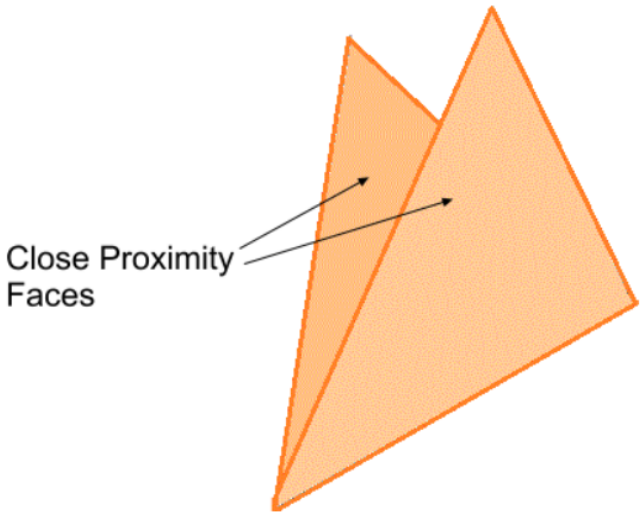

Figure 3.3: Example of face proximity [16]

- **Free edges**: A free edge is connected to only one face. Two adjoining faces share two vertices along the common edge. The color which to this kind of error is "green".

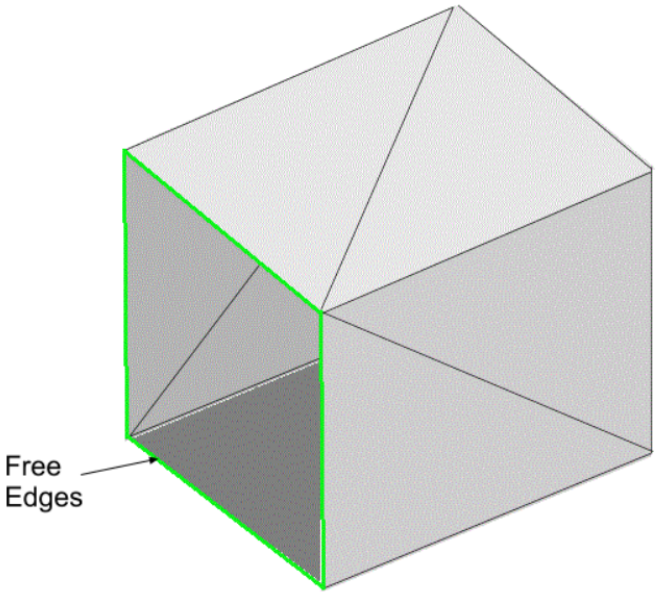

Figure 3.4: Example of free edges [16]

- **Non-manifold edges**: A non-manifold edge is an edge shared by three or more faces. The color which to this kind of error is "blue".

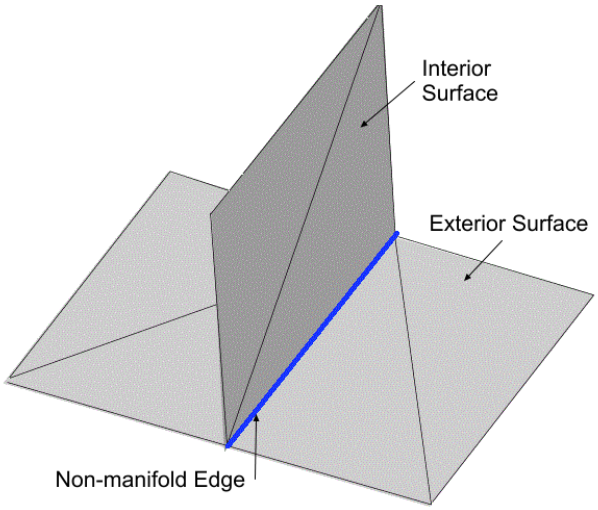

Figure 3.5: Example of non-manifold edges [16]

- **Non-manifold vertices**: A vertex is considered non-manifold if any of its connected faces do not have any other connections with the rest of the connected faces, except through the vertex itself. The color which to this kind of error is "blue".

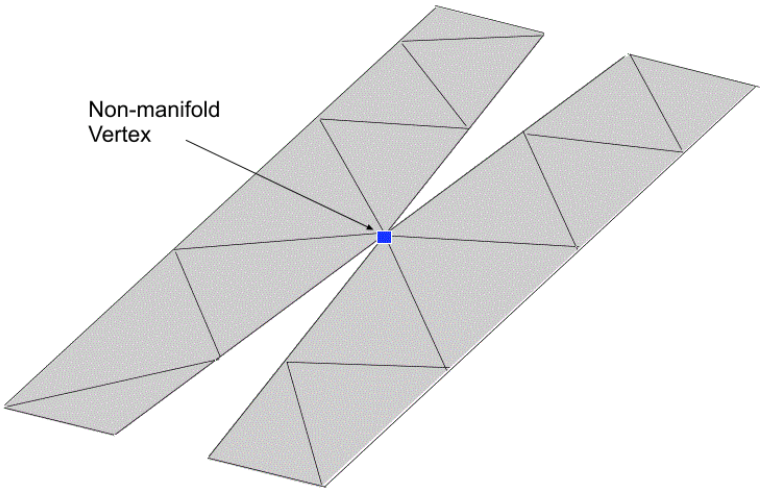

Figure 3.6: Example of non-manifold vertices [16]

Considering that the imported surface mesh had already passed the checks on ANSA BETA CAE, only few problems were found, so it was possible to solve them by using the auto-fix option of *Surface Repair Tool*.

The next step consisted in executing the following operations:

- **Bounded Shape Operation**: Bounded shapes are shape components linked to pre-existing geometry. They dynamically adjust their shape and dimensions in accordance with the reference geometry. In particular, the output part type was set on *Shape Aligned Box*, which creates a box around the input parts. After having built these boxes around different part of the vehicle, through the execution of some *Simulation Operation*, it has

been possible to evaluate the coordinate system of different components and also the dimension of the car. The use of this simulation operation is one major different from the first approach, where they were not used. The strength of *Simulation Operation* is that they can automate the solution process without the need of using a Macro Java. As a matter of facts, they can use loop or condition operations.

- **Part Curve Creator Operation**: it generates and manages part curves within the parts-based meshing pipeline.

- **Zip Edges Operation**: It is employed to address minor surface issues, such as closing small gaps or joining multiple parts together. Considering that the option for the output was *New Part - Discrete*, the operation produced a single output part which is the union between every input part.

- **Extract Volume Operation**: The "Extract Volume" mesh operation identifies enclosed volumes within chosen parts and creates a separate part to represent that volume. As input parts, this operation requires those geometry parts from which the operation extracts an internal volume.

- **Surface Extruder**: It elongates the edges of the provided surface to create the enclosing surfaces of the extended area. In properties windows, it is possible to define from which surface the extrusion action has to start and also the distance of the extrusion itself. The result of this operation is a new surface which extends outside the parts, at a specific distance from the surfaces of the parts themselves. This new surface can be used for example in the custom controls of the operation to generate the volumetric mesh, in order to give specific properties in those areas.

- **Offset Operation**: This operation creates an external surface at a defined distance from the surfaces of the parts. It can be useful to define some areas where the user wants to refine the mesh in order to catch the details in a more precise way.

- **Box Refinement Operation**: Similar to surface extruder and offset operations. it is possible to create boxes in particular areas where particular properties of the volumetric mesh are required (such as the wake of the vehicle).

- **Directed Mesh Operation/Subtract Operation/Contact Creator Operation/Automated Mesh Operation**: The importance and the use of these operations, has been presented in the *Section 3.2*.

The next step of the workflow, considering the use of *Simulation Operation*, consisted in the execution of the *Simulation Operation* to remove invalid cells. This operation sets properties of the cells belonging to the volumetric mesh such as *Minimum Face Validity, Minimum Cell Quality, Minimum Cell Volume, etc ...*, and remove those cells which would create problems

during the simulation.
Considering that some of the operation to generate the mesh are different between the two approaches and that parameters used in the automated mesh are dissimilar too, the result is a different volumetric mesh. So, in order to test the effectiveness of the way of meshing, tests were carried out either by using the same approach but changing turbulence models (so that the influence of the approximation of *Reynolds Stress Tensor* can be analyzed) or by using the same turbulence model with the two approaches (so that the influence of the mesh can be seen).

Once that the mesh has been created the attention turned to the physics of the problem.

3.4 Physics of the problem

As said in the previous section, all the different physics which are presented below were used for both approaches. Following are reported the model selection used:

- **Three Dimensional Model**: It is used to define the space modeling, which is utilized to provide methods for computing and accessing mesh metrics. Three Dimensional Model is intended for operation on meshes in three dimensions.

- **Steady**: It is used to define the time modeling. The chief purpose of the time models is to furnish solvers that manage the iteration and/or unsteady time-stepping.

- **Material Modeling**: It is used to define the material to simulate. The simulated substance oversees the diverse thermodynamic and transport characteristics pertinent to the material, as well as the physical processes being replicated in the continuum. Obviously, the material selected is Air.

- **Flow Solvers**: They are employed to address the conservation equations for mass and momentum in both non-compressible and compressible fluid flows. The solution space is divided into a finite set of small control volumes, aligning with the cells of a computational grid. Discrete adaptations of the integral form of conservation equations are applied to each control volume. This process leads to a collection of linear algebraic equations, where the total number of variables in each equation system corresponds to the number of cells in the grid. Typically, numerical techniques convert the mathematical model into a system of algebraic equations. This conversion entails discretizing the governing equations in both spatial and temporal dimensions. Subsequently, the resulting linear equations are resolved using an algebraic multigrid solver. There are two different solvers: Segregated Flow and Coupled Flow.

  - **Segregated Flow**: The segregated flow solver addresses the conservation equations for mass and momentum in a sequential way. The non-linear governing equations are tackled iteratively, one after the other, for the solution variables.

  - **Coupled Flow**: The equations of conservation for continuity and momentum are resolved in a coupled way, meaning they are solved concurrently as a system of equations. The velocity field is derived from the momentum equations. Pressure

is computed from the continuity equation, and density is determined through the equation of state. The coupled solver offers a notable advantage: the CPU time scales linearly with the number of cells. This means that the convergence rate remains consistent even as the mesh is refined.

- **Equation of State**: The equations of state are constitutive relationships that elucidate the connection between density and internal energy in relation to the fundamental thermodynamic variables, pressure, and temperature. There are different models which may be chosen, such as Ideal Gas (which calculates the density using the ideal gas equation), Real Gas (which takes into account also non-ideal behaviors) and Constant Density.

- **Viscous Regime**: it may be inviscid, laminar or turbulent.

- **Reynolds-Averaged Turbulence**: in this section the turbulence model must be defined. There are four different options:
  - *K-Epsilon Turbulence*;
  - *K-Omega Turbulence*;
  - *Reynolds Stress Turbulence*;
  - *Spalart-Allmaras Turbulence.*

  As said before, in this job, the turbulence model tested are the *Standard K-Epsilon Two-Layer*, *Lag EB K-Epsilon* and *SST K-Omega*, which have been explained in *Chapter 2.*

Once that the definition of the physical models has been done, the simulation was ready to be launched.

3.5 Application of the two approaches on different models of vehicles

In this section it will be seen which changes in the geometry have been implemented on ANSA BETA CAE using the workflow presented in *Section 3.1.* In addition, the results in terms of drag coefficient collected using the two different approaches will be reported.

The vehicles which have been studied are *Fiat 500X*, *Fiat Tipo*, *Alfa Romeo Stelvio* and *Alfa Romeo Giulia.*

Figure 3.7: View of Fiat 500X [6]

Figure 3.8: View of Fiat Tipo [18]

Figure 3.9: View of Alfa Romeo Stelvio [3]

Figure 3.10: View of Alfa Romeo Giulia [2]

3.5.1 Fiat 500X

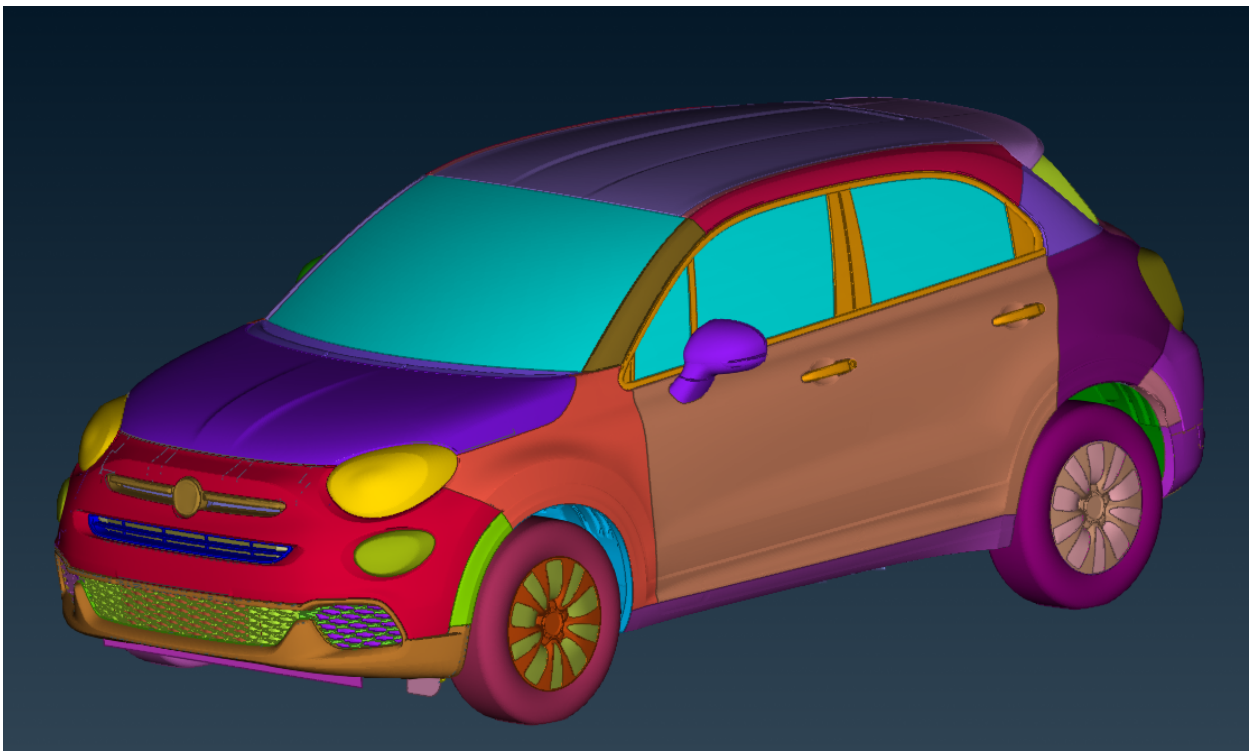

Figure 3.11: View of ANSA BETA CAE of Fiat 500X

Four different configurations of the vehicle have been studied. In particular, modifications focused on the C-Nolder and closed-grille simulations and they are resumed in the following table:

Configuration Number	Model Configuration
1	Opened-grille and Base C-Nolder
2	Opened Grille and No C-Nolder
3	Opened-Grille and C-Nolder-D-Node
4	Closed-Grille and Base C-Nolder

Table 3.2: Different configurations of Fiat 500X

The following pictures show the implementation of geometry modification applied on ANSA BETA CAE for the four different configurations.

Figure 3.12: Back view of the first configuration - Base C-Nolder with opened grille

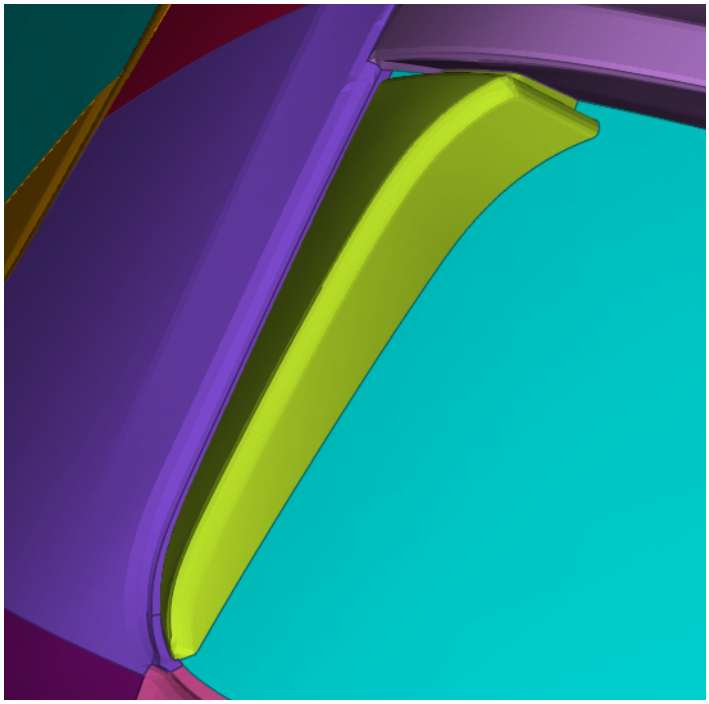

Figure 3.13: Zoom of the Nolder - Base C-Nolder with opened grille

Figure 3.14: Back view of the second configuration - No C-Nolder with opened grille

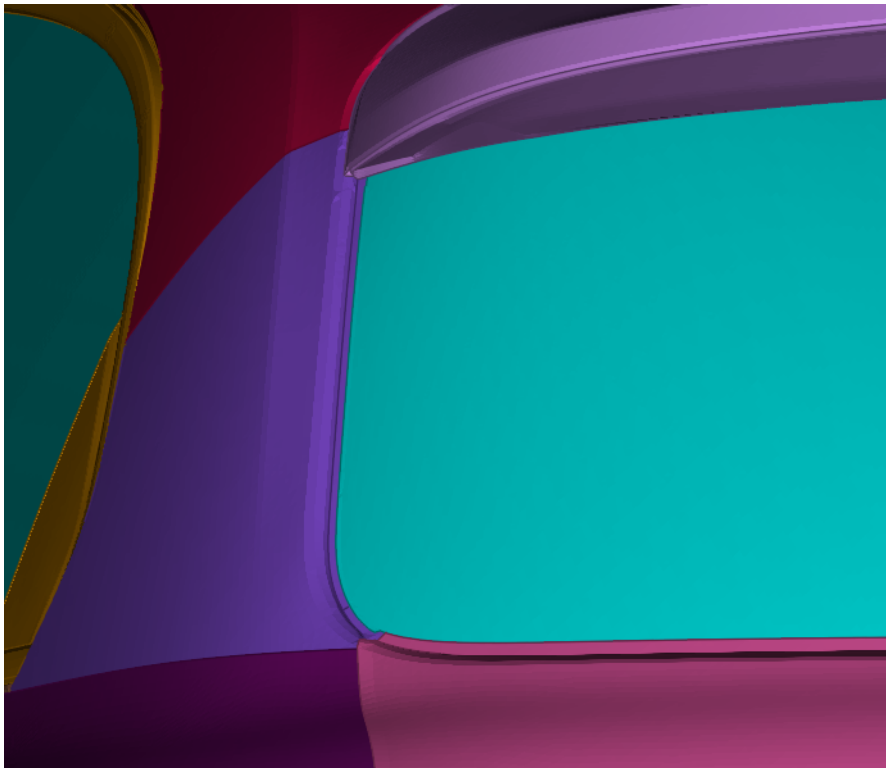

Figure 3.15: Zoom of the area without the C-Nolder - No C-Nolder with opened grille

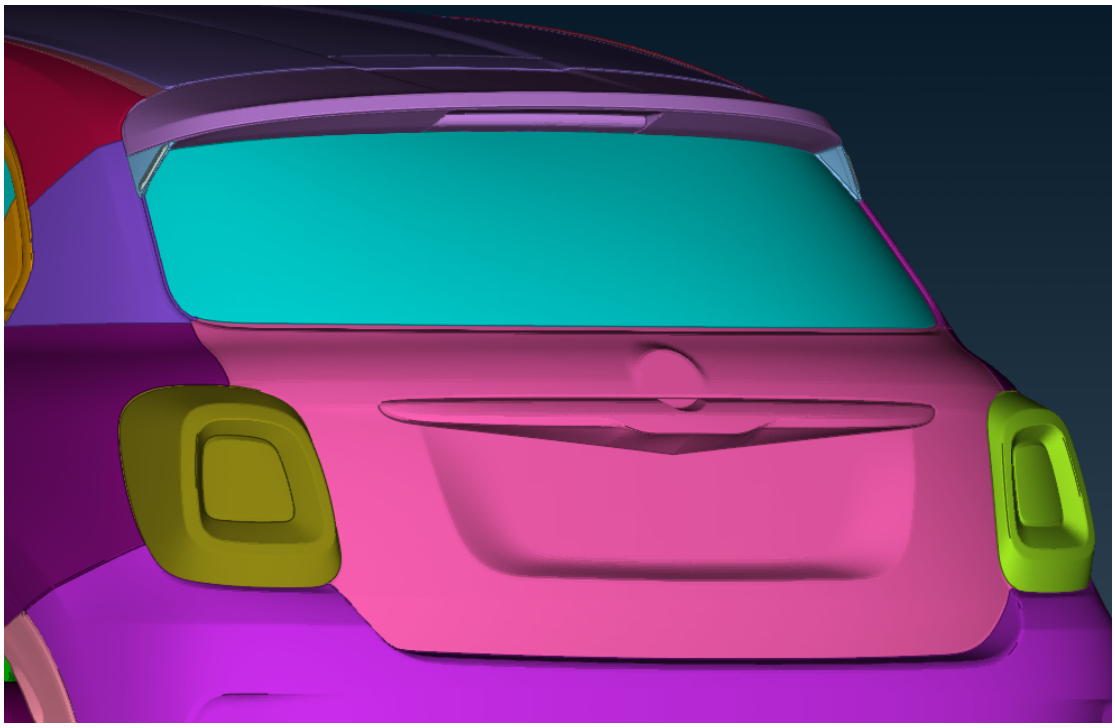

Figure 3.16: Back view of the third configuration - C-Nolder-D-Node with opened grille

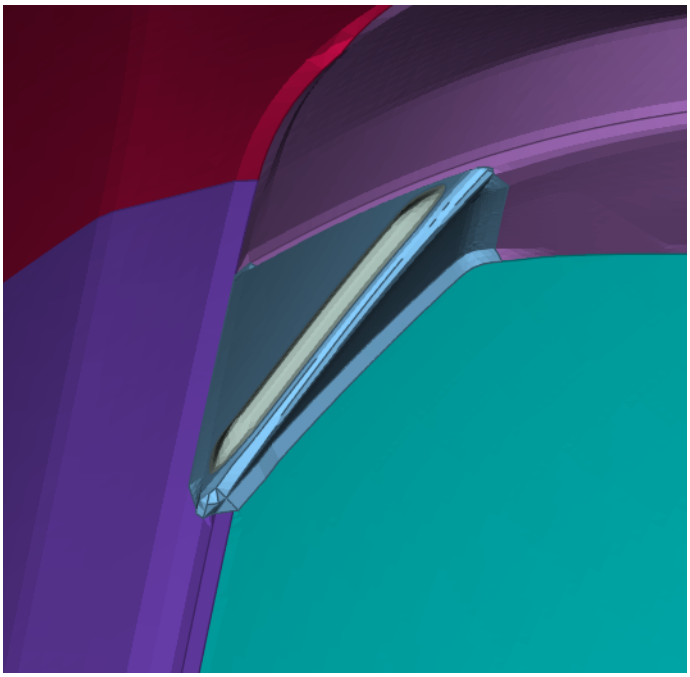

Figure 3.17: Zoom of the area with the C-Nolder-D-Node - C-Nolder-D-Node with opened grille

Considering that there is no modification of the geometry in the fourth configuration compared to the first one, it is not necessary to report pictures.

The tables which resume the results in term of absolute C_x are shown below. It is important

to underline that absolute values are obtain by dividing the value of C_x by a reference value, which is the drag coefficient collected during the tests in the wind tunnel.

500x base C-Nolder with opened grille	
Type of Analysis	**Cx**
Wind Tunnel	1
K-epsilon-1st strategy of meshing	0,96
K-omega-1st strategy of meshing	0,94
K-epsilon-2nd strategy of meshing	0,98
K-omega-2nd strategy of meshing	0,97
Lag-EB-2nd strategy of meshing	0,95

Table 3.3: Absolute C_x for the first configuration of Fiat 500x

500x base No C-Nolder with opened grille	
Type of Analysis	**Cx**
Wind Tunnel	1
K-epsilon-1st strategy of meshing	0,94
K-omega-1st strategy of meshing	0,92
K-epsilon-2nd strategy of meshing	0,96
K-omega-2nd strategy of meshing	0,95
Lag-EB-2nd strategy of meshing	0,94

Table 3.4: Absolute C_x for the second configuration of Fiat 500x

500x base C-Nolder Node-D with opened grille	
Type of Analysis	**Cx**
Wind Tunnel	1
K-epsilon-1st strategy of meshing	0,94
K-omega-1st strategy of meshing	0,92
K-epsilon-2nd strategy of meshing	0,96
K-omega-2nd strategy of meshing	0,95
Lag-EB-2nd strategy of meshing	0,93

Table 3.5: Absolute C_x for the third configuration of Fiat 500x

500x base C-Nolder with closed grille	
Type of Analysis	**Cx**
Wind Tunnel	1
K-epsilon-1st strategy of meshing	0,96
K-omega-1st strategy of meshing	0,93
K-epsilon-2nd strategy of meshing	1
K-omega-2nd strategy of meshing	0,98
Lag-EB-2nd strategy of meshing	0,96

Table 3.6: Absolute C_x for the fourth configuration of Fiat 500x

In the charts presented below, the results just reported in the tables are plotted on Cartesian axes. Specifically, on the y-axis, the values of absolute resistance coefficients C_x are shown, while on the x-axis, the corresponding meshing and turbulence models are displayed. It is important to say that to assess to the first strategy of meshing the word "Aerotools" is used, whereas to refer to the second strategy the words "No Wrap" are used.

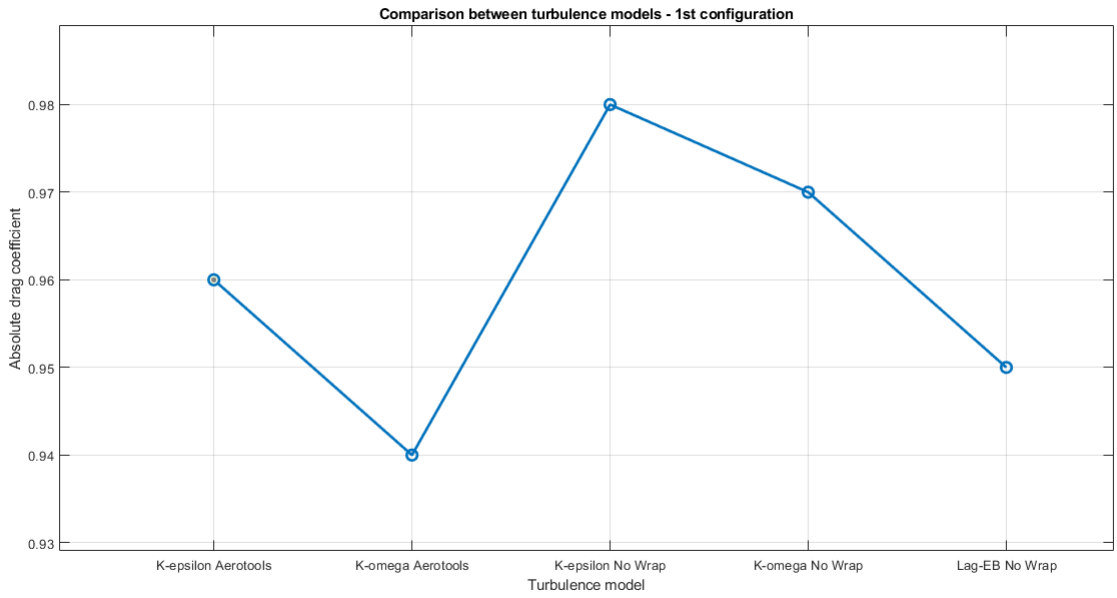

Figure 3.18: Comparison between turbulence models - 1st configuration

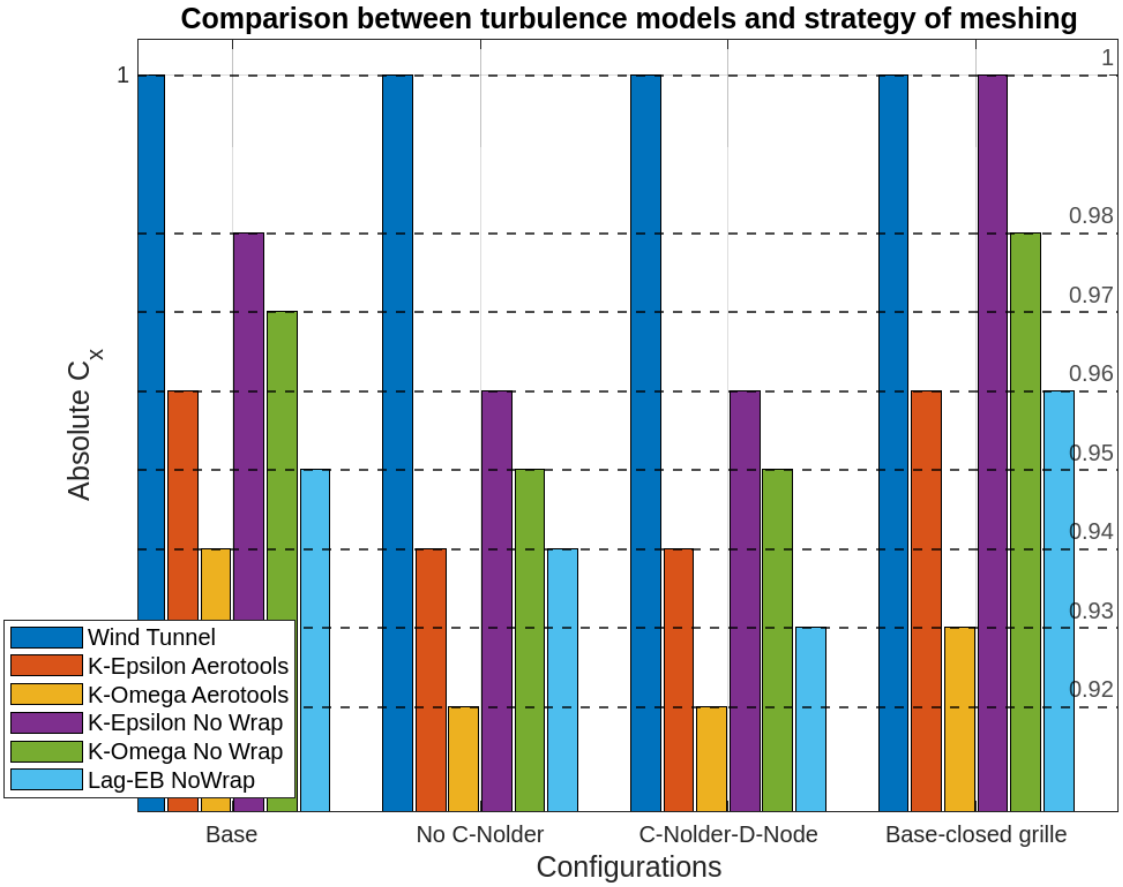

Figure 3.19: Comparison between turbulence models and configurations for Fiat 500x

Once that the drag coefficients C_x have been evaluated for each configuration with all turbulence models and strategies of meshing, it is important to see the values of the deltas predicted respect the base configuration (1st configuration). Obviously, the rows corresponding to the base configuration has all the values of ΔC_x equal to zero. The results are resumed in the following tables:

Model	**Delta Cx Wind Tunnel**
500x base C-Nolder with opened grille	0,000
500x No C-Nolder with opened grille	0,005
500x C-Nolder Node-D with opened grille	0,006
500x base C-Nolder with closed grille	-0,010

Table 3.7: ΔC_x-Wind Tunnel

Model	Delta Cx K-epsilon Aerotools
500x base C-Nolder with opened grille	0,000
500x No C-Nolder with opened grille	0,000
500x C-Nolder Node-D with opened grille	0,000
500x base C-Nolder with closed grille	-0,009

Table 3.8: ΔC_x-K-epsilon Aerotools

Model	Delta Cx K-omega Aerotools
500x base C-Nolder with opened grille	0,000
500x No C-Nolder with opened grille	-0,001
500x C-Nolder Node-D with opened grille	-0,001
500x base C-Nolder with closed grille	-0,011

Table 3.9: ΔC_x-K-omega Aerotools

Model	Delta Cx K-epsilon No Wrap
500x base C-Nolder with opened grille	0,000
500x No C-Nolder with opened grille	-0,001
500x C-Nolder Node-D with opened grille	-0,001
500x base C-Nolder with closed grille	-0,002

Table 3.10: ΔC_x-K-epsilon No Wrap

Model	Delta Cx K-omega No Wrap
500x base C-Nolder with opened grille	0,000
500x No C-Nolder with opened grille	-0,002
500x C-Nolder Node-D with opened grille	0,000
500x base C-Nolder with closed grille	-0,006

Table 3.11: ΔC_x-K-omega No Wrap

Model	Delta Cx Lag-EB No Wrap
500x base C-Nolder with opened grille	0,000
500x No C-Nolder with opened grille	0,000
500x C-Nolder Node-D with opened grille	0,000
500x base C-Nolder with closed grille	-0,005

Table 3.12: ΔC_x-Lag-EB No Wrap

In order to have a better view and comprehension of how the variation of the geometry affected the prediction of the deltas, the following graphs are reported:

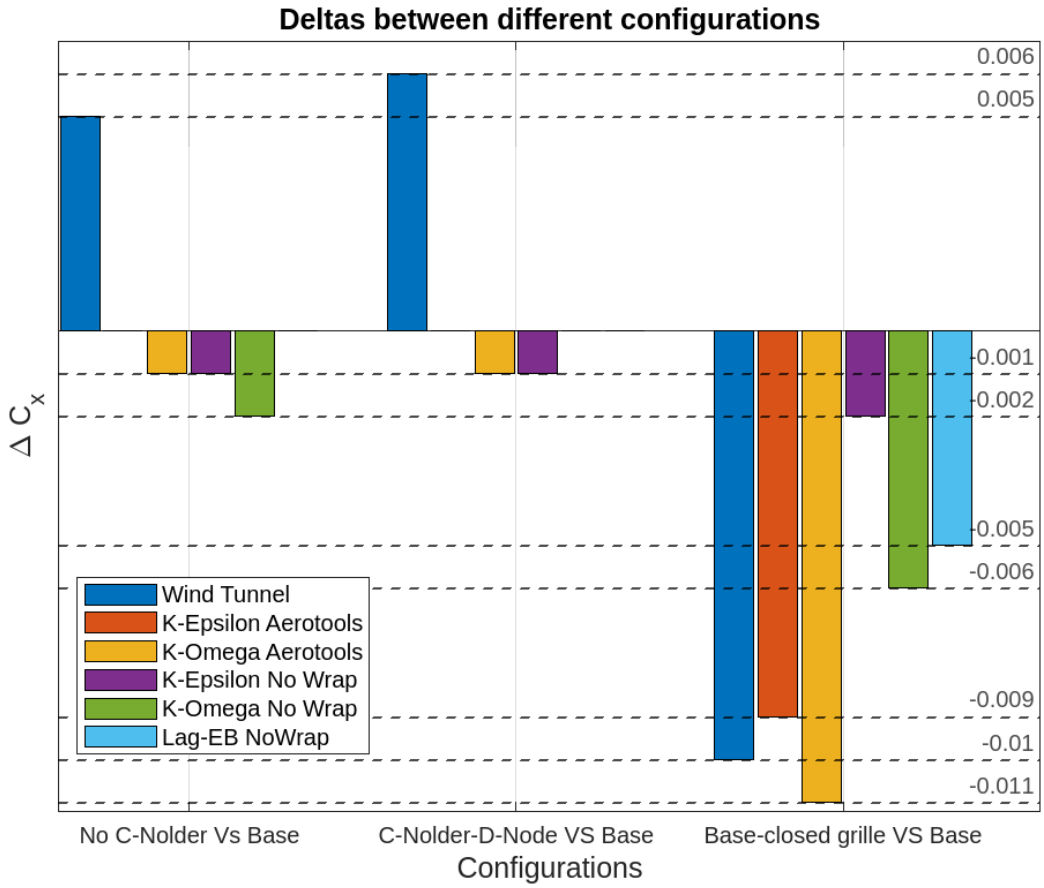

Figure 3.20: Variation in terms of drag coefficient respect to the base model

Conclusions and the additional analysis are reported in the next chapter.

3.5.2 Fiat Tipo

Figure 3.21: View of ANSA BETA CAE of Fiat Tipo

The analysis which has been conducted on this vehicle focused on the computation of the drag coefficient using the two different approaches and the 3 turbulence models. No geometry modifications have been implemented. The results in term of absolute drag coefficient are reported in the following table:

Type of Analysis	**Cx**
Wind Tunnel	1
K-epsilon-1st strategy of meshing	0,98
K-omega-1st strategy of meshing	0,95
K-epsilon-2nd strategy of meshing	0,98
K-omega-2nd strategy of meshing	0,98
Lag-EB-2nd strategy of meshing	0,96

Table 3.13: Absolute C_x for Fiat Tipo

In the charts presented below, the results just reported in the tables are plotted on Cartesian axes. Specifically, on the y-axis, the values of absolute resistance coefficients C_x are shown, while on the x-axis, the corresponding meshing and turbulence models are displayed. It is important to say that to assess to the first strategy of meshing the word "Aerotools" is used, whereas to refer to the second strategy the words "No Wrap" are used.

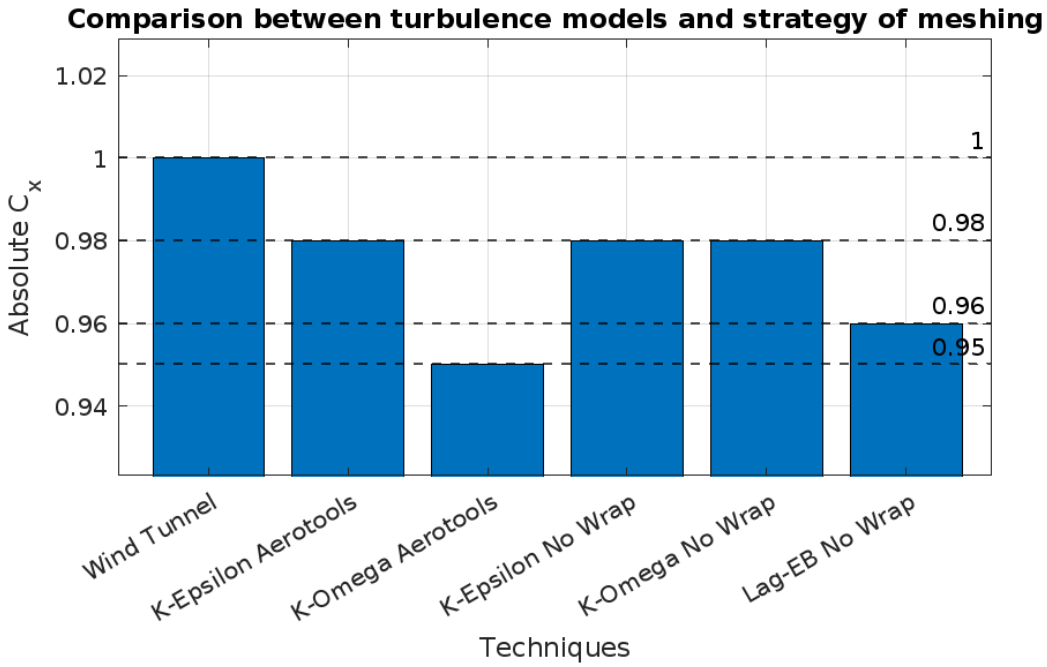

Figure 3.22: Absolute C_x of Fiat Tipo

Conclusions and the additional analysis are reported in the next chapter.

3.5.3 Alfa Romeo Stelvio

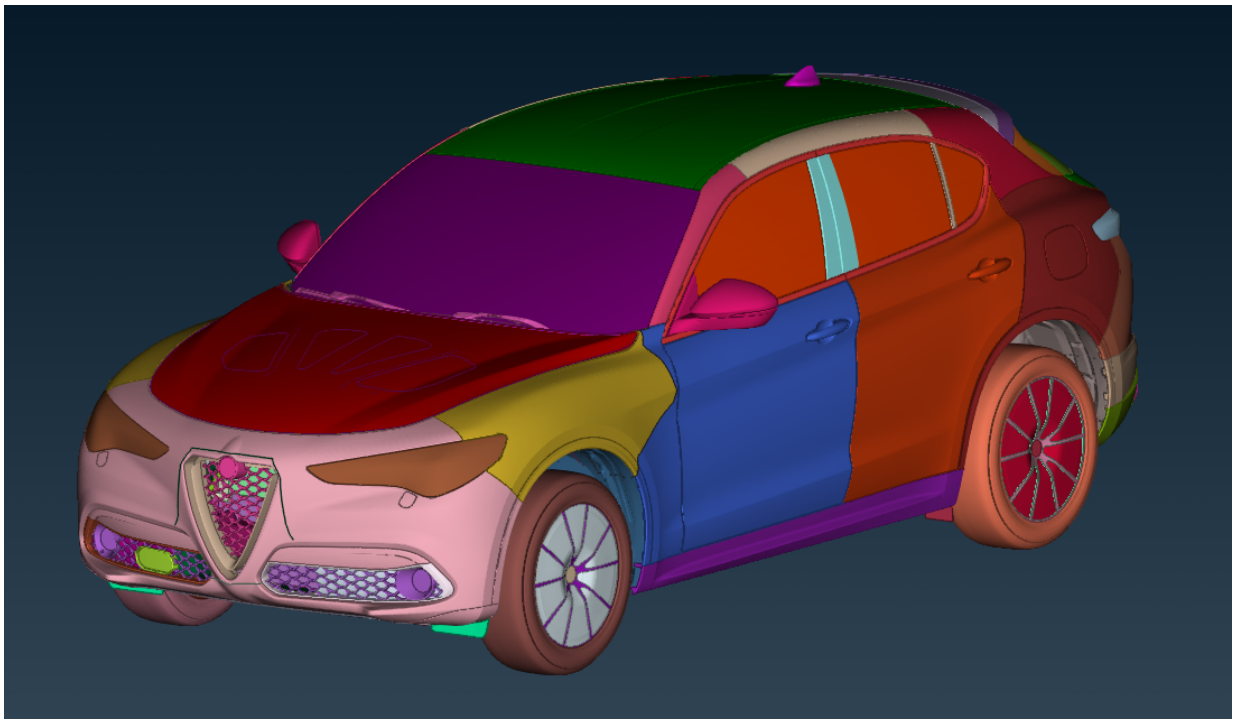

Figure 3.23: View of ANSA BETA CAE of Alfa Romeo Stelvio

The analysis which has been conducted on this vehicle focused on the computation of the drag coefficient using the two different approaches and the 3 turbulence models. One geometry modification has been implemented. In particular, using the software ANSA BETA CAE a component called Dam has been added in the rear of the vehicle, as it is shown in the following pictures.

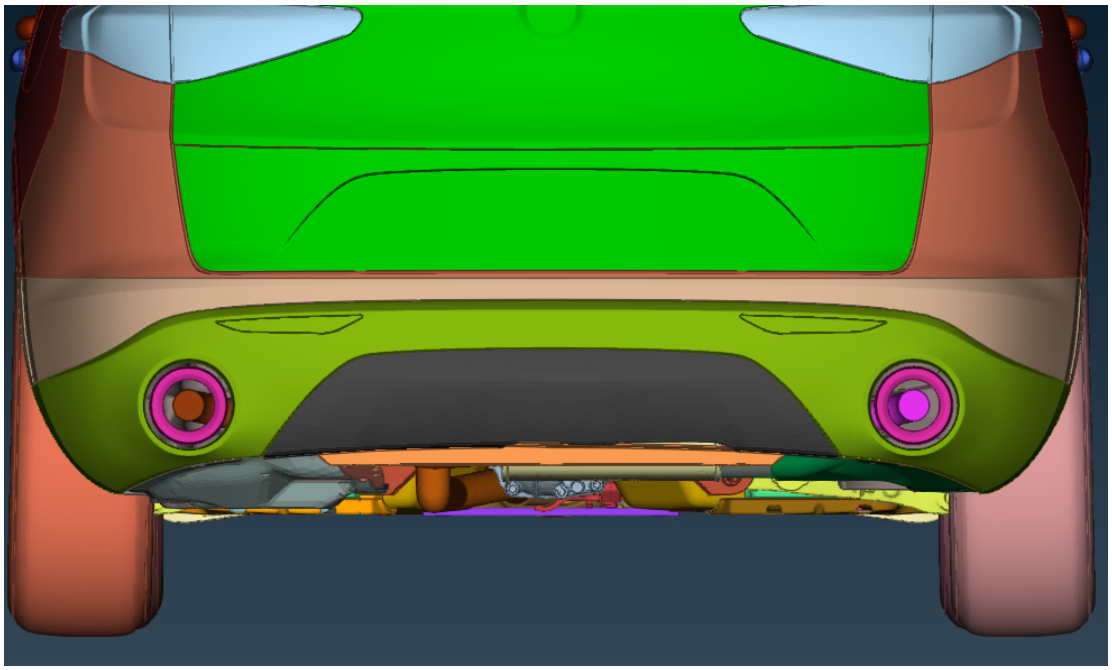

Figure 3.24: Back view of Alfa Romeo Stelvio

Figure 3.25: Dam added to Alfa Romeo Stelvio

The results in term of absolute drag coefficient are reported in the following table:

Type of Analysis	Cx
Wind Tunnel	1
K-epsilon-1st strategy of meshing	1.03
K-omega-1st strategy of meshing	1.05
K-epsilon-2nd strategy of meshing	1.05
K-omega-2nd strategy of meshing	1.05
Lag-EB-2nd strategy of meshing	1.05

Table 3.14: Absolute C_x for Alfa Romeo Stelvio

In the charts presented below, the results just reported in the tables are plotted on Cartesian axes. Specifically, on the y-axis, the values of absolute resistance coefficients Cx are shown, while on the x-axis, the corresponding meshing and turbulence models are displayed. It is important to say that to assess to the first strategy of meshing the word "Aerotools" is used, whereas to refer to the second strategy the words "No Wrap" are used.

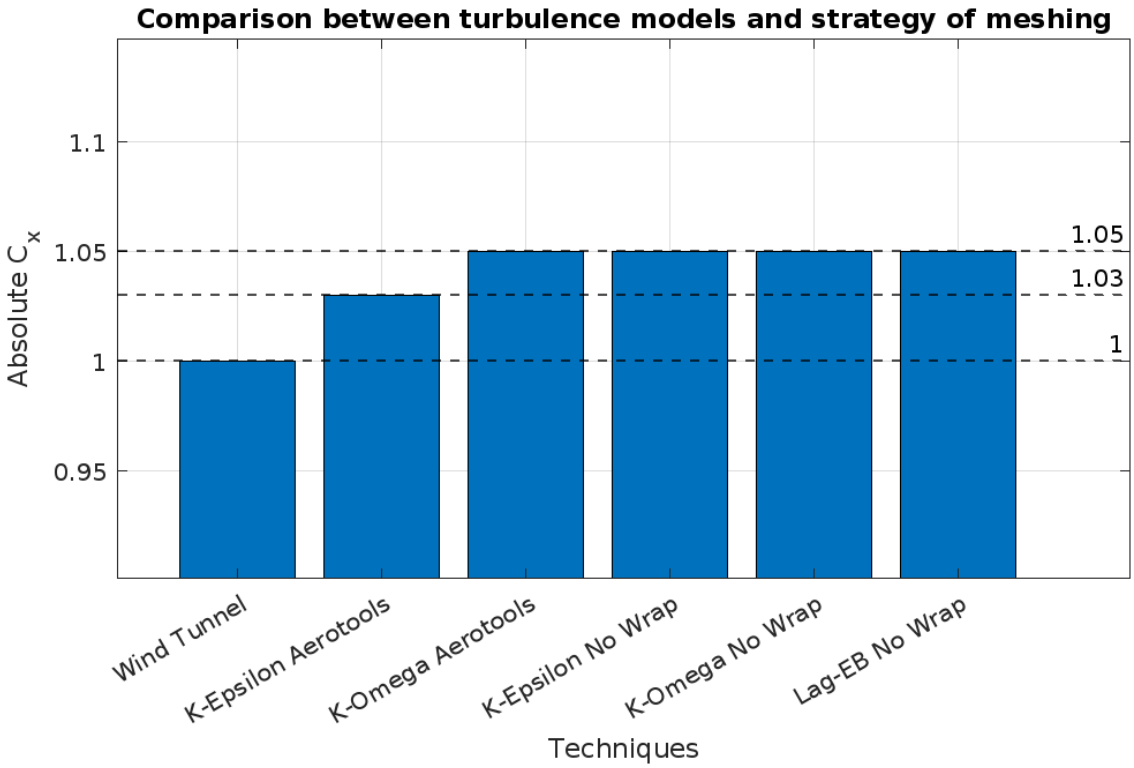

Figure 3.26: Absolute C_x of Alfa Romeo Stelvio

Conclusions and the additional analysis are reported in the next chapter.

3.5.4 Alfa Romeo Giulia

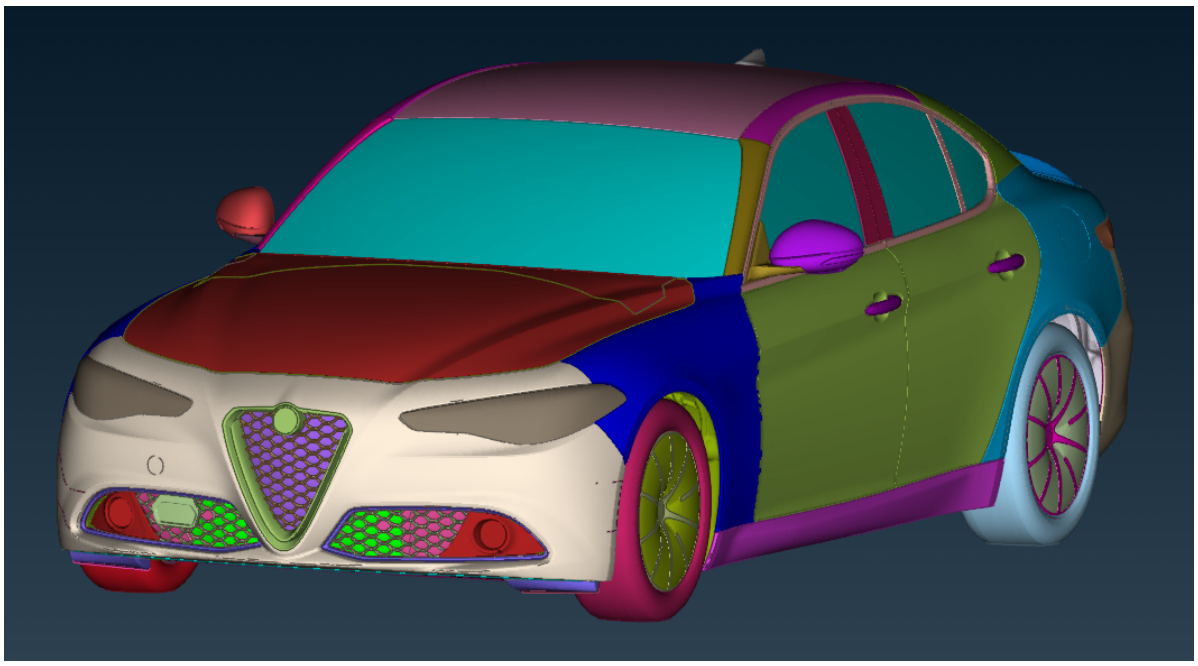

Figure 3.27: View of ANSA BETA CAE of Alfa Romeo Giulia

Two different configurations of the vehicle have been studied. In particular, modifications focused on the rear of the vehicle. In greater details, the modification applied to the first configuration (Baseline) consisted in the addition of a rear spoiler.

Configuration Number	Model Configuration
1	Baseline
2	Baseline with rear spoiler

Table 3.15: Different configurations of Alfa Romeo Giulia

The following pictures show the implementation of geometry modification applied on ANSA BETA CAE for the two different configurations.

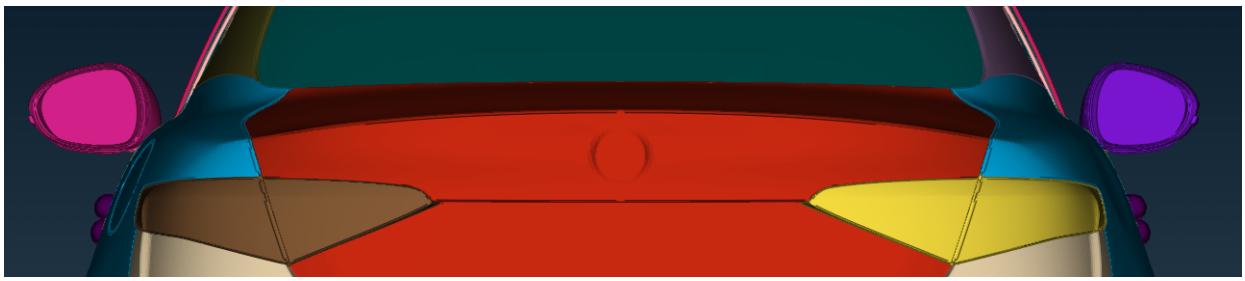

Figure 3.28: Back view of the first configuration - Baseline

Figure 3.29: Zoom of the rear of the vehicle - Baseline

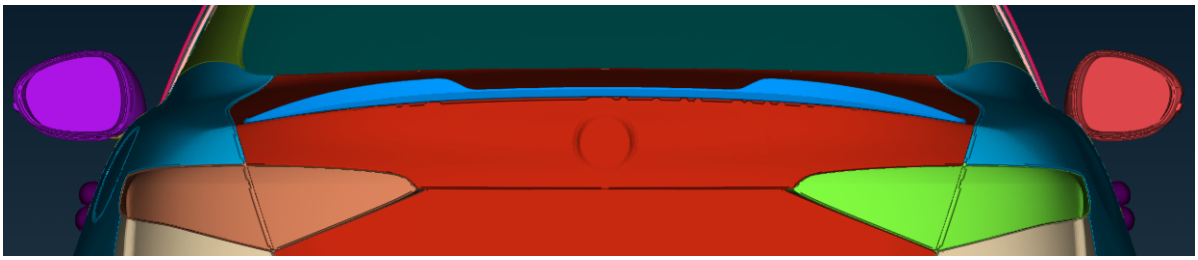

Figure 3.30: Back view of the second configuration - Baseline with spoiler

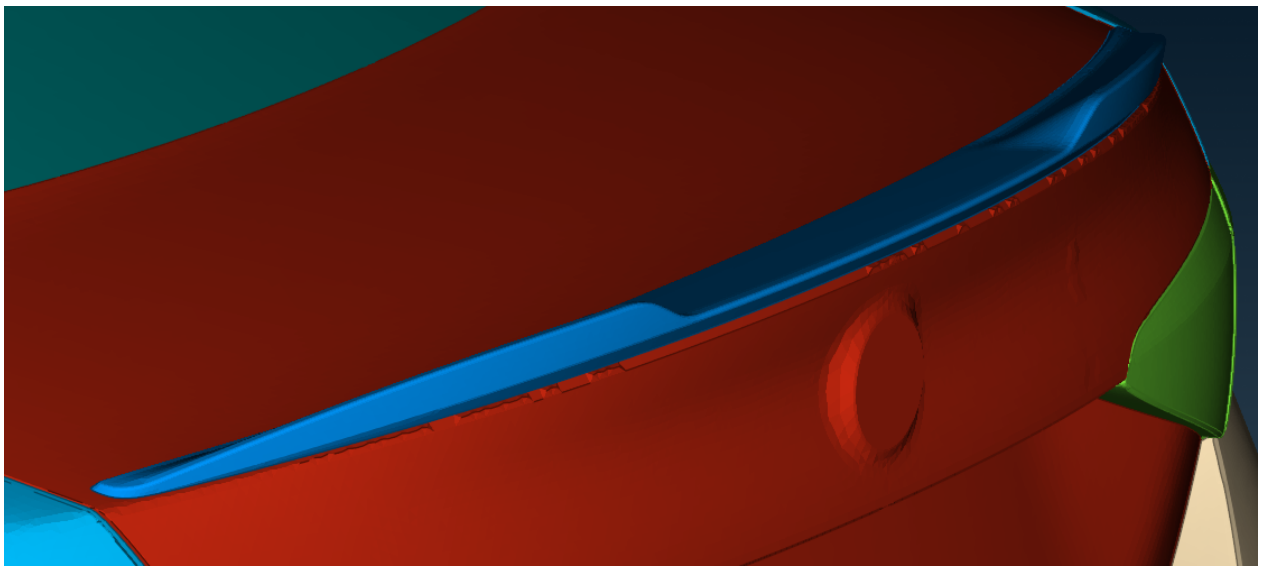

Figure 3.31: Zoom of the rear of the vehicle - Baseline with spoiler

The tables which resume the results in term of absolute Cx are shown below. It is important to underline that absolute values are obtain by dividing the value of C_x by a reference value, which is the drag coefficient collected during the tests in the wind tunnel.

Alfa Romeo Giulia Baseline	
Type of Analysis	**Cx**
Wind Tunnel	1
K-epsilon-1st strategy of meshing	1.02
K-omega-1st strategy of meshing	0,99
K-epsilon-2nd strategy of meshing	1.04
K-omega-2nd strategy of meshing	1.03
Lag-EB-2nd strategy of meshing	1.01

Table 3.16: Absolute C_x for the Baseline configuration of Alfa Romeo Giulia

Alfa Romeo Giulia Baseline with rear spoiler	
Type of Analysis	**Cx**
Wind Tunnel	1
K-epsilon-1st strategy of meshing	1.02
K-omega-1st strategy of meshing	0,99
K-epsilon-2nd strategy of meshing	1.03
K-omega-2nd strategy of meshing	1.02
Lag-EB-2nd strategy of meshing	1.01

Table 3.17: Absolute C_x for the Baseline configuration with spoiler of Alfa Romeo Giulia

In the charts presented below, the results just reported in the tables are plotted on Cartesian axes. Specifically, on the y-axis, the values of absolute resistance coefficients Cx are shown, while on the x-axis, the corresponding meshing and turbulence models are displayed. It is important to say that to assess to the first strategy of meshing the word "Aerotools" is used, whereas to refer to the second strategy the words "No Wrap" are used.

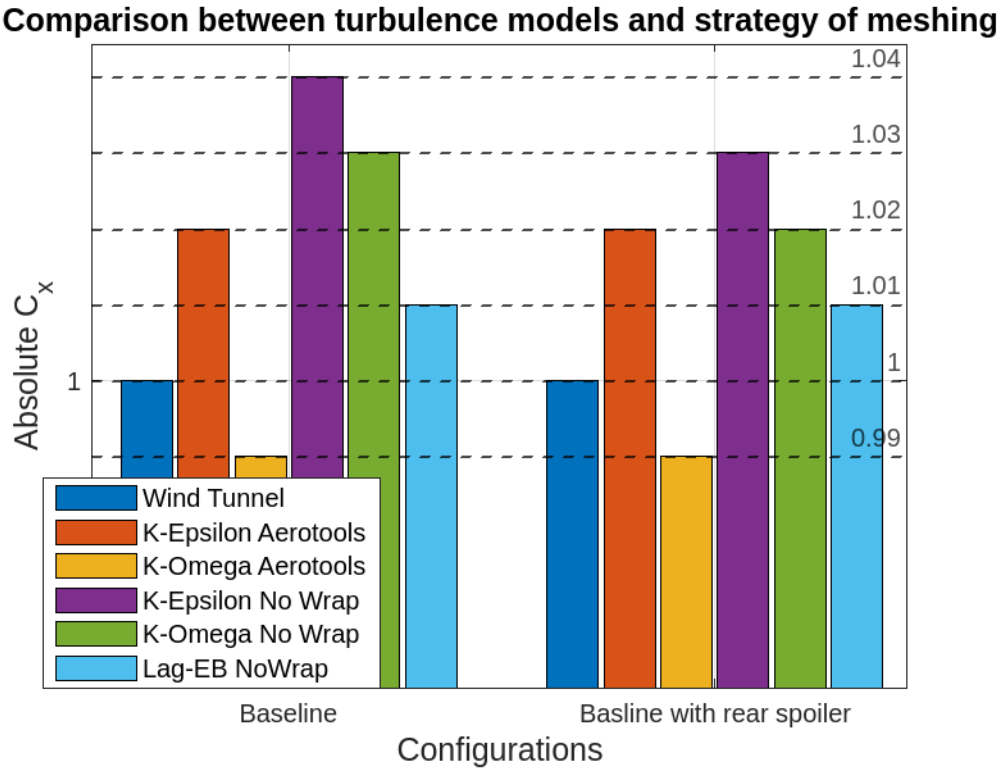

Figure 3.32: Comparison between turbulence models and configurations for Alfa Romeo Giulia

Once that the drag coefficients C_x have been evaluated for each configuration with all turbulence models and strategies of meshing, it is important to see the values of the deltas predicted respect the base configuration. The results are resumed in the following table:

Alfa Romeo Giulia prediceted Deltas	
Type of Analysis	**Delta Cx**
Wind Tunnel	0.007
K-epsilon-1st strategy of meshing	0.007
K-omega-1st strategy of meshing	0.007
K-epsilon-2nd strategy of meshing	0.006
K-omega-2nd strategy of meshing	0.005
Lag-EB-2nd strategy of meshing	0.005

Table 3.18: ΔC_x Baseline with spoiler VS Baseline of Alfa Romeo Giulia

In order to have a better view and comprehension of how the variation of the geometry affected the prediction of the deltas, the following graphs are reported:

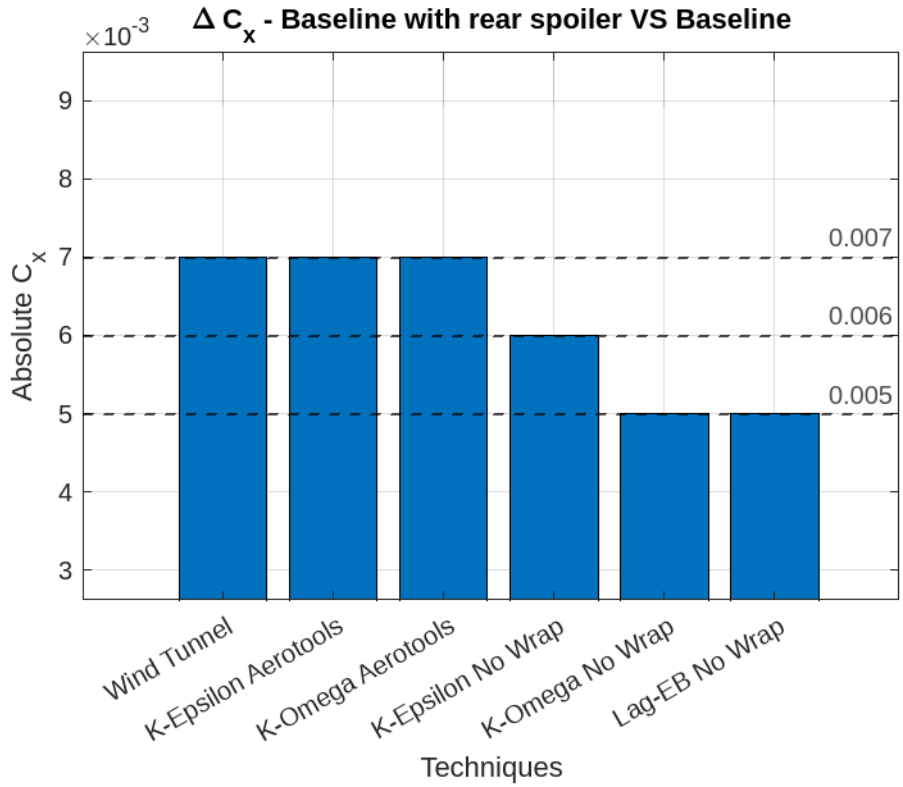

Figure 3.33: Variation in terms of drag coefficient respect to the base model for Alfa Romeo Giulia

Conclusions and the additional analysis are reported in the next chapter.

Chapter 4

Conclusions and additional analysis

In this chapter, conclusions are drawn based on the results presented in the preceding one. Additionally, further analyses will be conducted to explore in greater depth how geometric modifications and computational strategies have influenced the outcomes. This pivotal stage of the study aims to synthesize the data, offering insights into the broader implications of our findings. By examining the impact of geometric alterations alongside computational approaches, we aim to elucidate the nuanced interplay between these variables and their collective effect on the observed results. The chapter is divided in different sections for every different vehicle.

4.1 Fiat 500X

Referring to *Figure 3.19*, which reports values of absolute C_x for the vehicle, it shows a trend which is respected either with *Aerotools* and with *No Wrap* approach. As a matter of fact, with both strategies of meshing, the turbulence model which is closer to the value of the drag coefficient recorded in the wind tunnel is the *K-Epsilon*. Especially for the fourth configuration, the C_x computed is the same.

A different outcome results when deltas between different configurations are analyzed. None of the turbulence models studied were able to predict the deltas between the different configurations (compared with the base one). In greater details, the configuration without the nolder resulted in a slight decrease of the drag coefficient with almost every strategy and turbulence model, even though the data collected in the wind tunnel suggested an increase compared to the base configuration. Similar results may be observed in the comparison between the second configuration and the base one. The fourth configuration (the one with the close-grilled) has revealed that the first strategy of meshing is more precise than the second one in the prediction of the deltas, whereas the "No-Wrap" strategy turned out to be not equally accurate. Among all the turbulence model used in this study with the second strategy of meshing, the one which came closest to the experimental value is the K-omega. This big difference in the evaluation of the deltas in this fourth configuration (which main changing are in the front of the vehicle), are an be explained by observing the mesh in the grid area.

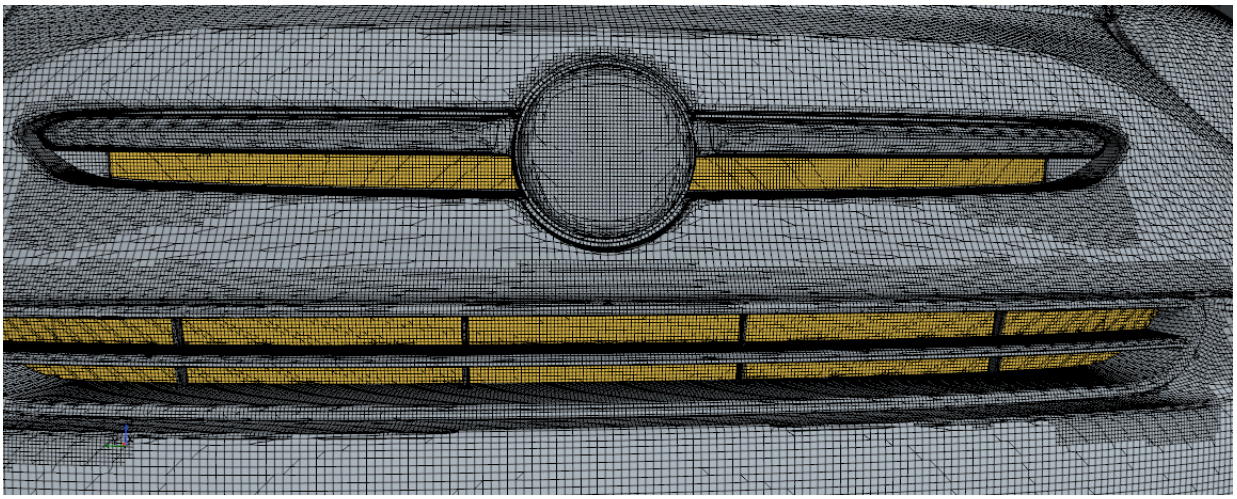

Figure 4.1: View of the mesh in the front of the vehicle using "Aerotools approach"

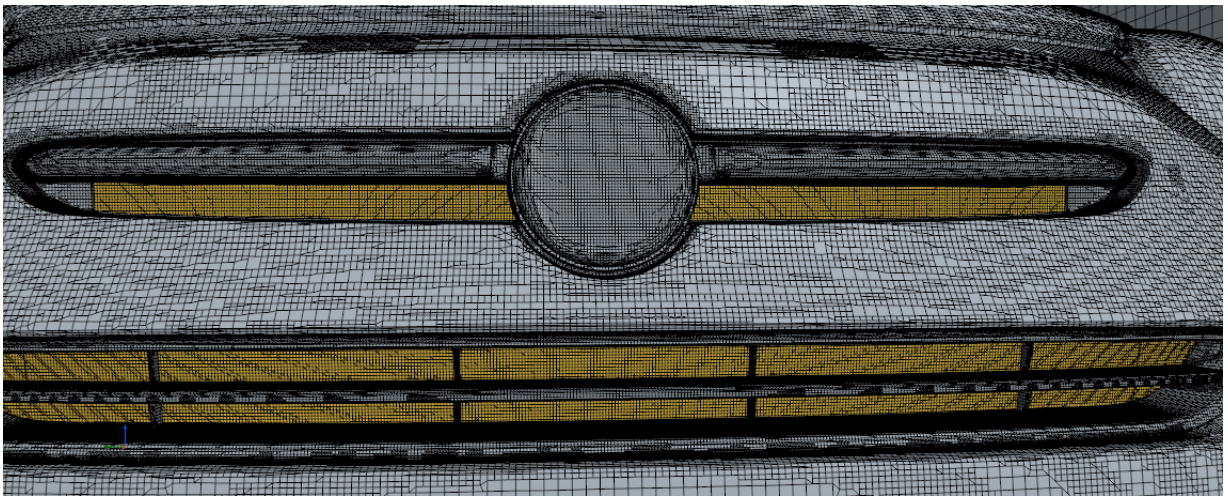

Figure 4.2: View of the mesh in the front of the vehicle using "No Wrap approach"

As it can be seen, in the areas close to the grill, the mesh generated more cells so the simulation in those areas is more accurate.

In order to see how the modification of the nolder affected the aerodynamics of the vehicle, it can be useful to check the skin friction coefficient which can give an idea of the separation of the flux, the pressure coefficient and a velocity plane which can show the develop of the wake downstream of the vehicle. Considering that the turbulence model which is accurate either in the prediction of the drag coefficient and in the prediction of deltas is the K-epsilon applied to the first strategy of meshing, the pictures below are those obtained with it.

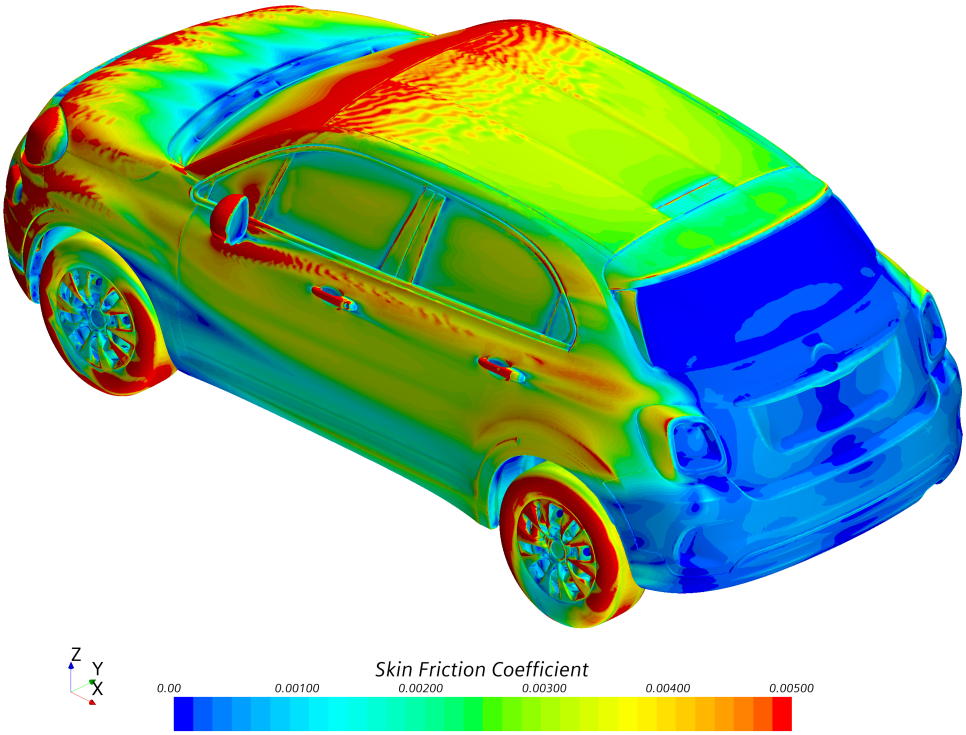

Figure 4.3: Back-Top-Left view of the skin coefficient obtained with the first strategy of meshing using K-epsilon turbulence model - Base configuration

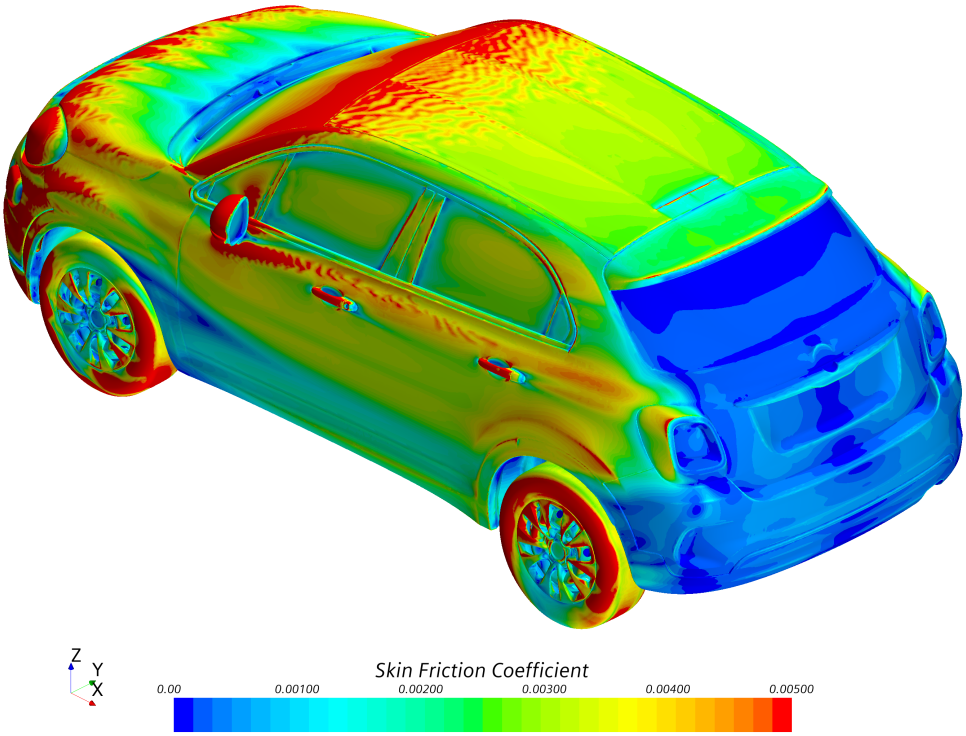

Figure 4.4: Back-Top-Left view of the skin coefficient obtained with the first strategy of meshing using K-epsilon turbulence model - 2nd configuration

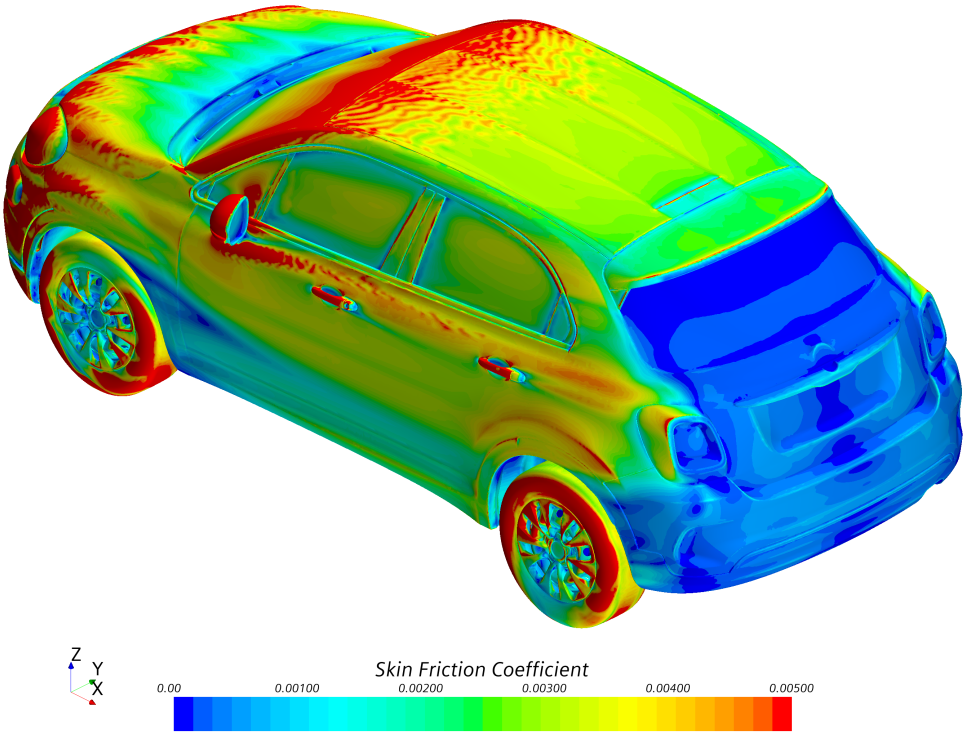

Figure 4.5: Back-Top-Left view of the skin coefficient obtained with the first strategy of meshing using K-epsilon turbulence model - 3rd configuration

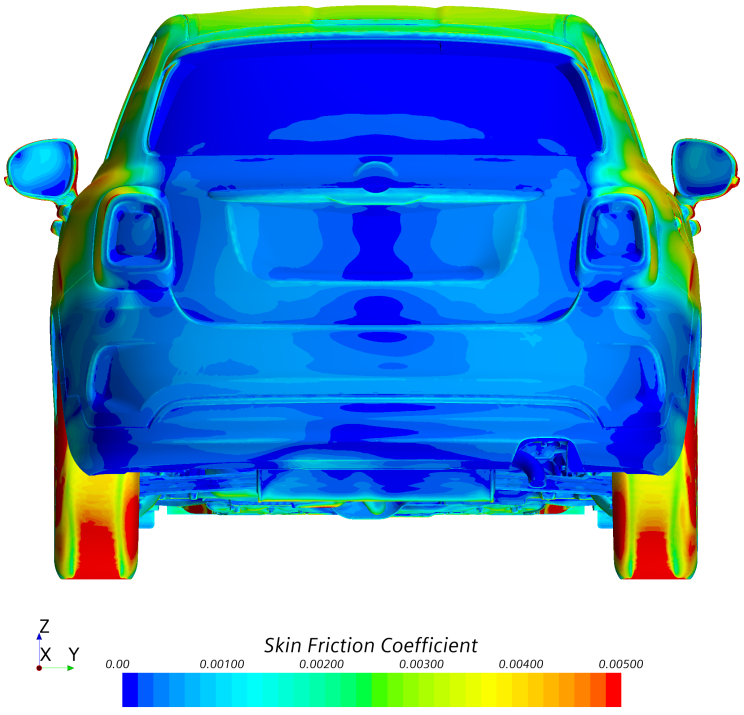

Figure 4.6: Back view of the skin coefficient obtained with the first strategy of meshing using K-epsilon turbulence model - Base configuration

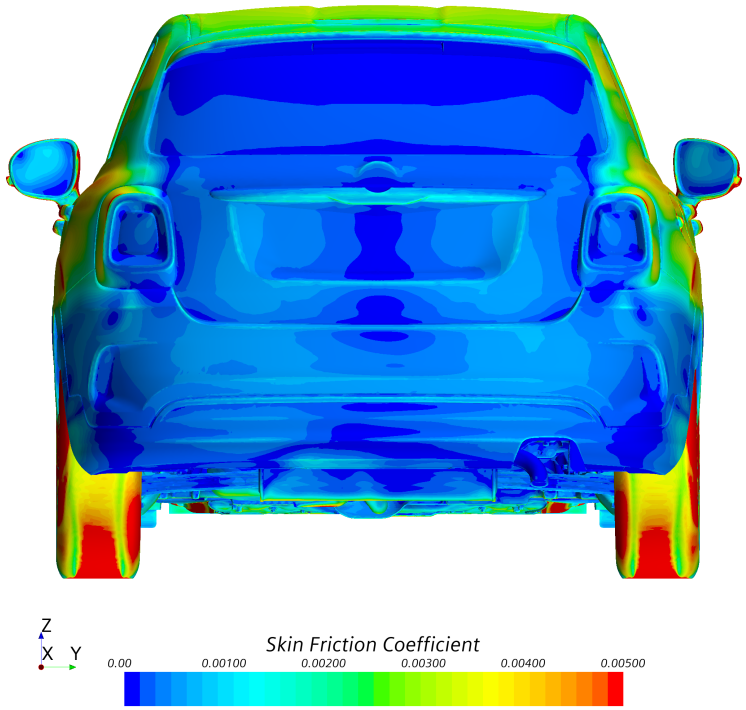

Figure 4.7: Back view of the skin coefficient obtained with the first strategy of meshing using K-epsilon turbulence model - 2nd configuration

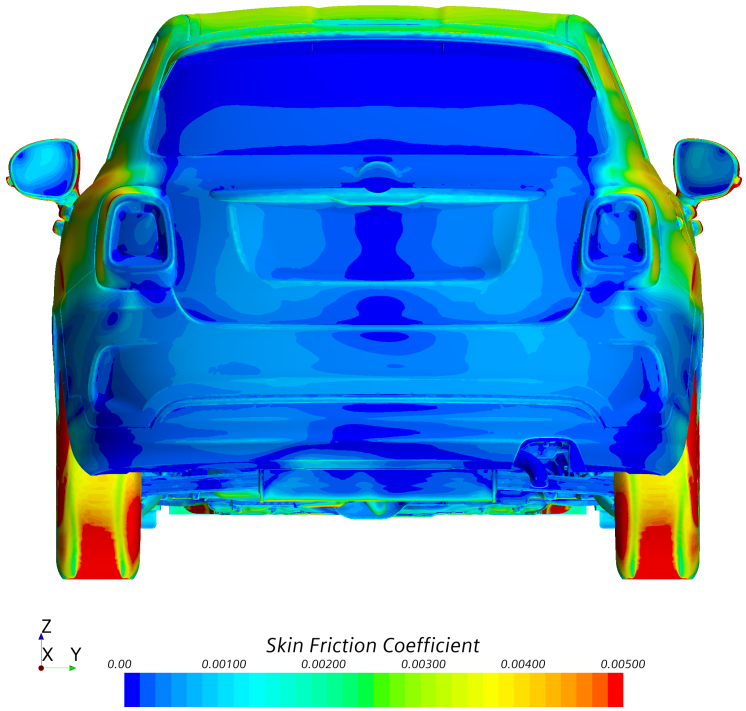

Figure 4.8: Back view of the skin coefficient obtained with the first strategy of meshing using K-epsilon turbulence model - 3rd configuration

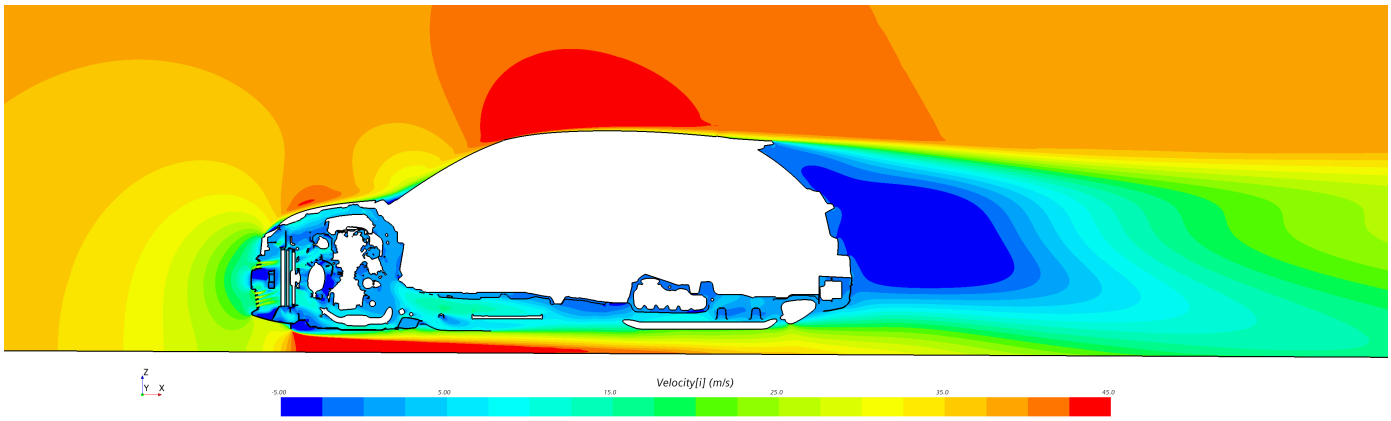

Figure 4.9: Cut plane of vehicle showing the velocity [i] obtained with the first strategy of meshing using K-epsilon turbulence model - Base configuration

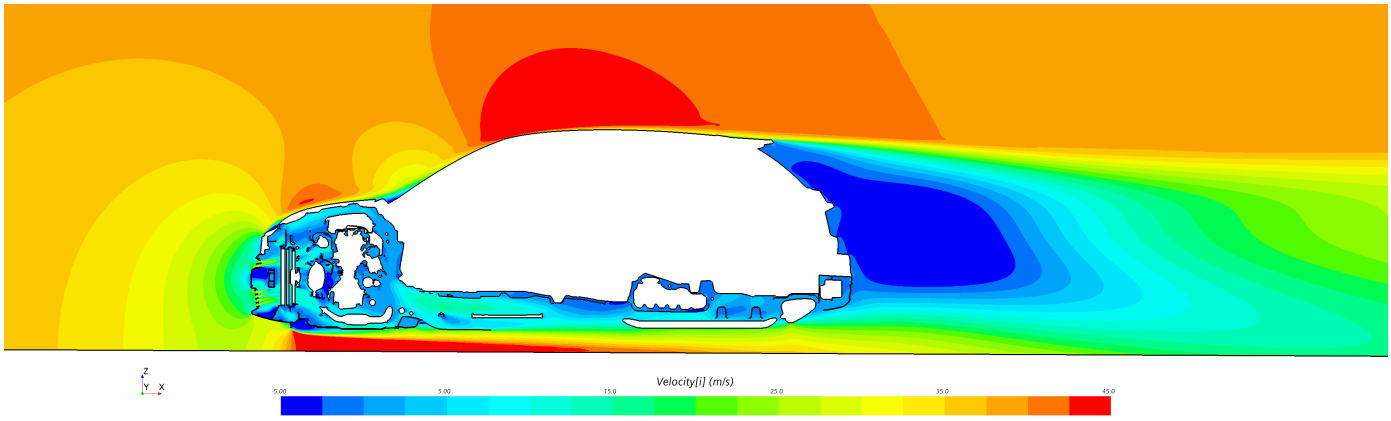

Figure 4.10: Cut plane of vehicle showing the velocity [i] obtained with the first strategy of meshing using K-epsilon turbulence model - 2nd configuration

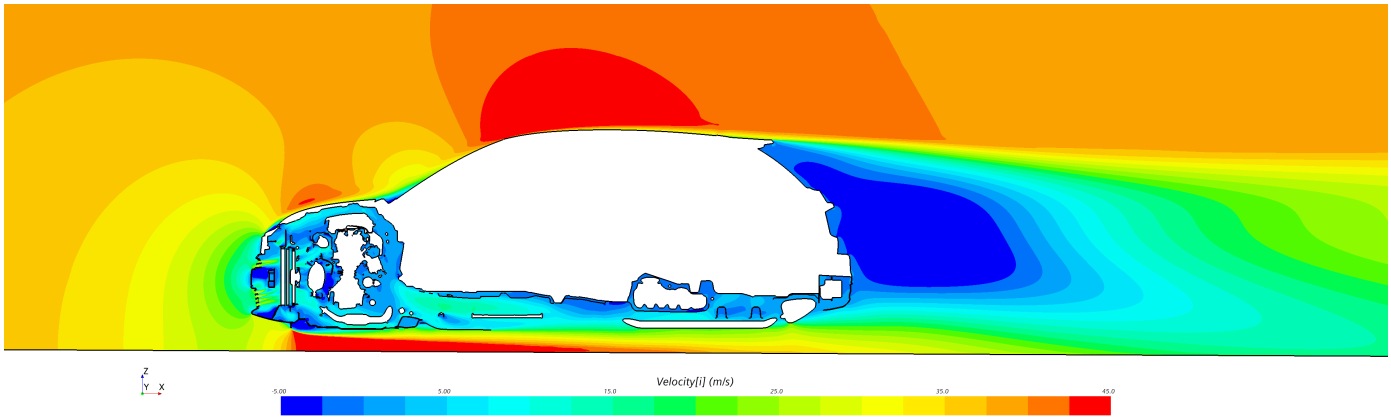

Figure 4.11: Cut plane of vehicle showing the velocity [i] obtained with the first strategy of meshing using K-epsilon turbulence model - 3rd configuration

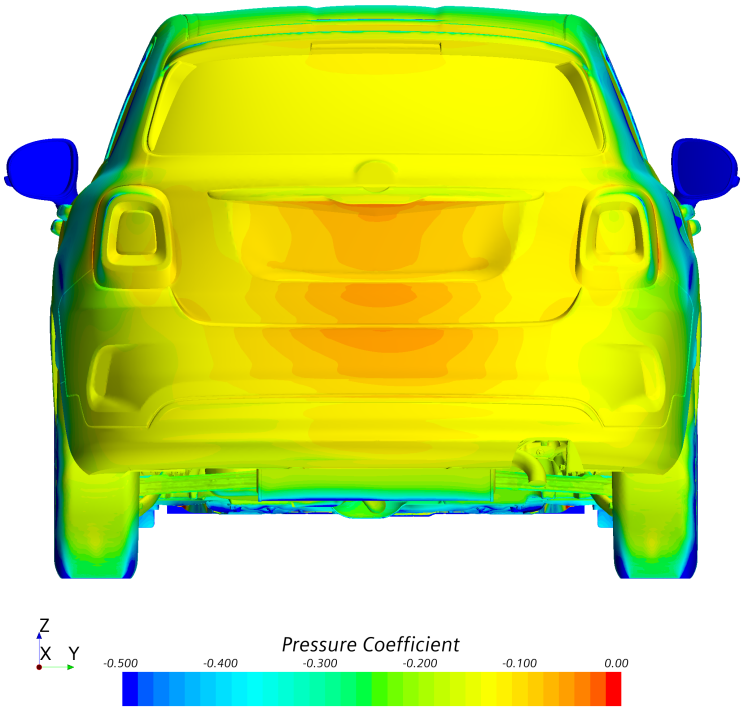

Figure 4.12: Cp obtained with the first strategy of meshing using K-epsilon turbulence model - Base configuration

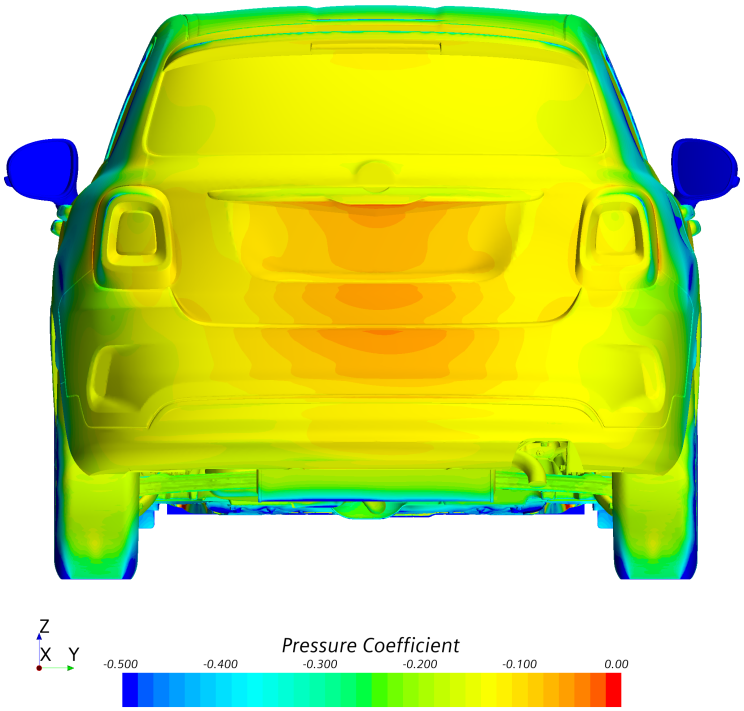

Figure 4.13: Cp obtained with the first strategy of meshing using K-epsilon turbulence model - 2nd configuration

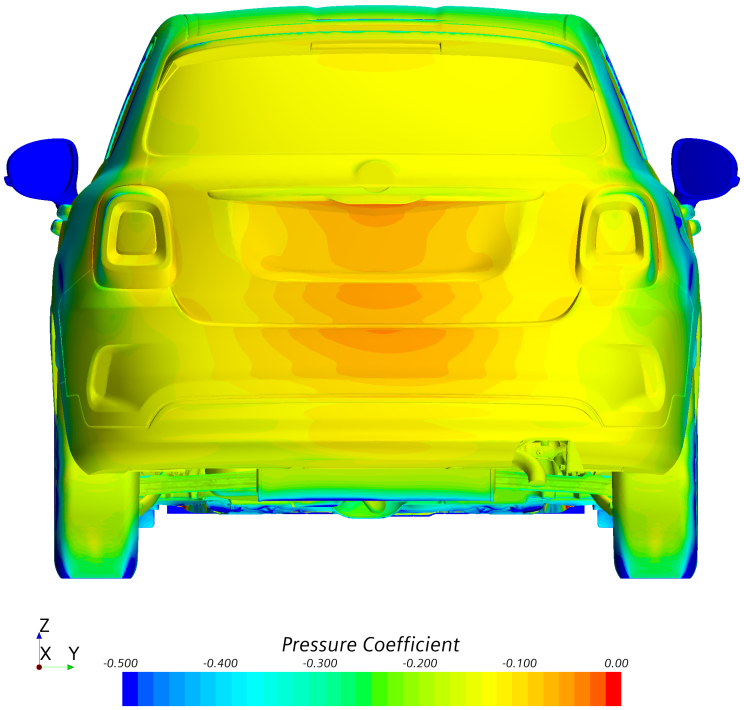

Figure 4.14: Cp obtained with the first strategy of meshing using K-epsilon turbulence model - rd configuration

As it can be seen from the previous images, it is clear how there are almost no changes in the prediction of the skin friction, the pressure coefficient and the shape and length of the low velocity area downstream the vehicle. This is in agreement with the incapacity of the simulation to collect the differences between the different configurations.

4.2 Fiat Tipo

Considering that only the Baseline configuration have been analyzed for this vehicle, no prediction of deltas between different configurations have been produced. The analysis focused on the prediction of the drag coefficient. Referring to *Figure 3.22*, which reports values of absolute C_x for the vehicle, it is shown how every different approach to the simulation predicted a drag coefficient which is lower than the one recorded in the wind tunnel. By comparing the values predicted with the simulations, it seems that the more effective turbulence model is the K-epsilon one, which turned out to be the closest to the value recorded in the wind tunnel. This result is in agreement with what was previously observed with the previous car model. It is important to underline that the fact that all the simulation predicted a lower drag coefficient compared to the wind tunnel one, may be due to several explanations. For example, in the wind tunnel there may be:

- **Edge interference**: If edge interferences generate turbulence or non-uniform flows around the model, they can increase the measured coefficient of resistance.

- **Effect of wind tunnel walls**: Wind tunnel walls can generate flow disturbances, especially near solid surfaces. This can increase the measured coefficient of resistance, particularly when the flow is affected by stagnation, vortices, or separations.

In addition to that, using the option to create probe points, an addition analysis has been conducted. As a matter of fact, in the wind tunnel many pressure taps have been used to register the pressure coefficient, so using some features of STAR CCM+ it was possible to record also the values predicted using the software of simulation. The pressure taps have been positioned as shown in the following images.

Figure 4.15: Pressure sensor position - 1

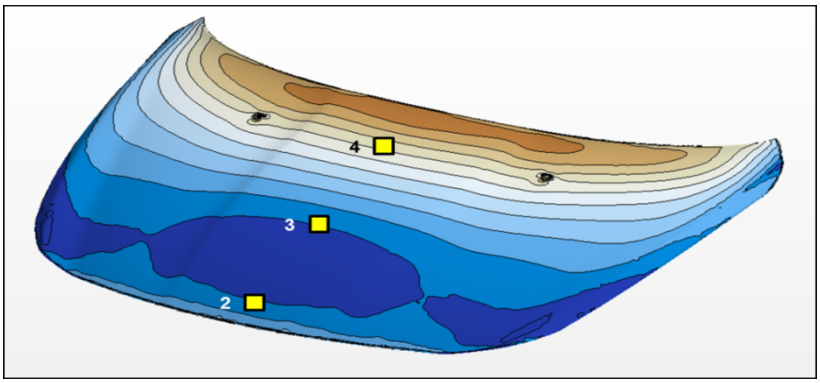

Figure 4.16: Pressure sensors position - 2

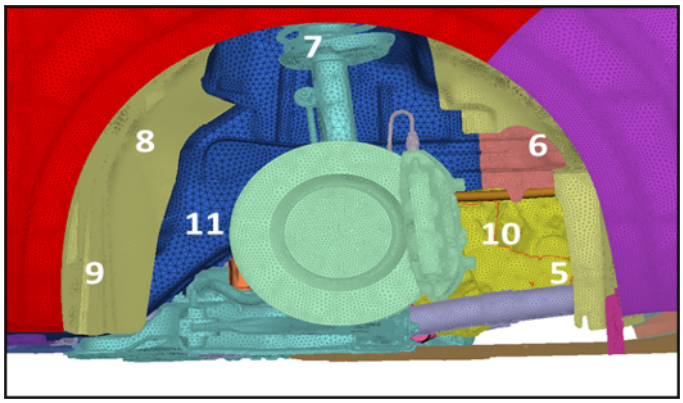

Figure 4.17: Pressure sensors position - 3

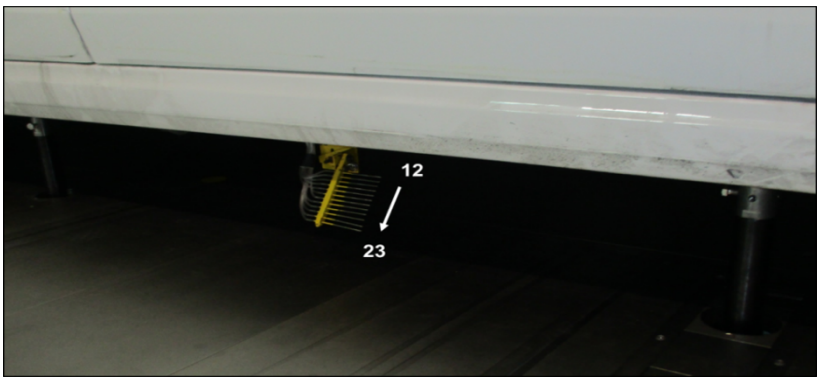

Figure 4.18: Pressure sensors position - 4

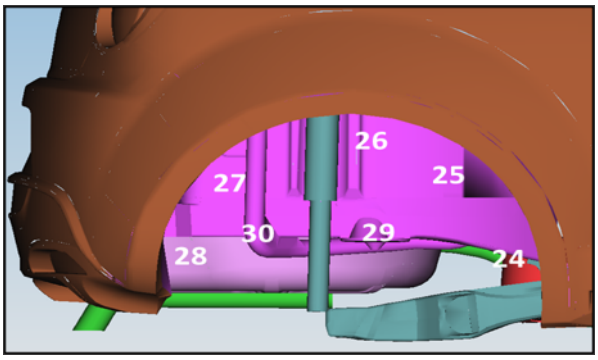

Figure 4.19: Pressure sensors position - 5

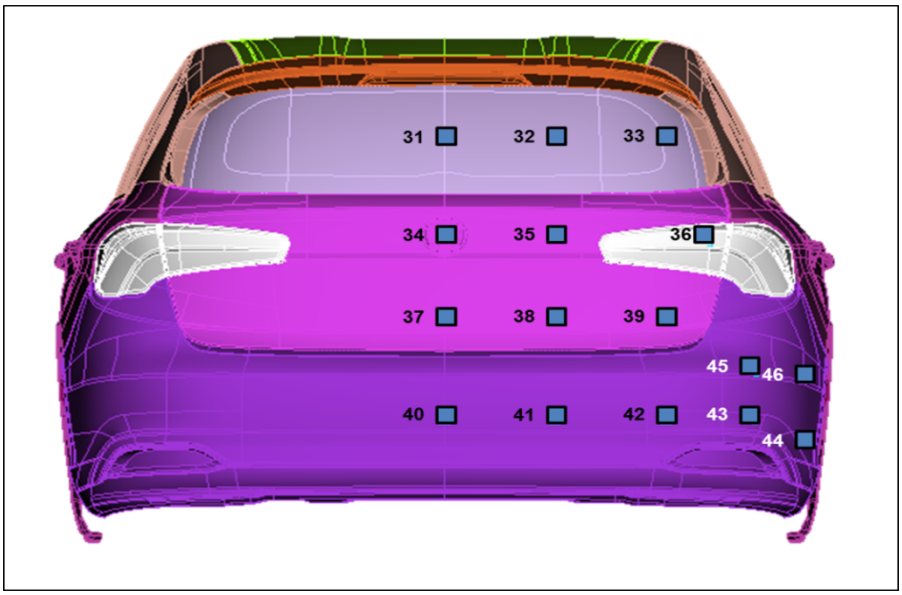

Figure 4.20: Pressure sensors position - 6

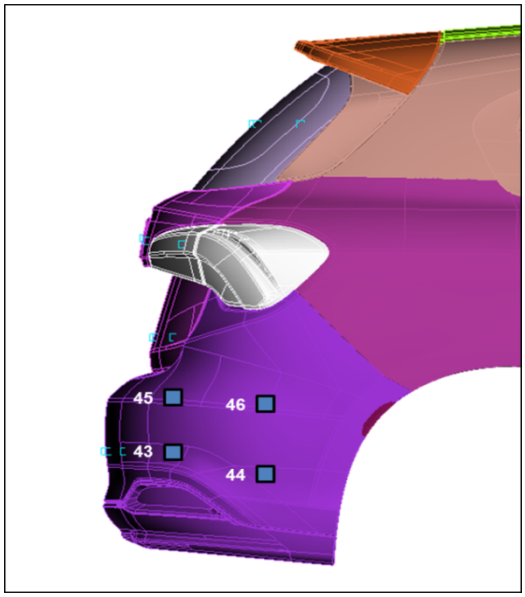

Figure 4.21: Pressure senso.sr position - 7

Considering that a good approximation of the results have also been obtained with the K-omega turbulence model with the second approach, in the following graph either the results accomplished with K-epsilon "Aerotools" and the K-omega "No Wrap" approaches are shown:

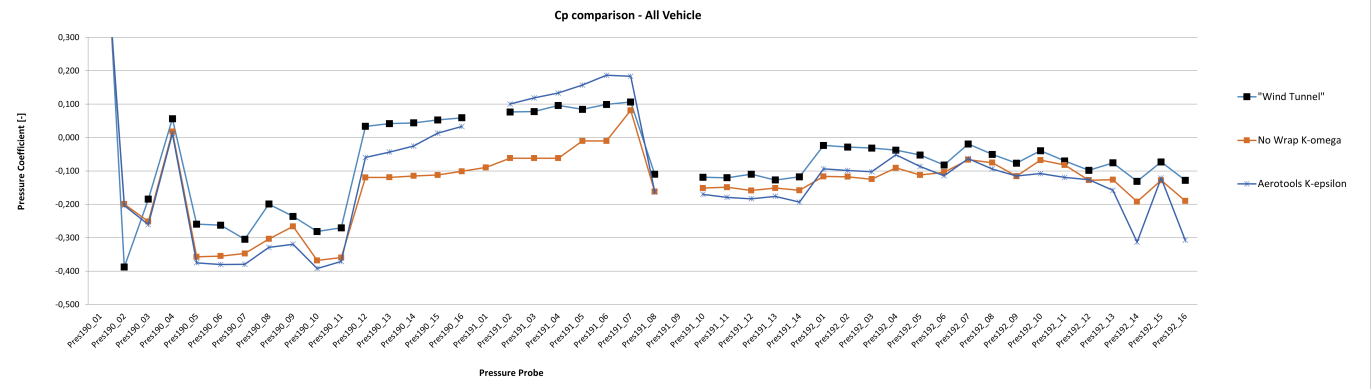

Figure 4.22: C_p prediction for Fiat Tipo

As it can be observed, there are different areas where one strategy of simulation is better than the other: for example in areas of the locary the K-omega with "No Wrap" approach is better than the other, whereas the K-epsilon "Aerotools" is closer to the data collected in the wind tunnel for the pressure rake close to the door of the vehicle. In addition to the fact that the mesh varies depending on the approaches used, one explanation of why SST K-omega model may perform better that K-epsilon in the locary area may be the following: the SST k-omega turbulence model tends to perform better than the standard k-epsilon due to its enhanced capability in handling flow separation and recirculation effects. This is especially important in complex flow areas such as the locary, where the flow behavior is influenced by the presence of the wheel and the associated complex geometry. The SST k-omega model is better equipped to model near-wall flows and is effective in predicting transitional flows from laminar to turbulent. It provides a more accurate representation of the flow physics near the wheel and accounts for the anisotropic nature of turbulence in regions with complex geometries.

4.3 Alfa Romeo Stelvio

Considering that only the Baseline configuration have been analyzed for this vehicle, no prediction of deltas between different configurations have been produced. The analysis focused on the prediction of the drag coefficient. Referring to *Figure 3.26*, which reports values of absolute C_x for the vehicle, it is shown how every different approach to the simulation predicted a drag coefficient which is higher than the one recorded in the wind tunnel. As it happened for the other the previous two vehicles, the strategy which revealed to be the closest to the drag coefficient recorded in the wind tunnel is the K-epsilon with "Aerotools" approach.

The pictures below show some field functions which may be useful to visualize how the flow follows the geometry of the vehicle and how the pressure coefficient changes along the vehicle. They have been produced by using "Aerotools" approach with either K-epsilon and K-omega turbulence models.

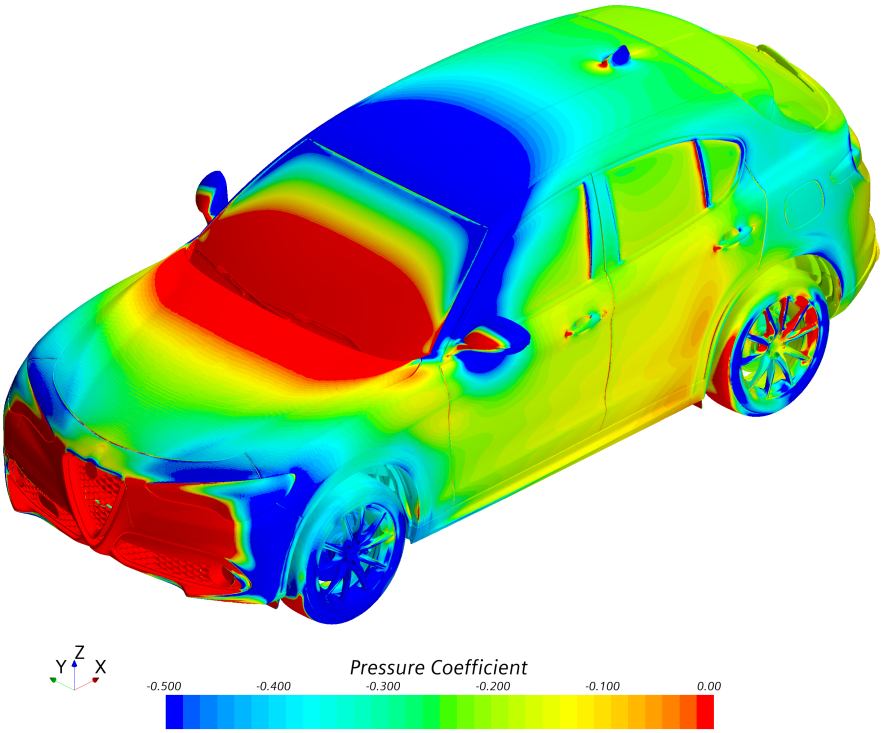

Figure 4.23: C_p Alfa Romeo Stelvio with K-epsilon "Aerotools"

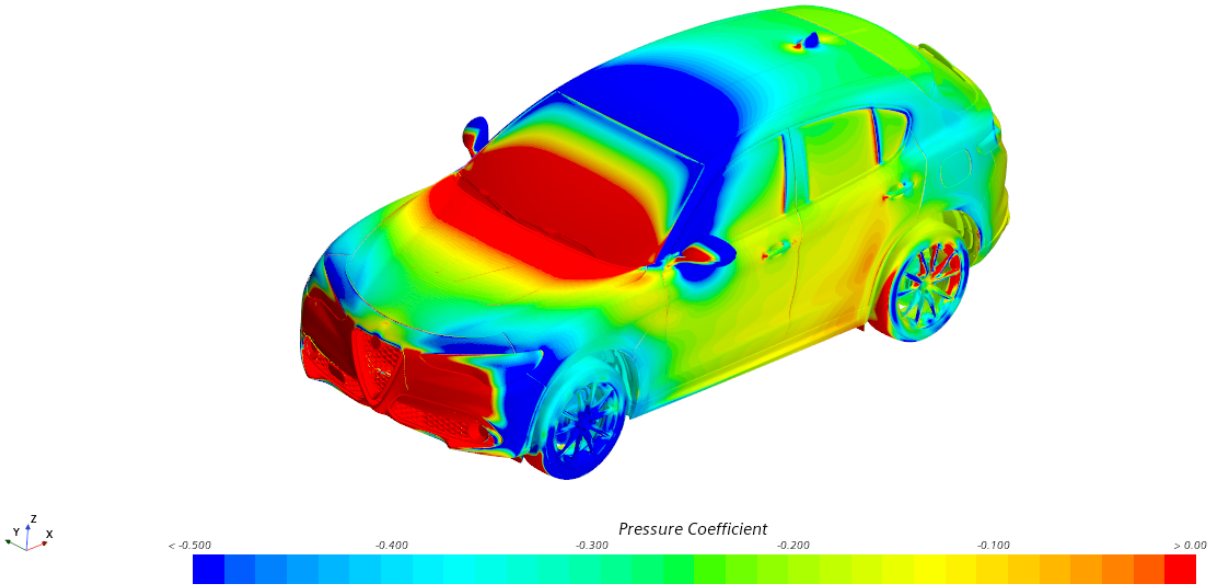

Figure 4.24: C_p Alfa Romeo Stelvio with K-omega "Aerotools"

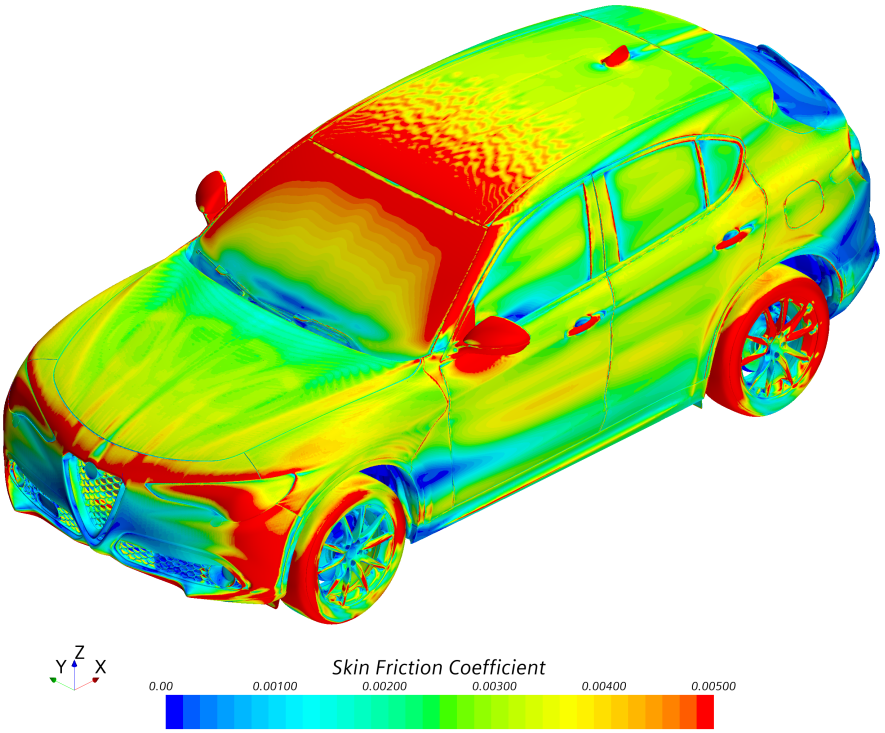

Figure 4.25: Skin Friction Coefficient Alfa Romeo Stelvio with K-epsilon "Aerotools"

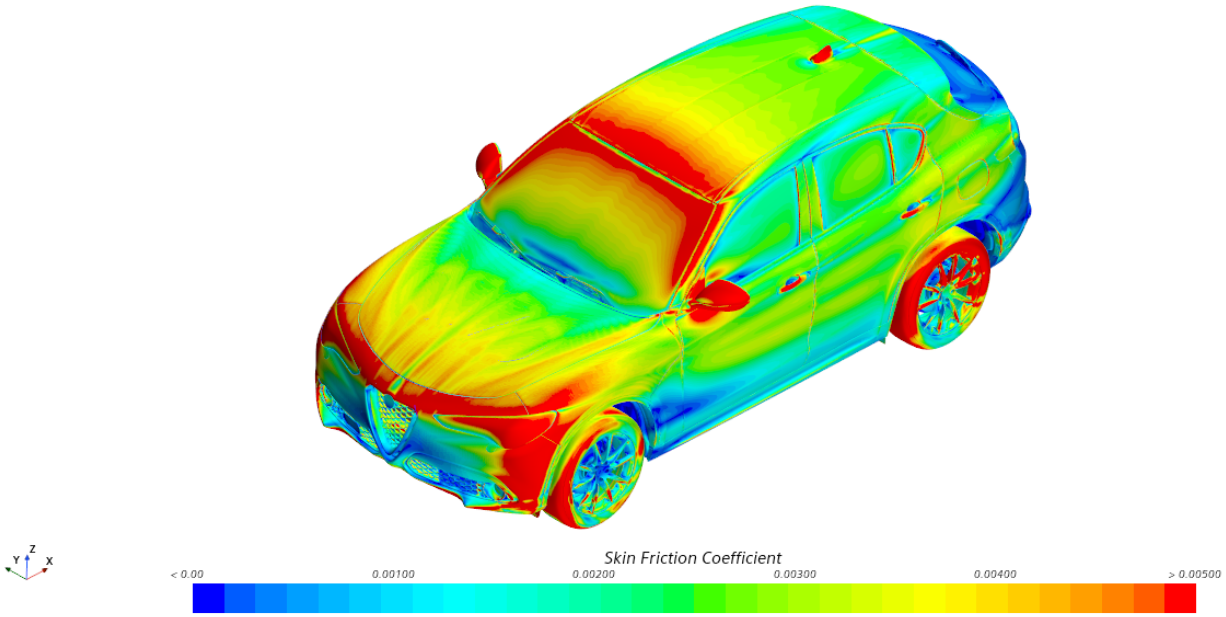

Figure 4.26: Skin Friction Alfa Romeo Stelvio with K-omega "Aerotools"

If no major changes can be visualized in the C_p images, there is a substantial difference in the picture which reports the skin friction coefficient in the area of the front door. As a matter

of fact, the simulation which uses the K-epsilon predicted a coefficient which is higher than the one computed with the K-omega, passing the information that the flux is following more than in the other case.

4.4 Alfa Romeo Giulia

Referring to *Figure 3.32*, which reports values of absolute Cx for the vehicle, it shows a trend which is respected either with Aerotools and with No Wrap approach. As a matter of fact, with both strategies of meshing, the turbulence model which is closer to the value of the drag coefficient recorded in the wind tunnel is the K-Omega. As a matter of fact, not only it produced the closest value to the one recorded in the wind tunnel, but also predicts the same delta between the two different configurations.

In order to see how the modification of the back of the vehicle affected its aerodynamics, it can be useful to check the skin friction coefficient which can give an idea of the separation of the flux, the pressure coefficient and a velocity plane which can show the develop of the wake downstream of the vehicle. Considering that the turbulence model which is accurate either in the prediction of the drag coefficient and in the prediction of deltas is the K-omega applied to the first strategy of meshing, the pictures below are those obtained with it.

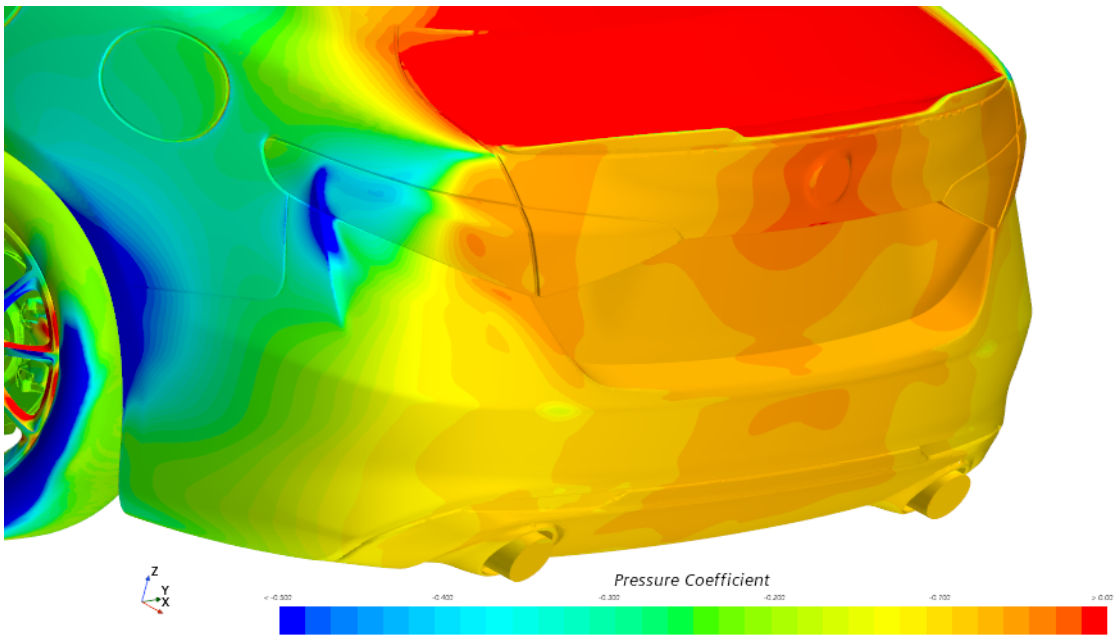

Figure 4.27: C_p Alfa Romeo Giulia with spoiler with K-omega "Aerotools"

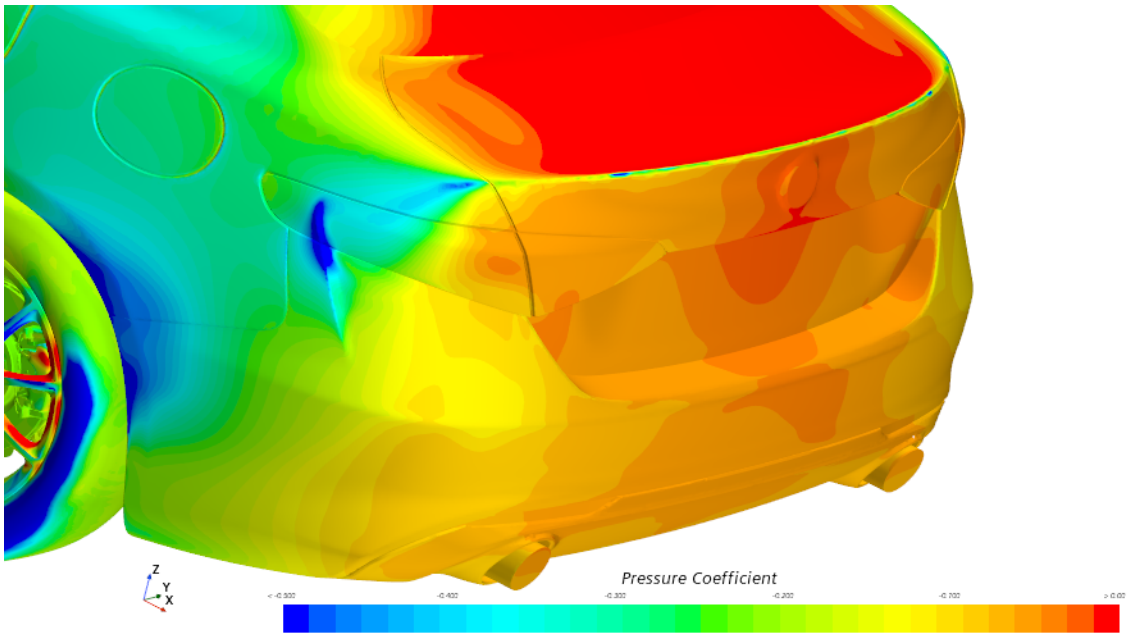

Figure 4.28: C_p Alfa Romeo Giulia without spoiler with K-omega "Aerotools"

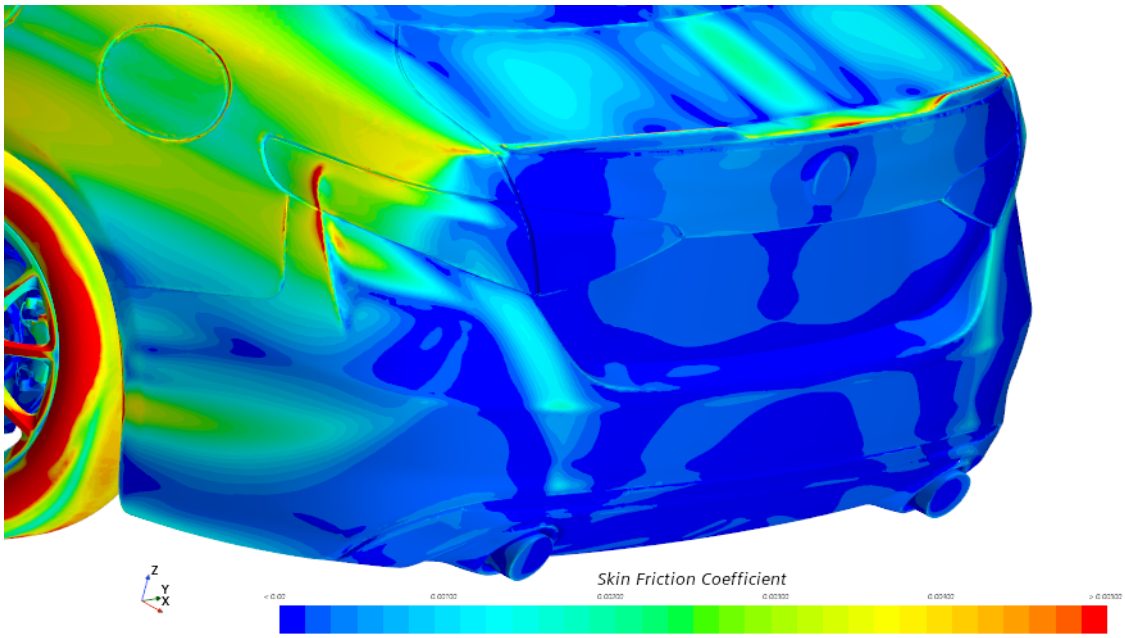

Figure 4.29: Skin Friction - 1 - Alfa Romeo Giulia with spoiler with K-omega "Aerotools"

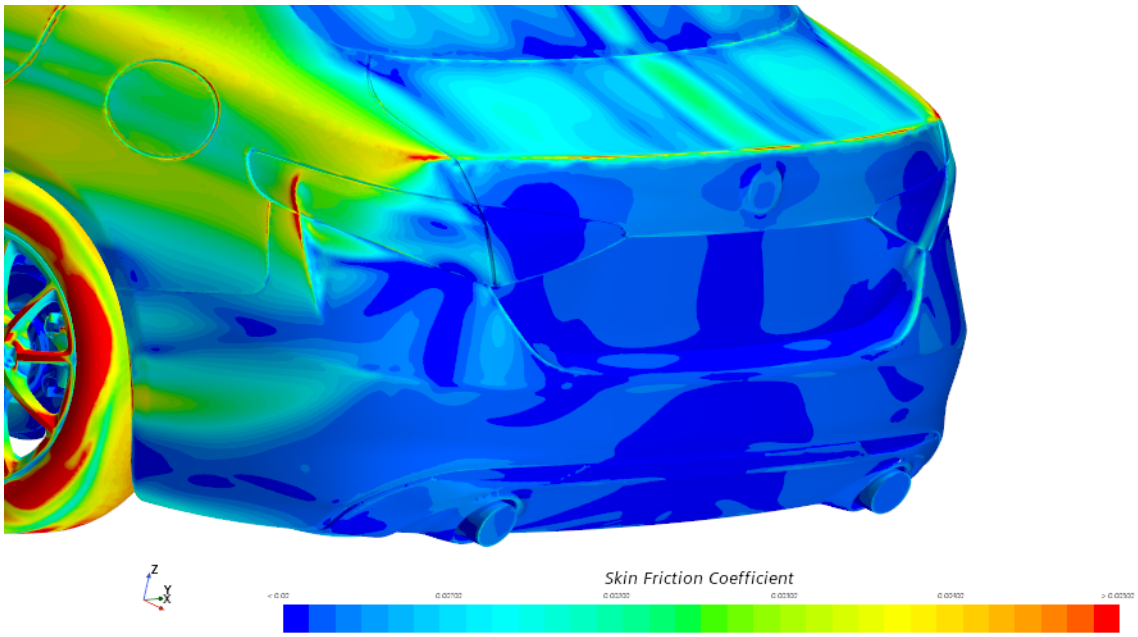

Figure 4.30: Skin Friction - 1 - Alfa Romeo Giulia without spoiler with K-omega "Aerotools"

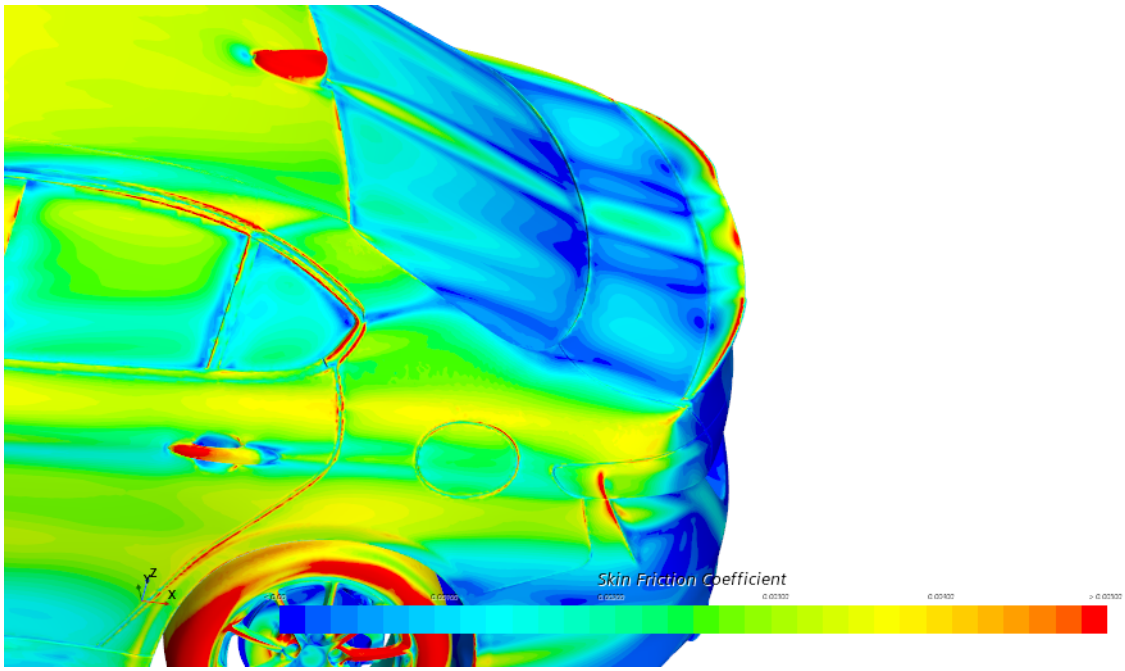

Figure 4.31: Skin Friction - 2 - Alfa Romeo Giulia with spoiler with K-omega "Aerotools"

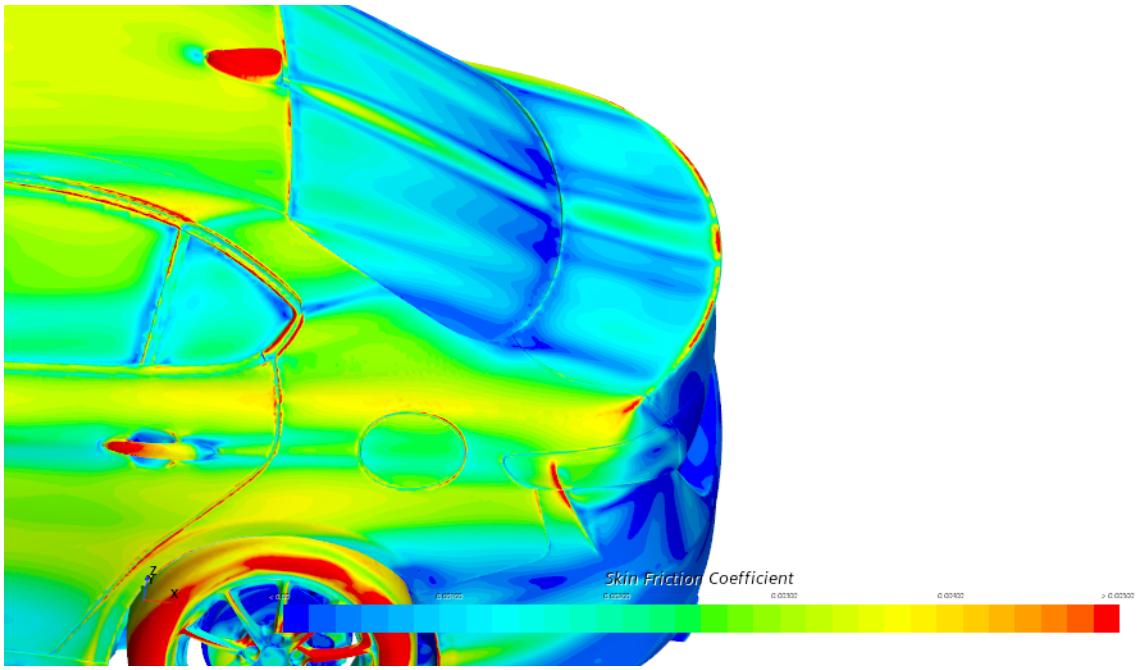

Figure 4.32: Skin Friction - 2 - Alfa Romeo Giulia without spoiler with K-omega "Aerotools"

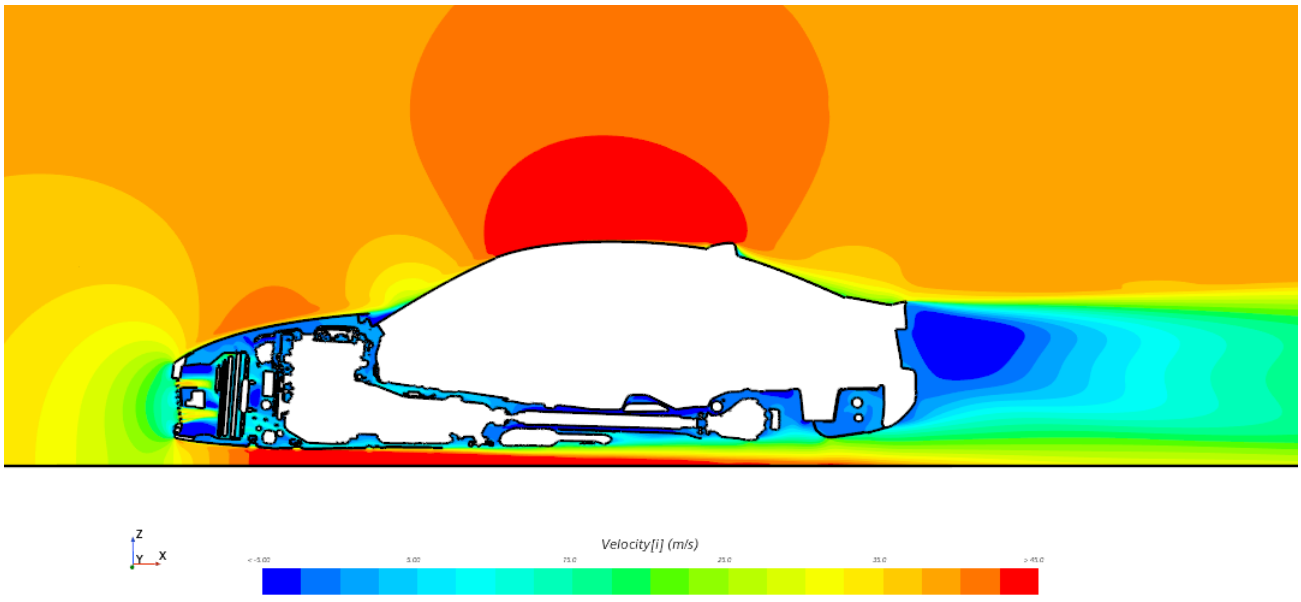

Figure 4.33: Cut plane of vehicle Alfa Romeo Giulia with spoiler showing the velocity [i] obtained with K-omega "Aerotools"

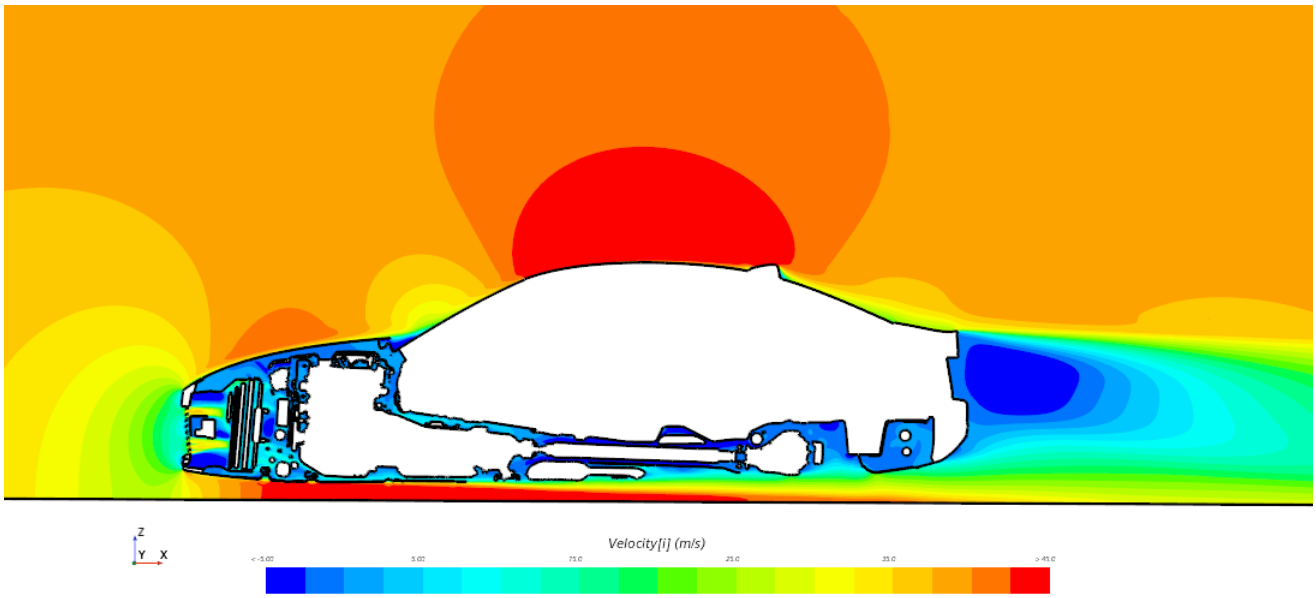

Figure 4.34: Cut plane of vehicle Alfa Romeo Giulia without spoiler showing the velocity [i] obtained with K-omega "Aerotools"

One of the biggest things which may be observed is in the images related to the C_p. As a matter of fact, it can be seen that in the back of the vehicle there is a bigger pressure recovery in the configuration without the spoiler than in the one with it. This thing supports the fact that the Baseline configuration presents a lower drag coefficient. Another thing that can be seen is that the wake which develops in the configuration with the spoiler is wider than the one without it. It is explained by the fact that the geometry of the spoiler forces the flow to go upwards.

Another thing which must be said is that every simulation executed with "No Wrap" approach gave as a result an underestimation of the variation of the drag coefficient. This slight difference in the results with the two approaches may be explainable in the settings of the mesh. As a matter of fact, from the pictures below it is possible to see how the dimension of the cells with "Aerotools" approach are smaller than the ones built with "No Wrap" approach.

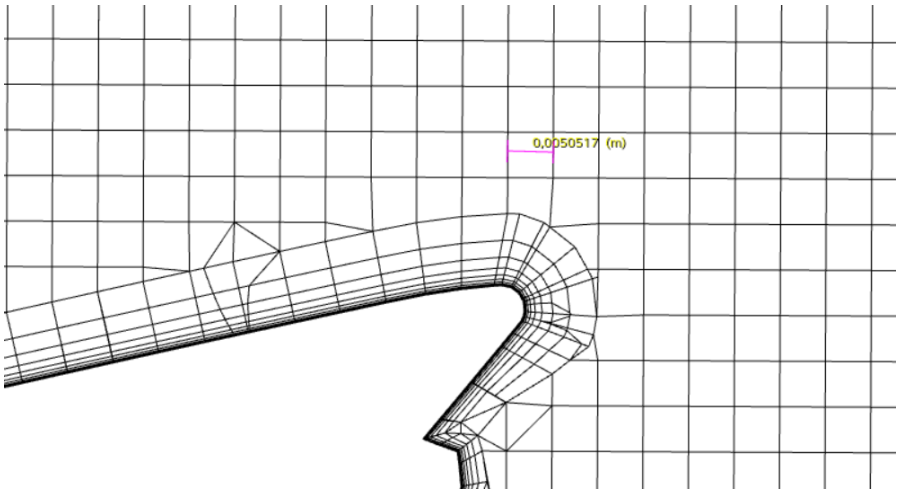

Figure 4.35: Dimension of the cells built with "Aerotools" approach near the spoiler

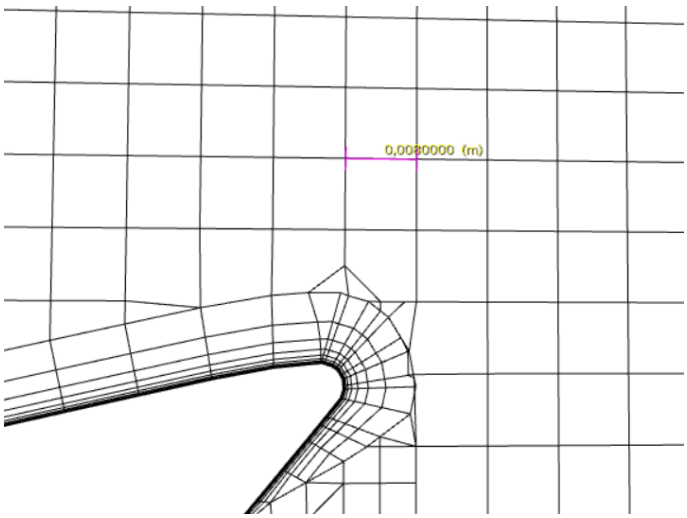

Figure 4.36: Dimension of the cells built with "No Wrap" approach near the spoiler

Considering that the spoiler affects also the downforce, it can be useful to see how the different mesh strategies and turbulence models affected it. The results obtained are resumed in the following table.

Alfa Romeo Giulia prediceted Deltas	
Type of Analysis	**Delta Cx**
K-epsilon-1st strategy of meshing	-0.060
K-omega-1st strategy of meshing	-0.063
K-epsilon-2nd strategy of meshing	-0.060
K-omega-2nd strategy of meshing	-0.061
Lag-EB-2nd strategy of meshing	-0.056

Table 4.1: ΔC_z Baseline with spoiler VS Baseline of Alfa Romeo Giulia

As it can be observed from the previous table, every different strategy of simulation agrees with the expected fact that the geometry modification applied, resulted in an increasing of the downforce (the z-axis is directed upwards), which may give more stability to the vehicle.

4.5 Conclusion

As analyzed in the previous sections, the turbulence model which have revealed to be the best to predict the absolute C_x and deltas between different configuration is the *Standard K-epsilon Two Layer* and the strategy of meshing which has been more effective is the "Aerotools" one. As a matter of fact, the "Aerotools" approach with K-epsilon turbulence model have proved to be able to predict a Cx, which is accurate on all different models even though, as all the other strategies of computation, it could not find how the changes of geometry in the Fiat 500X influenced the value of the drag coefficient itself. It must be noted that SST K-Omega turbulence model has been precise in a vehicle such as the Alfa Romeo Giulia.

Bibliography

[1] "Aerodinamica Sperimentale – Gaetano Iuso – Politecnico di Torino". In: 2023.

[2] Alfaromeo. *ALFA ROMEO GIULIA*. Accessed on October 17, 2023. 2023. URL: https://www.alfaromeo.it/modelli/giulia.

[3] Alfaromeo. *ALFA ROMEO STELVIO*. Accessed on October 17, 2023. 2023. URL: https://www.alfaromeo.it/modelli/stelvio.

[4] Renzo Arina. *Fondamenti di aerodinamica*. Levrotto & Bella, 2015.

[5] BETA CAE Systems. *ANSA User Guide*. 2022.

[6] blizauto. *Fiat 500X*. Accessed on October 17, 2023. 2023. URL: https://www.blizauto.it/v/12082-fiat-500x-1-0-t3-120cv.

[7] "Computational Fluid Dynamics – Domenic D'Ambrosio – Politecnico di Torino". In: 2022.

[8] Burt David. *Improved Design of Settling Tanks Using an Extended Drift Flux Model*. 2010.

[9] PA Durbin. "A Reynolds stress model for near-wall turbulence". In: *Journal of Fluid Mechanics* 249 (1993), pp. 465–498.

[10] "Flussi turbolenti – Daniela Tordella – Politecnico di Torino". In: 2022.

[11] C. Fukushima and J. Westerweel. *Work from Technical University of Delft, The Netherlands*. 2007.

[12] J.O.Hinze. *Turbulence*. 1975.

[13] Michael Kraus et al. "Rheological modelling of linear viscoelastic materials for strengthening in bridge engineering". In: Aug. 2016.

[14] Brian Landers. "Mixing Characteristics of Turbulent Twin Impinging Axisymmetric Jets at Various Impingement Angles". PhD thesis. June 2016. DOI: 10.13140/RG.2.1.1028.2482.

[15] Florian R Menter. "Two-equation eddy-viscosity turbulence models for engineering applications". In: *AIAA journal* 32.8 (1994), pp. 1598–1605.

[16] Siemens Digital Industries Software. "Simcenter STAR-CCM+ User Guide, version 2021.1". In: *Spalart-Allmaras Model*. Siemens, 2021.

[17] P.R Spalart. "Strategies for turbulence modelling and simulations". In: *International Journal of Heat and Fluid Flow* (June 2000).

[18] Stellantis. *Debutta la nuova gamma Tipo*. Accessed on October 17, 2023. 2023. URL: https://www.media.stellantis.com/it-it/fiat/press/debutta-la-nuova-gamma-tipo.

[19] David C Wilcox. "Formulation of the kw turbulence model revisited". In: *AIAA journal* 46.11 (2008), pp. 2823–2838.

List of Figures

List of Tables